

Contents

1 General introduction	5
1.1 Industrial background and motivation	5
1.2 Outline of the work	5
2 Fatigue life calculation methods	5
2.1 Basic fatigue criteria	5
2.1.1 Criteria based on stress	5
2.1.2 Criteria based on energy	10
2.2 Basquin curve	12
2.3 Calculation method without cycle counting	13
3 Space gradient effects	19
3.1 Introduction	19
3.2 A first gradient approach [1]	20
3.2.1 General formulation	20
3.2.2 Recall of the classical Crossland criterion	21
3.2.3 Formulation of Crossland criterion with gradient effect	22
3.3 Optimized Crossland Criterion formulation	22
3.4 Optimized Papadopoulos Criterion formulation	23
3.5 Optimized Dang Van Criterion formulation	24
3.6 Calibration of the criteria	25
3.6.1 Fully reversed 4-point bending and rotating cantilever bending fatigue tests	25
3.6.2 Bending-torsion fatigue tests	29
3.7 Discussion	32
3.8 Conclusion	32
4 Time varying load : the standard approach	33
4.1 The notion of damage in fatigue	33
4.1.1 Linear and nonlinear accumulation of damage	33
4.1.2 Classic Chaboche damage law	36
4.2 Verification method of Chaboche law	42
4.3 Chaboche law containing different criteria	42
4.3.1 Chaboche law with Crossland criterion	42
4.3.2 Chaboche law with Dang Van criterion	43
4.4 Numerical testing on different loading patterns	43
4.4.1 Test on pure rotation	44
4.4.2 Test on 4-point bending	45
4.4.3 Test on rotative bending	47
5 Handling general loadings	49
5.1 Cycle Counting Method	49
5.2 Multiaxial loading: existing models and limitations(Roux)	51
5.3 Multiscale energy dissipation approach	52
5.4 Kinematic Hardening Models	53
5.4.1 Linear Kinematic Hardening	53
5.4.2 Non-linear Kinematic Hardening	54
5.5 Weakening scales and yield function	54
5.5.1 The concept of weakening scales	54
5.5.2 Distribution of weakening scales	55

5.5.3	Yield function with mean stress effect	55
5.5.4	Local plastic model	58
5.5.5	Energy dissipation in shear cycle with mean stress	58
5.6	Construction of an energy based fatigue approach	58
5.7	Nonlinearity of damage accumulation	63
5.7.1	Energy approach with Chaboche law	63
5.7.2	Generalized damage accumulation	63
6	Numerical implementation and validation	63
6.1	Integration rules for \dot{W} and δD	63
6.2	Regime determination under multiple scales	65
6.3	Test on different load histories	68
6.3.1	One dimensional application to simple cyclic data	68
6.3.2	One dimensional application to PSA data	69
6.3.3	Multi-dimensional application to PSA data	71
6.4	Discussion	75
7	Multi-dimensional application	76
Reference		79
Appendices		80



Available online at www.sciencedirect.com



Thesis 00 (2017) 1–80

Journal
Logo

www.elsevier.com/locate/procedia

International Conference on Fatigue Damage of Structural Materials XI

A new strategy for fatigue analysis in presence of general multiaxial time varying loadings

Ma Zepeng^{a,*}, Patrick Le Tallec^b, Habibou Maitournam^c

^a*Laboratory of Solid Mechanics, Ecole Polytechnique, 91128 Palaiseau Cedex, France*

^b*Laboratory of Solid Mechanics, Ecole Polytechnique, 91128 Palaiseau Cedex, France*

^c*IMSIA, ENSTA ParisTech, CNRS, CEA, EDF, Universit Paris-Saclay, 828 bd des Marchaux, 91762 Palaiseau cedex France*

Abstract

The object of this paper is to propose an energy based fatigue approach which takes into account impurities and hardness in the material which affect the fatigue life while handling multidimensional time varying loading histories.

Our fundamental thought is to assume that the local dissipated energy at small scale governs fatigue at failure. The proposal of our model is to consider a plastic behavior at the mesoscopic scale with a dependence of the yield function not only on the deviatoric part of the stress but also on the hydro static part. A kinematic hardening under the assumptions of associative plasticity is also considered. We follow the Dang Van paradigm. The structure is elastic at the macroscopic scale. At each material points, there is a stochastic distribution of weak points which will undergo strong plastic yielding, which contribute to energy dissipation without affecting the overall macroscopic stress.

Instead of using the number of cycles, we use the concept of loading time. To elaborate real life loading history more accurately, mean stress effect is taken into account in mesoscopic yield function and non-linear damage accumulation law are also considered in our model. Fatigue will then be determined from the plastic shakedown cycle and from a phenomenological fatigue law linking lifetime and accumulated mesoscopic plastic dissipation.

Keywords: Fatigue; Energy; High cycle; Plasticity; Mean stress

^{*}Corresponding author. Email address: zepeng.ma@polytechnique.edu

Nomenclature

Σ_{max}	maximum stress during the loading cycles
σ_m	mean stress
σ_H	hydrostatic stress
σ_{-1}	fatigue limit for fully reversed condition
b	back stress
σ_y	macroscopic yield stress
N	current number of cycles
N_F	number of cycles to failure
\dot{p}	accumulated plastic strain rate given as $\sqrt{\frac{2}{3}}\ \dot{\varepsilon}_p\ $
D	damage variable
$M(), \alpha()$	functions in the nonlinear continuous damage model
M_0, a, b, γ	coefficients of the nonlinear continuous damage model
σ_{σ_m}	fatigue limit for a non-zero mean stress
σ_a	stress amplitude
σ_u	ultimate tensile stress
$\langle \rangle$	Macaulay bracket symbol. $\langle \rangle$ is defined as $\langle m \rangle = 0$ if $m \leq 0$, $\langle m \rangle = m$ if $m > 0$
S_{max}	maximum deviatoric stress during the loading cycles
\dot{w}	energy dissipation rate at a certain scale
\dot{W}	energy dissipation rate at all scales
W	dissipated energy
W_{cyc}	dissipated energy per cycle
$\dot{\varepsilon}_p$	rate of effective plastic strain
\dot{p}	accumulated plastic strain rate given as $\sqrt{\frac{2}{3}}\ \dot{\varepsilon}_p\ $
W_F	dissipated energy to failure per unit volume
E	Young's modulus
$k = 500 \sim 800 MPa$	hardening parameter
$\beta = 1 \sim 50$	weakening scales distribution exponent
$\gamma = 0 \sim 50$	material parameter from Chaboche law(Wohler curve exponent)
$\alpha = 1 - a \left(\frac{\max_t \sqrt{J_{2,a}(t)} + a_c P_{max}(t) - b_c}{\sigma_u - 2 \max \sqrt{J_{2,a}}} \right)$	characterizes non-linearity of damage accumulation
a	material parameter from Chaboche law
σ_y	macroscopic yield stress(normal or shear)
$\lambda = 0 \sim 5$	hydrostatic pressure sensitivity
$\underline{\underline{S}} = dev \underline{\underline{\Sigma}}$	deviatoric part of the stress tensor
σ_H	macroscopic hydrostatic pressure
$A_{II} = \tau_{oct,a} = \sqrt{\frac{1}{3} J_{2,a}}$	the amplitude of octahedral shear stress
s_{-1}	tensile fatigue limit for $R = -1$

1 General introduction

1.1. Industrial background and motivation

The search for the best performance at the best cost in the mechanical and transport leads to conditions of use of the mechanical components increasingly severe. Fatigue failures are widely studies because it accounts for 90% of all service failures due to mechanical causes. Fatigue failures occur when metal is subjected to a repetitive or fluctuating stress and will fail at a stress much lower than its tensile strength and the process happens without any plastic deformation (no warning).

These can lead to the emergence of fatigue for very high level of stress gradient(for small scale or complex geometric structures) and non-constant multiaxial loading history . For these so-called "extreme" solicitations, the mechanisms of damage as well as fatigue resistance levels are mostly completely unknown. This poses an important problem during the dimensioning phase since, on the one hand, the existing endurance criteria struggle to account for behavior for this type of loading, and on the other hand, the fatigue data that would allow to identify a model adapted to this problem are almost non-existent.

1.2. Outline of the work

2 Fatigue life calculation methods

2.1. Basic fatigue criteria

This bibliographic chapter enables to present the methods to calculate the lifetime of multiaxial high cycle fatigue. In fact, the equivalent stress of multiaxial loading and variable amplitude loading reveals the necessity of study these methods. These criteria allows to determine whether the stress trajectory in the stress space leads to the failure of the points concerned.

Papadopoulos suggested, in particular, to group families of fatigue criteria into four categories:

- Criteria based on strain
- Criteria based on stress
- Criteria based on energy
- Criteria based on plasticity-damage coupling

Generally, the criteria developed in strain(and sometimes in energy) are adapted to the oligocyclic fatigue where the tests are often carried out with imposed strain. Approaches in stress(and sometimes in energy), as well as those based on the coupling plasticity and damage(which have begun to emerge in recent years) are being applied in the domain of endurance. In particular, we will focus on the last three categories and analyze the different approaches.

2.1.1. Criteria based on stress

Three types of approach can be distinguished:

- Critical Plan Approaches
- Approaches based on stress invariants
- The criteria based on mean stress in an elementary volume

For simplicity and to avoid too costly identification procedures of fatigue data, criteria are often expressed using two parameters. The first relates generally to a shear stress (on a plane or on average over an elementary volume) while the second reflects the normal stress effects (mean and amplitude) through the hydrostatic stress or the normal stress. The criteria using the hydrostatic stress are the most numerous [Crossland 1956, Sines 1959 Morel 1999 Huyen Thi Thu 2008]. The micro-macro approach applied to the field of endurance

was born with the work of [Dang Van 1973], and since it has been used many times by including [Papadopoulos 1993] to take better account of loading path effects. The normal stress acting on the material planes is sometimes used on a critical plane [Findley 1959], or through integration at every plane of an elementary volume [Liu and Zenner 1993]. [Huyen Thi Thu 2008] proposes, in particular, a probabilistic approach that shows this type of integration.

Crossland Criterion

In several industries, the required design lifetime of many components often exceeds 10^8 cycles. This requirement is applicable to aircraft (gas turbine disks 10^{10} cycles), automobiles (car engine 10^8 cycles), and railways (high speed train 10^9 cycles). Although a large amount of fatigue data has been published in the form of S-N (where S is stress and N cycles numbers) curves, the data in the literature has been usually limited to fatigue lives up to 10^7 cycles. Using traditional fatigue criteria, a near hyperbolic relationship between stress and fatigue life is assumed, with an asymptotic limit defined as the endurance stress. To predict this asymptotic limit, the Crossland Criterion is probably the most widely known. Crossland proposed that the second invariant of the deviatoric stress tensor and the hydrostatic pressure are the variables governing the endurance limit.

Many fatigue limit criteria can be written as:

$$f(\tau) + g(\sigma) \leq 0 \quad (1)$$

where f and g are given functions of the shear stress and of the normal stress respectively, as applied to different interfaces within the material.

The classical Crossland criterion defines the fatigue limit of metallic specimens subjected to multi-axial in-phase cyclic stress[2] :

$$f(\sqrt{J_{2,a}}, P_{max}) = \tau_{eq} + aP_{max} - b \leq 0 \quad (2)$$

where $\tau_{eq} = \sqrt{J_{2,a}}$ measures the amplitude of variation of the second invariant of the deviatoric stress and P_{max} is the maximum hydrostatic stress observed during a loading cycle. If $f(\sqrt{J_{2,a}}, P_{max})$ is negative or null, there is no damage. If $f(\sqrt{J_{2,a}}, P_{max})$ is positive, there is likely to be damage. The physical constants a and b are material's constants that needs to be determined experimentally. The amplitude of the square root of the second invariant of the stress deviator can be defined, in general case, as the half-length of the longest chord of the deviatoric stress path[3]

$$\sqrt{J_{2,a}} = \frac{1}{2\sqrt{2}} \min_{\underline{\underline{S}}} \{ \max_t \sqrt{(\underline{\underline{S}}(t) - \underline{\underline{S}}_1) : (\underline{\underline{S}}(t) - \underline{\underline{S}}_1)} \} \quad (3)$$

Recall that the deviatoric stress $\underline{\underline{S}}$ associated to a stress tensor $\underline{\underline{\sigma}}$ is defined by

$$\underline{\underline{S}} = \underline{\underline{\sigma}} - \frac{1}{3} \text{tr} \underline{\underline{\sigma}} \underline{\underline{1}} \quad (4)$$

The maximum value that the hydrostatic stress reaches during the loading cycle is on the other hand:

$$P_{max} = \max_t \{ \frac{1}{3} \text{tr} (\underline{\underline{\sigma}}(t)) \}. \quad (5)$$

For a proportional cyclic loading, if one introduces the two extreme stress tensors $\underline{\underline{\sigma}}^A$ and $\underline{\underline{\sigma}}^B$ observed during the loading path, together with the stress amplitude

$$\underline{\underline{\Delta\sigma}} = \underline{\underline{\sigma}}^B - \underline{\underline{\sigma}}^A \quad (6)$$

and its deviatoric part $\underline{\underline{\Delta s}}$, the variation of the second invariant of the stress deviator reduces to

$$\sqrt{J_{2,a}} = \frac{1}{2} \max_t \sqrt{\frac{1}{3} \underline{\underline{\Delta s}} : \underline{\underline{\Delta s}}} = \frac{1}{2} \max_t \sqrt{\frac{1}{3} (\Delta s_{11}^2 + \Delta s_{22}^2 + \Delta s_{33}^2 + 2\Delta s_{12}^2 + 2\Delta s_{13}^2 + 2\Delta s_{23}^2)}. \quad (7)$$

The physical constants a and b can be related to the limit t_{-1} of endurance in alternate pure shears and to the limit f_{-1} of endurance in alternate pure traction and compression by

$$a = \frac{(t_{-1} - \frac{f_{-1}}{\sqrt{3}})}{\frac{f_{-1}}{3}}, \quad b = t_{-1}. \quad (8)$$

Thus the classical Crossland criterion can be written as:

$$\sqrt{J_{2,a}} + aP_{max} - b \leq 0 \quad (9)$$

Dang Van Criterion

In multiaxial fatigue with large number of cycles, the important role of local plasticity on the appearance of a fatigue limit is widely accepted and fully justifies the use of a multi-scale approach. Among the existing approaches, one of the most known and used is that of [Dang Van 1999]. This criterion is used in particular in the design of certain automotive structures at PSA and Renault. The criterion [Dang Van 1973] belongs to the family of critical plane type approaches. The main physical basis of this criterion focuses on the theory of elastic adaptation to two scales, mesoscopic and macroscopic. The macroscopic behavior of the material often remains elastic, only a grain oriented unfavorably undergo plastic deformation. The author states the following hypothesis: " The multiscale approach is settled on the assumption that under high cycle fatigue loading a structure will not be fractured by fatigue if an elastic shakedown is reached at the macroscopic scale as well as at mesoscopic scale " [Dang Van 1999]. The approach developed first is to describe the plasticity across the grain, assuming a yield criterion. The yield criterion is the law of Schmid with a linear supposed isotropic hardening. The author then search the elastic adaptation Fig. 1 formula and a fatigue test locally (represents the tensor defining the orientation of the sliding system, γ is the plastic slip and τ is the amplitude of shear stress on the defined plan). Finally, a micro to macro is applied to determine

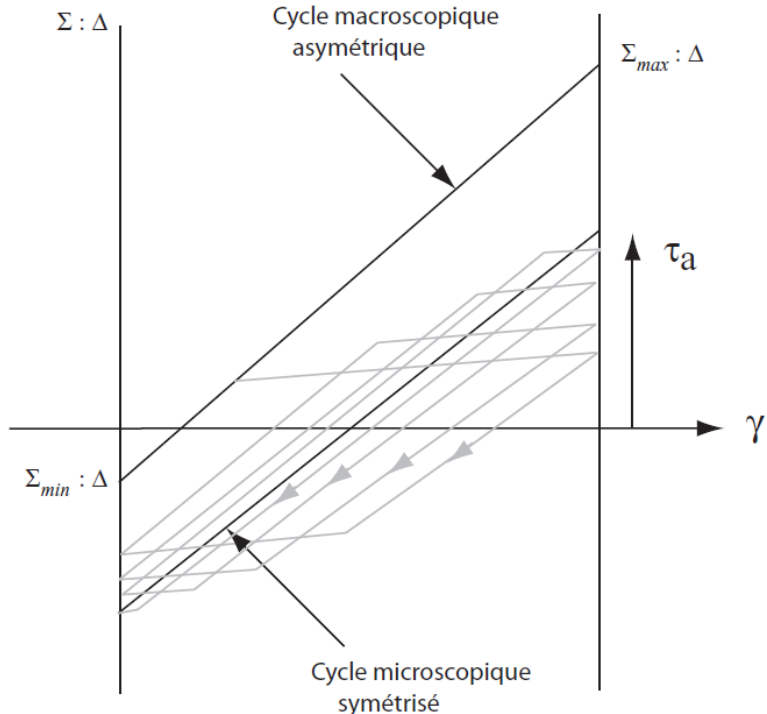


Fig. 1: Elastic adaptation at the two scales [Dang Van 1999]

the criteria on the macroscopic scale. The localization law used is Lin-Taylor model that assumes equality

of deformations at two scales. Using empirical relationships, the harmful role of the mean stress on the fatigue strength of the material is shown for type of uniaxial tensile stress. Dang Van shows the effect of the mean stress with hydrostatic stress term in the criteria expressed as a linear combination of mesoscopic shear stress on the maximum shear plane τ_a and the hydrostatic stress Σ_h .

The Dang Van criterion presented in [4] is expressed as:

$$\max_{\vec{n}} \left\{ \max_t \{ \tau_a(\vec{n}, t) + a_D \Sigma_h(t) \} \right\} \leq b_D. \quad (10)$$

τ_a denotes the mesoscopic shear stress amplitude and is obtained from a mesoscopic stress tensor $\hat{\sigma}$ defined by:

$$\hat{\sigma}(t) = (\sigma(t) - s^*).$$

s^* is the center of the smallest hypersphere circumscribed to the loading path in deviatoric stress space. It is obtained by solving a “min-max” problem as follows:

$$s^* = \arg \min_{s_1} \left\{ \max_t \| s(t) - s_1 \| \right\}.$$

In the case of fully reversed loading, the values $s^* = 0$ can be directly deduced without solving the “min-max problem” as in general case.

The principal stress values of stress tensor $\tilde{\sigma}$ denoting by $\hat{\sigma}_{III}(t) \leq \hat{\sigma}_{II}(t) \leq \hat{\sigma}_I(t)$, one gets the amplitude of shear stress by:

$$\tau(t) = \frac{1}{2}(\hat{\sigma}_I(t) - \hat{\sigma}_{III}(t)).$$

$\Sigma_h(t)$ is the hydrostatic stress as a function of the time, given by:

$$\Sigma_h(t) = \frac{\sigma_{kk}(t)}{3}.$$

The material characteristic parameters a_D and b_D of the Dang Van criterion, can be related to the fully reversed bending (or tension- compression because of the same stress state between them) fatigue limit, denoted by f_{-1} (or S_{-1}), and to the torsion fatigue limit, denoted by t_{-1} ,

$$a_D = \frac{3t_{-1}}{s_{-1}} - \frac{3}{2};$$

$$b_D = t_{-1}.$$

In the particular case of the uniaxial tension, the criterion is written as:

$$\Sigma_{xx,a} \left(\frac{1}{2} + \frac{a_D}{3} \right) + \Sigma_{xx,m} \left(\frac{a_D}{3} \right) = b_D$$

Papadopoulos Criterion

The approach proposed by [5] also uses the concept of elastic adaptation and even the localization law. According to him, “the observations at the mesoscopic scale show that the initiation of a fatigue crack is defined as the occurrence of micro-cracks corresponding to the rupture of the most deformed crystal grains in an aggregate. Thus, a fatigue limit criterion can be modeled by a limit value of the accumulated plastic strain in the most distorted grain.”

$$\gamma_{cum} \leq \gamma_{\infty}$$

He proposes to opt for a mean value of the accumulated plastic strain on all possible slip systems of representative elementary volume(REV). So he chose to use a average value of accumulated plastic deformation rather than looking at failure of a single crystal. A spherical coordinate system(Fig. 10) to guide the vector of normal in material plane, and the unit direction vector r linked to a sliding direction of this plan is used to conduct the integration over all possible orientations.

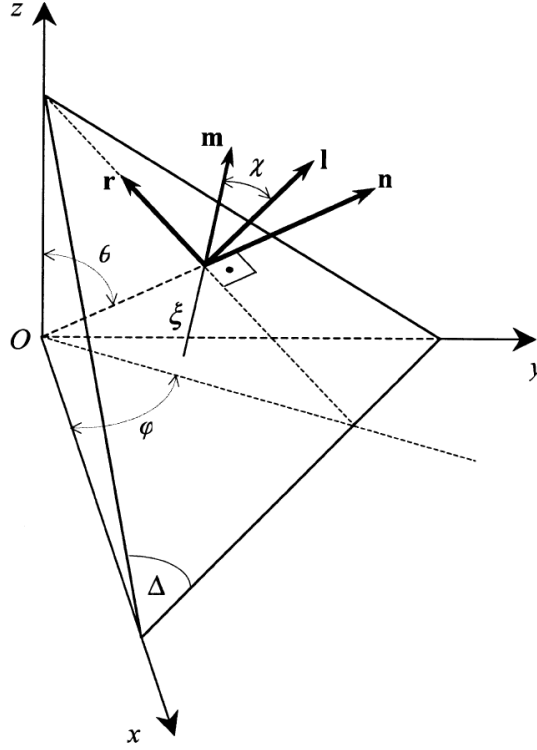


Fig. 2: Material plane Δ passing through point O of a body and its associated (n, l, r) frame.

At any point O of a body, a material plane Δ can be defined by its unit normal vector \mathbf{n} . This vector \mathbf{n} makes an angle θ with the z -axis of a $Oxyz$ frame attached to the body, and its projection on the xy plane makes an angle φ with axis x . For each plane Δ a new quantity is introduced called *generalised shear stress* amplitude and denoted as T_a . This shear stress quantity was first introduced in Papadopoulos [6] and was subsequently used by other researchers. The critical plane according to our proposal is that onto which $T_a(\varphi, \theta)$ achieves its maximum value. The fatigue limit criterion is written as:

$$\max T_a + \alpha_\infty \Sigma_{h,max} \leq \gamma_\infty \quad (11)$$

where α_∞ and γ_∞ are material parameters to be determined [6].

$$\Sigma_{h,max} = \max_t \left\{ \frac{1}{3} \operatorname{tr}(\underline{\underline{\sigma}}(t)) \right\}$$

He introduced the resolved shear stress τ :

$$\begin{aligned} \tau = & [\sin\theta \cos\varphi \sigma_{xx} + \sin\theta \sin\varphi \sigma_{xy} + \cos\theta \sigma_{xz}](-\sin\varphi \cos\chi - \cos\theta \cos\varphi \sin\chi) + \\ & [\sin\theta \cos\varphi \sigma_{xy} + \sin\theta \sin\varphi \sigma_{yy} + \cos\theta \sigma_{yz}] (\cos\varphi \cos\chi - \cos\theta \sin\varphi \sin\chi) + \\ & [\sin\theta \cos\varphi \sigma_{xz} + \sin\theta \sin\varphi \sigma_{yz} + \cos\theta \sigma_{zz}] \sin\theta \sin\chi \end{aligned} \quad (12)$$

It is clear that the resolved shear stress is a function of φ, θ, χ and of time t in the case of variable loading, i.e. $\tau = \tau(\varphi, \theta, \chi, t)$. Upon fixing a couple (φ, θ) (i.e. a plane Δ) and an angle χ (i.e. a line ξ on Δ), one can define the amplitude of the resolved shear stress τ_a , acting on Δ along ξ by the formula:

$$\tau_a(\varphi, \theta, \chi) = \frac{1}{2} [\max_{t \in P} \tau_a(\varphi, \theta, \chi, t) - \min_{t \in P} \tau_a(\varphi, \theta, \chi, t)] \quad (13)$$

Finally, for a given plane Δ , i.e. for a fixed couple (φ, θ) , the generalized shear stress amplitude T_a is defined as:

$$T_a(\varphi, \theta) = \sqrt{\frac{1}{\pi} \int_{x=0}^{\frac{\pi}{2}} \tau_a^2(\varphi, \theta, \chi) d\chi} \quad (14)$$

We note the fatigue limit in fully reversed torsion t_{-1} and the fatigue limit in fully reversed bending f_{-1} . From these two tests we get the parameters:

$$\begin{aligned} \gamma_\infty &= t_{-1}, \\ \alpha_\infty &= 3 \left(\frac{t_{-1}}{f_{-1}} - \frac{1}{2} \right). \end{aligned}$$

The Papadopoulos fatigue limit criterion achieves the form:

$$\max T_a + 3(t_{-1}/f_{-1} - 1/2) \Sigma_{h,max} \leq t_{-1}. \quad (15)$$

In the particular case of the uniaxial tension, the criterion is written as:

$$\Sigma_{xx,a} \left(\frac{1}{\sqrt{3}} + \frac{\alpha_\infty}{3} \right) + \Sigma_{xx,m} \left(\frac{\alpha_\infty}{3} \right) = \gamma_\infty$$

2.1.2. Criteria based on energy

Energy dissipation based on law of thermodynamics

In case of shell model. We assume the temperature in the thickness direction does not change. Based on the first and second law of thermodynamics, for any point M , we define $T(M, t)$ is the temperature field of M at time t . Its 2D heat transfer function is [7]:

$$\rho C \frac{\partial T(M, t)}{\partial t} - k \Delta_2 T(M, t) + \frac{2\sigma_e \varepsilon_m T(M, t)^4}{e} + \frac{2h}{e} [T(M, t) - T(M, t)^{air}] = d_1(M, t) + S_{th}(M, t) + r(M, t)$$

ρ is the density of the steel, C is specific heat capacity, k is heat transfer coefficient, σ_e is the bolzmann constant, ε_m is the surface thermal emissivity, h is heat convection factor, $T(M, t)^{air}$ is the environment temperature at point M , Δ_2 is two dimensional Laplace operator. $d_1(M, t)$ is the dissipative source of fatigue relevant irreversible strain ε_{ir} , strain hysteresis ε_{ve} and micro structure deformation; $S_{th}(M, t)$ is the thermoelastic source composing of elastic strain ε_e ; $r(M, t)$ is thermal radiation term.

In a single cycle the dissipated energy is only a function of dissipative source $d_1(M, t)$:

$$E_{d_1}(t) = \int_{t-\frac{t_f}{2}}^{t+\frac{t_f}{2}} d_1(t) dt$$

Experiments with different stress amplitude loadings shows that the correlation coefficient between dissipated energy in one cycle and fatigue life is more than S-N curve.

$$\lg E_{d_1}^m = -0.77 \lg N_F + 8.33 \text{ correlation coefficient: 0.94}$$

$$\lg \sigma_a = -0.13 \lg N_F + 2.85 \text{ correlation coefficient: 0.89}$$

Energy dissipation based on strain energy density

In their fatigue criterion, Froustey et al. (1992) have considered a complete cycle of stresses. They use the mean value on one cycle of the volumic density of the elastic strain energy, W_a , whatever the point M in the mechanical part.

$$W_a(M) = \frac{1}{T} \int_0^T \frac{1}{2} \sigma_{ij}(M, t) \varepsilon_{ij}^e(M, t) dt$$

where $\sigma_{ij}(M, t)$ and $\varepsilon_{ij}^e(M, t)$ are respectively the tensor of stresses and the tensor of elastic strains at the considered point M function of time T . Usually the endurance limit is low enough to consider that

the material remains elastic at the macroscopic scale (Lemaitre and Chaboche, 1988). Thus, W_a can be considered as the mean value on one cycle of the total strain energy density at the considered point.

In 1998 Thierry PALIN-LUC and Serge LASSEUR [8] proposed the failure criterion of W_a :

Their studies show that another limit, called σ^* , can be defined below the usual endurance limit of the material, σ_D . At a considered point a stress amplitude below this new limit does not initiate observable damage at the microscopic scale (no micro-cracks).

From σ^* and by analogy with a sinusoidal traction load the corresponding mean value of the strain energy volumetric density, W_{a^*} , can be calculated, where E is the Young modulus of the material.

$$W_{a^*} = \frac{\sigma^{*2}}{4E}$$

Around each point it is always possible to define the volume $V^*(C_i)$ by the set of points M where $W_a(M)$ is higher than $W_{a^*}(C_i)$. They postulate that the part of $W_a(M)$ exceeding $W_{a^*}(C_i)$ is the damaging part of the strain energy volumetric density. $\bar{\omega}_a(C_i)$ is the volumetric mean value of the strain energy around the critical point C_i

$$V^*(C_i) = \{ \text{points } M(x, y, z) \text{ around } C_i \text{ such that } W_a(M) \geq W_{a^*}(C_i) \}$$

$$\bar{\omega}_a(C_i) = \frac{1}{V^*(C_i)} \int \int \int_{V^*(C_i)} [W_a(x, y, z) - W_{a^*}(C_i)] d\nu$$

This stress limit σ^* can be estimated from fatigue test results in fully reversed tension and in rotating bending

$$\sigma^* = \sqrt{2(\sigma_{Ten,-1}^D)^2 - (\sigma_{RotBend,-1}^D)^2}$$

A critical plane approach based on energy concepts

$$W(t) = \frac{1}{2} \sigma(t) \varepsilon(t) \operatorname{sgn}[\sigma(t), \varepsilon(t)]$$

$$\operatorname{sgn}(x, y) = \frac{\operatorname{sgn}(x) + \operatorname{sgn}(y)}{2}$$

$\operatorname{sgn}(x), \operatorname{sgn}(y) = 0, 1, -1$ for distinguishing positive and negative works in a fatigue cycle[9].

If the stress and strain reach their maximum values, σ_a and ε_a , then the maximum energy density value is

$$W_a = \frac{1}{2} \sigma_a \varepsilon_a$$

In the case of high-cycle fatigue, when the characteristic $(\sigma_a - N_F)$ is used, the axis σ_a should be replaced by W_a , where

$$W_a = \frac{\sigma_a^2}{2E}$$

In the case of low and high-cycle fatigue, when the characteristic $(\varepsilon_a - N_F)$ is used, we can do similar rescaling. We assume

$$\sigma_a = \sigma'_f (2N_F)^b$$

From Manson-Coffin-Basquin equation we obtain

$$\varepsilon_a = \varepsilon_a^e + \varepsilon_a^p = \frac{\sigma'_f}{E} (2N_F)^b + \varepsilon'_f (2N_F)^c$$

$$W_a = \frac{1}{2} \sigma_a \varepsilon_a = \frac{\sigma_a}{2} \left[\frac{\sigma'_f}{E} (2N_F)^b + \varepsilon'_f (2N_F)^c \right] = \frac{(\sigma'_f)^2}{2E} (2N_F)^{2b} + 0.5 \varepsilon'_f \sigma'_f (2N_F)^{b+c}$$

Fatigue characteristic for high-cycle fatigue takes the form

$$W_a = \frac{(\sigma'_f)^2}{2E} (2N_F)^{2b}$$

For the stress model we have:

$$\lg N_F = A - m \lg \sigma_a$$

For the energy model we have:

$$\lg N_F = A' - m' \lg W_a$$

m' is slope of fatigue curve expressed by energy.

2.2. Basquin curve

Stress-Life Diagram (S-N Diagram)

The basis of the Stress-Life method is the Wohler S-N diagram, shown schematically for two materials in Fig. 3. The S-N diagram plots nominal stress amplitude S versus cycles to failure N . There are numerous testing procedures to generate the required data for a proper S-N diagram. S-N test data are usually displayed on a log-log plot, with the actual S-N line representing the mean of the data from several tests.

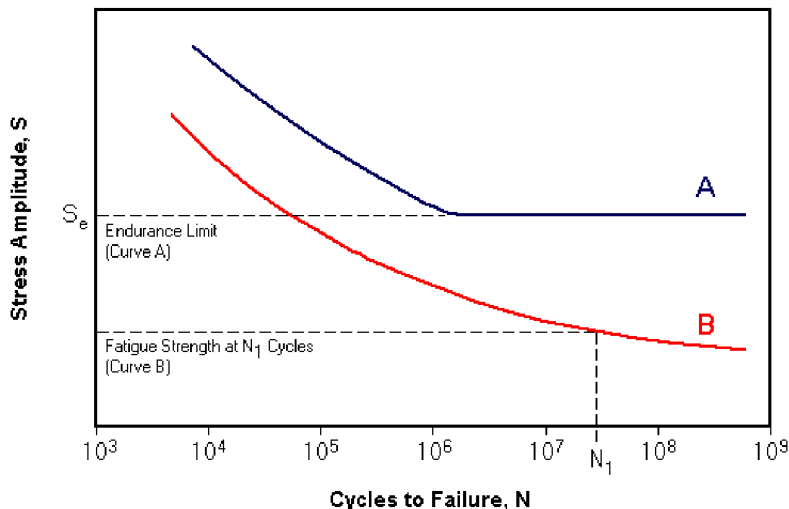


Fig. 3: Typical S-N curve.

Endurance Limit

Certain materials have a fatigue limit or endurance limit which represents a stress level below which the material does not fail and can be cycled infinitely. If the applied stress level is below the endurance limit of the material, the structure is said to have an infinite life. This is characteristic of steel and titanium in benign environmental conditions. A typical S-N curve corresponding to this type of material is shown Curve A in Fig. 3.

Many non-ferrous metals and alloys, such as aluminum, magnesium, and copper alloys, do not exhibit well-defined endurance limits. These materials instead display a continuously decreasing S-N response, similar to Curve B in Fig. 3. In such cases a fatigue strength S_f for a given number of cycles must be specified. An effective endurance limit for these materials is sometimes defined as the stress that causes failure at 1×10^8 or 5×10^8 loading cycles.

The concept of an endurance limit is used in infinite-life or safe stress designs. It is due to interstitial elements (such as carbon or nitrogen in iron) that pin dislocations, thus preventing the slip mechanism

that leads to the formation of microcracks. Care must be taken when using an endurance limit in design applications because it can disappear due to:

- Periodic overloads (unpin dislocations)
- Corrosive environments (due to fatigue corrosion interaction)
- High temperatures (mobilize dislocations)

The endurance limit is not a true property of a material, since other significant influences such as surface finish cannot be entirely eliminated. However, a test values (S'_e) obtained from polished specimens provide a baseline to which other factors can be applied. Influences that can affect the endurance limit include:

- Surface Finish
- Temperature
- Stress Concentration
- Notch Sensitivity
- Size
- Environment
- Reliability

Power Relationship

When plotted on a log-log scale, an S-N curve can be approximated by a straight line as shown in Fig. 4. Basquins equation is a power law relationship¹⁶ which describes the linear relationship between the applied stress cycles (S) in the y-axis and the number of cycles to failure in the x-axis plotted on a log-log scale.

$$N = BS^{\frac{1}{b}} \quad (16)$$

To calculate the slope of the Basquin equation, solve the system of equations:

$$N_1 = N_2 \left(\frac{S_1}{S_2} \right)^{\frac{1}{b}},$$

$$b = \frac{\log S_1 - \log S_2}{\log N_1 - \log N_2},$$

where b is the slope of the line.

$$B = N_1 S_1^{-\frac{1}{b}} = N_2 S_2^{-\frac{1}{b}}.$$

For the constant B, in industry the stress range value (from the maximum cyclic stress to the minimum cyclic stress) is often considered. If the stress values of the S-N curve are given as alternating stresses (which is the common practice), multiply these stresses by 2 to calculate the constant B (stress range = 2* alternating stress, assuming a zero mean stress and full reversal of the cyclic load). If the S-N curve data are given in stress range values, apply them directly in the equation for estimating the constant B.

The power relationship is only valid for fatigue lives that are on the design line. For ferrous metals this range is from 1×10^3 to 1×10^6 cycles. For non-ferrous metals, this range is from 1×10^3 to 5×10^8 cycles.

2.3. Calculation method without cycle counting

This part presents the existing method of prediction of lifetime, which does not need the algorithm of cycle counting. These kind of methods are still minority and usually more delicate to implement, but present the advantage of free the choice of variable of counting proved to be “dangerous”. The method presented here is the morel method which is based on stress.

Morel's method is based on a mesoscopic approach to critical plane type with the choice of plastic deformation as mesoscopic cumulative damage variable. Multiaxial and variable amplitude loading can be analyzed with this method.

Macroscopic quantities

Mesoscopic quantities

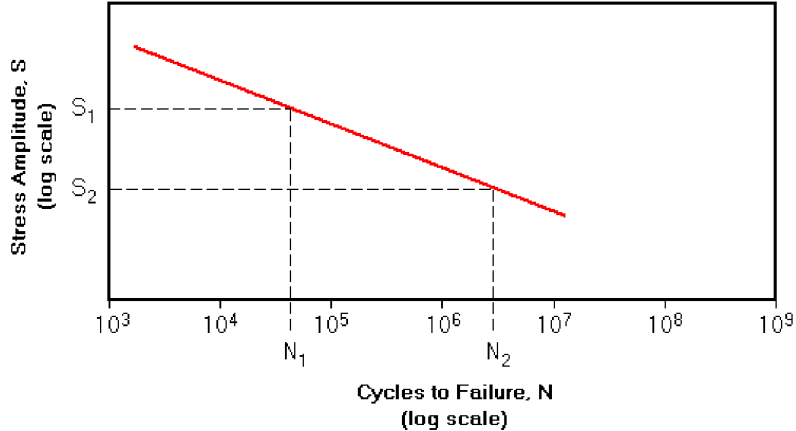


Fig. 4: Idealized S-N curve for high cycle fatigue.

Σ	macroscopic stress tensor
E	macroscopic strain tensor
C	macroscopic shear stress vector
T	macroscopic resolved shear stress vector acting on an easy glide direction
T_a	amplitude of the macroscopic resolved shear stress
P	macroscopic hydrostatic stress

Constant amplitude loading

Local stress estimation in high cycle fatigue

By assuming that only one glide system (defined by a normal vector \underline{n} to a plane and a vector (direction) \underline{M} within this plane) is active for every plastically deforming grain of the metal, Papadopoulos [9] established a macromeso passage for a glide system activated in a flowing crystal:

$$\underline{\tau} = \underline{T} - \mu \gamma^P \underline{m} \quad (17)$$

where $\underline{\tau}$ and \underline{T} are the mesoscopic and macroscopic resolved shear stresses acting along the slip direction \underline{m} and defined by:

$$\underline{\tau} = (\underline{m} \cdot \underline{\Sigma} \cdot \underline{n}) \underline{m} \quad (18)$$

$$\underline{T} = (\underline{m} \cdot \underline{\Sigma} \cdot \underline{n}) \underline{m} \quad (19)$$

γ^P is the plastic mesoscopic shear strain.

Initiation of slip in the crystal

The plasticity criterion is determined by Schmid's law with isotropic and kinematic hardening:

$$f(\underline{\tau}, \underline{b}, \tau_y) = (\underline{\tau} - \underline{b}) \cdot (\underline{\tau} - \underline{b}) - \tau_y^2 = 0 \quad (20)$$

where \underline{b} is the kinematical hardening parameter back stress.

In the description of his method, the author draws heavily on the work developed by Papadopoulos including the use of a measure of plastic deformation mesoscopic Cumulative T_σ associated with a particular material plane and modeling the behavior of grain in three distinct phases (hardening, saturation and softening); he considers the cumulative mesoscopic plastic deformation Γ as damage parameter and assumes that the initiation of a fatigue crack occurs when the latter reaches a critical value $D = D_R = \Gamma_R$ (Fig. 6).

Loading limit estimation

$\underline{\underline{\sigma}}$	mesoscopic stress tensor
$\underline{\underline{\varepsilon}}$	mesoscopic strain tensor
$\underline{\tau}$	mesoscopic resolved shear stress vector acting on an easy glide direction
γ^p	mesoscopic shear plastic strain
Γ	accumulated plastic mesostrain
T_σ	measure proportional to an upper bound of the plastic mesostrain accumulated on an elementary material plane Δ , also av
T_Σ	maximum value of T_σ
H	phase-difference coefficient

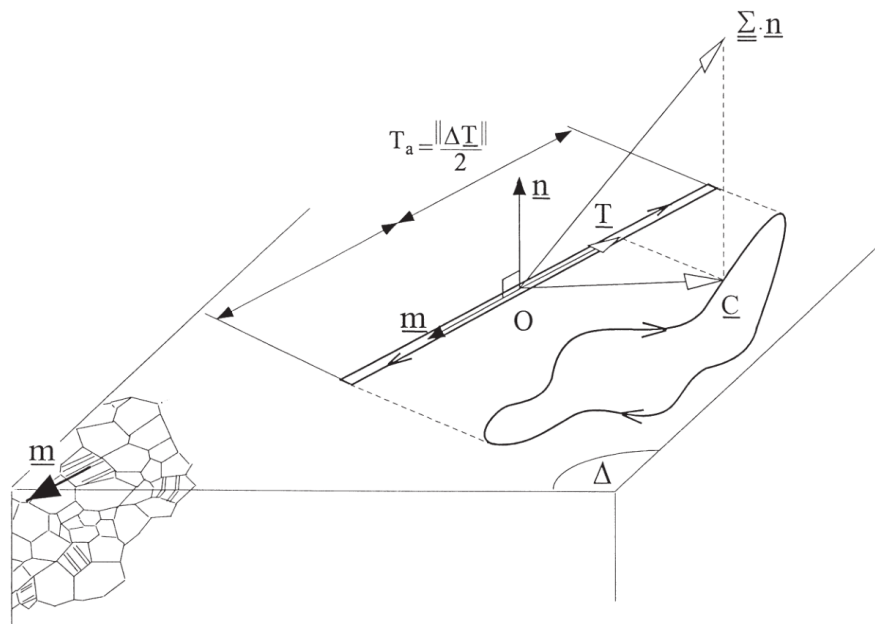


Fig. 5: Path of the macroscopic shear stress \underline{C} acting on a material plane Δ and the corresponding path of the macroscopic resolved shear stress \underline{T} acting on an easy glide direction.

The estimation of the yield limit in the saturation phase τ_s (defining the cyclic behavior of the crystal) is carried out by the definition of a limit loading.

$$T_{\Sigma lim} + \alpha P_{maxlim} = \beta \quad (21)$$

$$T_{\Sigma lim} = \frac{-\alpha P_m + \beta}{\alpha + \frac{T_\Sigma}{P_a}} \cdot \frac{T_\Sigma}{P_a} \quad (22)$$

Now we need to establish τ_{lim} . The corresponding actual amplitude of the shear stress, defined as half of the longest chord of the closed curve, is denoted as C_A .

$$H = \frac{T_\Sigma}{C_A} = \frac{T_{\Sigma lim}}{\tau_{lim}} \Rightarrow \tau_{lim} = \frac{T_{\Sigma lim}}{H} \quad (23)$$

where H constitutes a phase-difference coefficient. It is worth mentioning that the more open the elliptic path, the higher the coefficient H .

For a proportional loading, H is equal to $\sqrt{\pi}$. In the case of a particular circular path, H reaches the maximum value $\sqrt{2\pi}$ (Fig. 7).

Number of cycles to failure

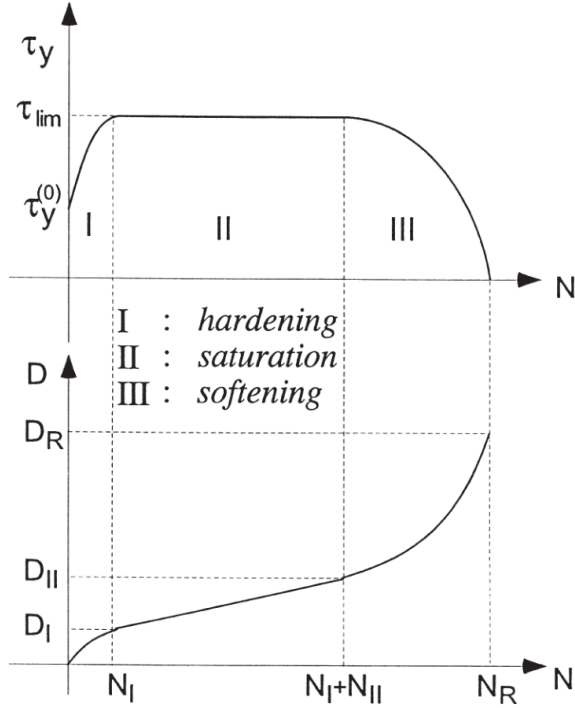


Fig. 6: Yield limit and damage evolutions in the three behavior phases (hardening, saturation and softening) when a cyclic loading is applied.

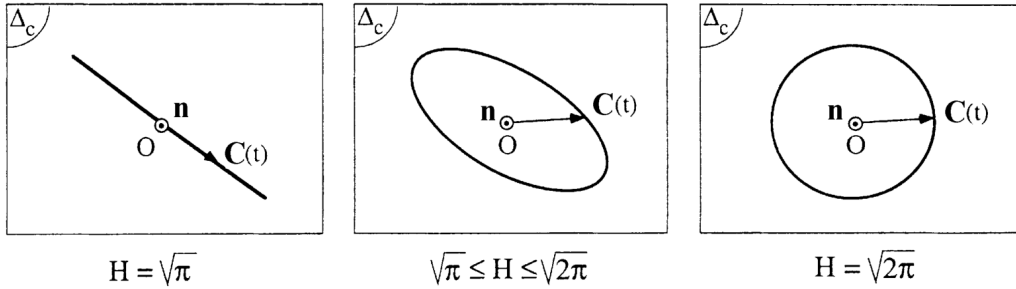


Fig. 7: Different paths and corresponding values of the phase-difference coefficient H .

Once the accumulated plastic mesostrain Γ along the particular gliding system reaches a critical value Γ_R , these grains are said to be broken. An analytical expression of the number of cycles to initiation (SN curve) can be achieved:

$$\Gamma = \Gamma_R \Rightarrow N_F = p \ln \left(\frac{C_A}{C_A - \tau_{lim}} \right) + q \left(\frac{\tau_{lim}}{C_A - \tau_{lim}} \right) - \frac{r}{C_A} \quad (24)$$

where p , q and r are functions of the hardening parameters of the three phases defined above.

From Eq.(22) and Eq.(23) we can find the yield point τ_s of the crystal in the saturation phase as a function of the amplitude P_a and the mean value P_m of the hydrostatic pressure, the phase difference coefficient H and two material related parameters α and β :

$$\tau_{lim} = \tau_s = \frac{-\alpha P_m + \beta}{\alpha \frac{P_a}{C_A} + H} \quad (25)$$

In the last relation Eq.(90), the detrimental effect of out-of-phase loading is introduced through τ_{lim} . As the coefficient H increases, τ_{lim} decreases, therefore N_F decreases which leads to more accumulated damage. The identification of the model parameters requires two endurance limits and a single SN curve (parameters p , q and r).

Variable amplitude loads

To determine the life time in the case of multiaxial variable amplitude loads, the author performs the following steps:

1. Identification of the critical plane Δ_c by maximizing the standard deviation of the macroscopic resolved shear stress in different directions. The author introduces a new parameter $T_{\sigma rms}$:

$$T_{\sigma rms}(\theta, \varphi) = \sqrt{\int_{\psi=0}^{2\pi} T_{rms}^2(\theta, \varphi, \psi) d\psi} \quad (26)$$

where $T_{rms}(\theta, \varphi, \psi)$ is the standard deviation of the macroscopic resolved shear stress.

2. Regarding the estimation of the phase difference coefficient H , it seems reasonable when the phase shift is not explicitly defined (or cannot be estimated) to use the most conservative value $\sqrt{2\pi}$.
3. On each direction (m) of the critical plane Δ_c :
 - (a) determination of the macroscopic changes in hydrostatic pressure $P(t)$ and the macroscopic resolved shear stress $T_a(t)$;
 - (b) evaluation of the saturation point by averaging the mesoscopic resolved shear stress thresholds calculated over the whole sequence, $\tau_s = (\tau_{lim})_{mean}$, τ_{lim} is calculated with Eq.(25);
 - (c) estimation of the cumulative mesoscopic plastic strain Γ by following the evolution of the mesoscopic yield stress σ_y according to the three phases (hardening, saturation and softening);
 - (d) calculating the number of sequences (associated with m direction) necessary to achieve Γ_R ;
4. For complex multiaxial loadings, the author assumes that the hardening and softening phases are small compared to the saturation phase[10]. In such a case, the yield limit remains constant for the whole lifetime and damage accumulation is purely linear. The analytical expression of the SN curve(Eq.(90)) becomes:

$$\Gamma = \Gamma_R \Rightarrow N_F = q \left(\frac{\tau_{lim}}{C_A - \tau_{lim}} \right) \quad (27)$$

where

$$q = \frac{c + \mu}{4} \frac{1}{l}$$

The final linear summation of individual damage from different critical planes would then lead to damage assessment:

$$\sum_i \frac{\Gamma^{(i)}}{\Gamma_R^{(i)}} = 1 \quad (28)$$

Experimental verification

In case of constant amplitude test

The author [11] consider the example of an out-of-phase bendingtorsion test on a high strength steel (30NCD16). The endurance limits of this material in reversed bending and torsion are, respectively, $f = 680MPa$ and $t = 426MPa$. The multiaxial sinusoidal loading is characterized by the amplitudes $\Sigma_{11a} = 600MPa$, $\Sigma_{12a} = 335MPa$ (no mean stresses) and the phase difference $\beta_{12} = 90^\circ$.

The maximum value of T_σ (denoted as T_Σ) can be deduced numerically. For this loading, we find $T_\Sigma = 697MPa$. On the critical material plane (where T_Σ is reached), C_A is estimated to be $282MPa$. The phase difference coefficient H is then simply deduced: $H = T_\Sigma/C_A = 2.47$.

Besides noting that $P_m = 0MPa$, $P_a = 200MPa$ and $a = 0.67$, $b = 775MPa$, $T_{\Sigma lim}$ is readily computed with the help Eq.(25): $T_{\Sigma lim} = 633MPa$. Finally, $\tau_{lim} = T_{\Sigma lim}/H = 256MPa$. Once p , q and r have been identified from a SN curve with the least squares line method, C_A and τ_{lim} can be introduced into Eq. (90) and the number of cycles to initiation can be finally calculated, i.e. $N_F = 210^5$ cycles.

In case of variable amplitude test

According to the previous endurance data and the definition of the generalized fatigue limit (for bending $\tau_{lim} = f/2$ and for torsion $\tau_{lim} = t$), one can estimate the parameter $q = 20800$.

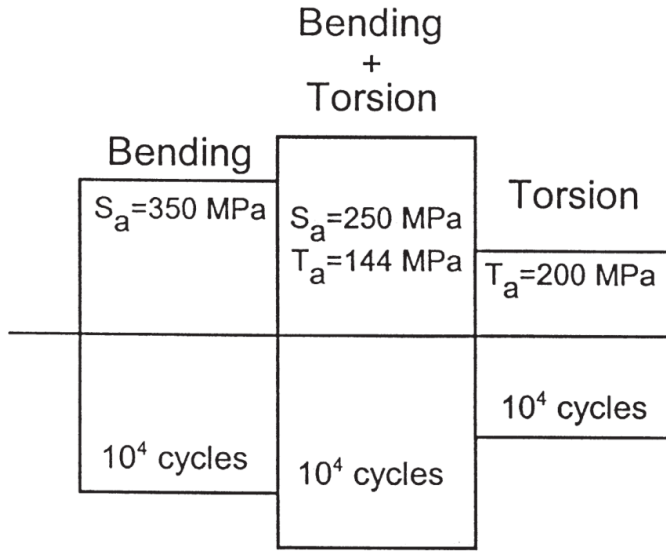


Fig. 8: block sequence tests (bending/bending+torsion/torsion) performed on a mild steel XC18.

Let us consider now a block sequence composed of 10^4 cycles of bending ($\Sigma_a = 350MPa$) followed by 10^4 cycles of combined in-phase bendingtorsion ($\Sigma_a, T_a = 250MPa, 144MPa$) followed by 10^4 cycles of torsion ($T_a = 200MPa$). This sequence is repeated until the initiation of a crack. The mean lifetime is found to be $N = 1.7310^5$.

The three generalized fatigue limits relative to the three blocks are estimated according to Eq.(25):

$$\tau_{lim}^{bending} = 155MPa$$

$$\tau_{lim}^{torsion} = 179MPa$$

$$\tau_{lim}^{bend+tors} = 157MPa$$

These three values and the parameter q are enough to accumulate the damage in the three blocks using Eq.(27):

$$\frac{\Gamma^{(bending)}}{\Gamma_R^{(bending)}} + \frac{\Gamma^{(bend+tors)}}{\Gamma_R^{(bend+tors)}} + \frac{\Gamma^{(torsion)}}{\Gamma_R^{(torsion)}} = 1$$

The corresponding number of cycles to initiation is: $N_{prediction} < 1.510^5$, that is to say five successive applications of the sequence. This prediction, close to the experimental result $N = 1.7310^5$, is a conservative one.

It is important to note that if only one critical plane (either from bending, torsion or bending+torsion loading) is used for damage accumulation, one-third of the damage would be calculated, resulting in a nonconservative prediction.

Morel's method is promising in its description aspect of limited endurance fatigue phenomenon, through the choice of the mesoscopic plastic deformation. By using cumulative plasticity, a fatigue mechanisms occurring at the mesoscopic scale takes into account the main factors affecting the lifetime cycle fatigue (hydrostatic pressure and influence of phase shift).

However, at the present stage, it does not completely meet the demand of a predictive tool. Indeed, it is a relatively complicated method (search critical plane Δ_c and accumulated damage in each direction in the plan); its application for multiaxial variable amplitude fatigue loads application data that are still not available (an S-N curve, two endurance limits and a particular damage accumulation test). In addition, it is limited to soft materials. On the other hand, it is not completely free of counting method because its author uses the counting of the extrema of the evolution to get the macroscopic resolved shear stress $T(t)$ and the corresponding amplitude P_a and mean values P_m of the hydrostatic stress in each direction (m) in Δ_c . With one purpose of calculating the limit of mesoscopic elasticity τ_{lim} in the saturation phase of the crystal. Again, this makes it difficult and daunting task.

3 Space gradient effects

The objective of the work is first to extend some classic high cycle fatigue (HCF) criteria (as Crossland, Dang Van, Papadopoulos, ...) in order to take into account a sensitivity of the criteria to stress spatial variations occurring at length scale l_g , and second to compare the performances of the extensions through several experimental fatigue tests. After an introduction of the basic criteria and their gradient based extensions proposed by Luu et al., we focus on the Crossland criterion and we propose a more practical and simple expression taking into account the gradient of the stress amplitude and the maximum hydrostatic stress. The generalization of the approach to other multiaxial fatigue criteria is also proposed. The proposition is then tested and applied to different simple situations such as 4-point bending and cantilever rotative bending. The relative errors between the exact solutions and the experimental data are estimated. Biaxial bending-torsion tests are also simulated to demonstrate the capabilities of the approach. In this work only stress gradient with a beneficial effect on fatigue have been considered.

3.1. Introduction

In several industries, the required design lifetime of many components often exceeds 10^8 cycles. This requirement is applicable to aircraft (gas turbine disks 10^{10} cycles), automobiles (car engine 10^8 cycles), and railways (high speed train 10^9 cycles). Although a large amount of fatigue data has been published in the form of S-N (where S is stress and N the number of cycles to fatigue) curves, the data in the literature have been usually limited to fatigue lives up to 10^7 cycles. Using traditional fatigue criteria, a near hyperbolic relationship between stress and fatigue life is assumed, with an asymptotic limit defined as the fatigue limit (or endurance stress). A large number of multiaxial fatigue criteria, generalizing this notion of fatigue limit, are available in the literature [3][4][12]. They are used to design industrial components against failure. Nevertheless, most of these criteria present some drawbacks, for instance when dealing with out-of-phase loading or with metals of different kinds from those used to develop the criteria. In fact, most of them are not designed to cope with high stress gradients such as those introduced by surface treatments or notches, or to handle scale effects as specially present in nano or micro components.

More precisely, as mentioned by Luu et al. [1], in problems related to small electronic components and electro-mechanical devices, at sufficiently small sizes, factors as size, gradient and loading effects affecting fatigue limits are not captured by classical fatigue criteria. In particular, for the same in-state stress distribution as well as nominal maximum stress and material, the smaller the sample size is, the smaller the surface or the volume of the most stressed zone is, the higher the fatigue limit is. Moreover, the nominal fatigue limit increases in the presence of stress gradient corresponding to a decreasing stress from the surface. Experimental example illustrates and makes clearer "beneficial gradient effect" [13]. The results of the constant moment tests on specimens of the same radius but different lengths shows that the gradient effect is an order of magnitude higher than the pure size effect. In this case, size effect is proved insignificant compared to the gradient effect at the considered scale.

From above it is concluded that the stress gradient factor is the most important contributer to this phenomenon. Fatigue criteria have been generalized by several authors by including a gradient dependence [13] in order to introduce a sensitivity of the endurance limit to space variations occurring at length scale l_g . Uniaxial normal cyclic stress states with non-zero and zero normal stress gradients, respectively, give some indication about the normal stress gradient effect. The larger the normal stress due to bending, the larger the difference between bending test points and tension-compression ellipse arc (as is shown in Fig. 9).

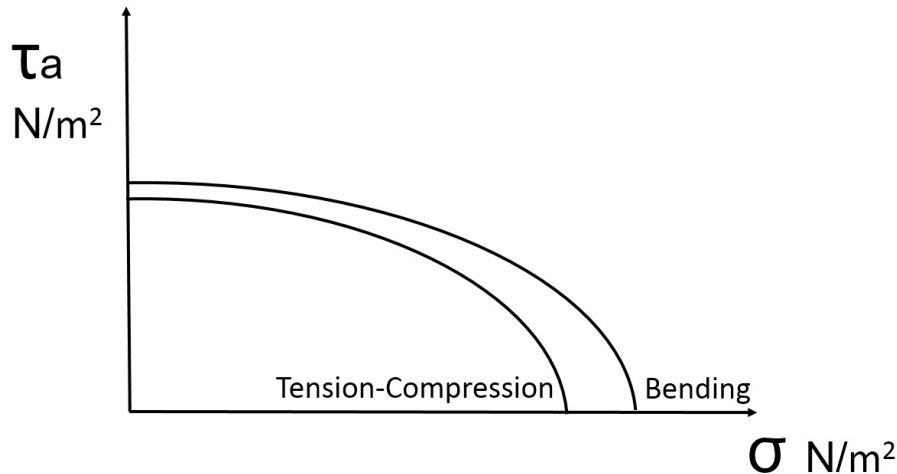


Fig. 9: Schematic representation of the nominal fatigue limit (ellipse arc) for two different tests: the arc is larger in the case of bending-torsion (presence of stress gradient) than in tension-compression.

Apart from gradient approaches[14][13], to take account of these effect, others approaches such critical volume [15], critical distance[16][17], critical layer[18], averaging over a specific volume [19][20] are used. In fact, all the approaches are equivalent to introducing a length scale. In the paper, we consider specifically the gradient approach. We start from the proposition of Luu et al., and propose a simpler way to account for the gradient. The Crossland criterion, one of the most widely known HCF criteria, is used to illustrate the approach. Crossland proposed that the second invariant of the deviatoric stress tensor and the hydrostatic stress are the variables governing the endurance limit. The new proposition adds two gradient terms ; it is then calibrated and its predictions are compared to experimental results to check its relevancy.

3.2. A first gradient approach [1]

3.2.1. General formulation

Luu et al. [1] proposed extensions of classical HCF fatigue criteria using the gradients of the shear and normal stress to account for the gradient effect. In the case of critical plane type criteria, they defined a generalized shear stress amplitude including shear stress gradient and a generalized maximum normal (or hydrostatic) stress. A general form of classical fatigue limit criteria can be written as follows:

$$f(C_a(n^*), N_{max}(n^*)) = C_a(n^*) + aN_{max}(n^*) - b \geq 0, \quad (29)$$

with a, b being two material parameters. f is a function, chosen in many cases as linear, and n^* is the normal vector of the critical plane; $C_a(n^*), N_{max}(n^*)$ are respectively the amplitude of shear stress and the maximum value of the normal stress on the critical plane.

A new class of fatigue criteria extended from classical ones with stress gradient terms introducing not only in the normal stress but also in the shear stress components, was proposed. It concerns only free defect materials and can model both phenomena “smaller is Stronger and Higher Gradient is Stronger”.

Besides the stress gradient term appearing in the normal stress part in form of $G = \Delta(\sigma_{11} + \sigma_{22} + \sigma_{33})$, another gradient term, the gradient of the stress tensor amplitude (or alternatively of deviatoric stress tensor

amplitude) $\| Y_a \| = \Delta\sigma_a$ is added to the shear stress amplitude part. Basing on all these analyses a new form of fatigue criteria taking into account gradient effects, is proposed:

$$f(\widetilde{C}_a(n^*), \widetilde{N}_{max}(n^*)) = \widetilde{C}_a(n^*) + a\widetilde{N}_{max}(n^*) - b \geq 0, \quad (30)$$

where $\widetilde{C}_a(n^*)$ and $\widetilde{N}_{max}(n^*)$ are extended definitions of the amplitude of shear stress and of the normal stress taking into account the presence of local gradient.

In the following we first focus on the Crossland criterion and its extension.

3.2.2. Recall of the classical Crossland criterion

The classical Crossland criterion defines the fatigue limit of metallic specimens subjected to multi-axial cyclic stress[2] by :

$$f(\sqrt{J_{2,a}}, \sigma_{H,max}) = \sqrt{J_{2,a}} + a\sigma_{H,max} - b \leq 0 \quad (31)$$

where $\sqrt{J_{2,a}}$ measures the amplitude of variation of the second invariant of the deviatoric stress and $\sigma_{H,max}$ is the maximum hydrostatic stress observed during a loading cycle. The parameters a and b are material constants to be calibrated experimentally. The amplitude of the square root of the second invariant of the stress deviator can be defined, in general case, as the half-length of the longest chord of the deviatoric stress path or as the radius of the smallest hypersphere circumscribing the stress deviator loading path [3]

$$\sqrt{J_{2,a}} = \frac{1}{2\sqrt{2}} \min_{\underline{S}_1} \left\{ \max_t \sqrt{(\underline{S}(t) - \underline{\underline{S}}_1) : (\underline{S}(t) - \underline{\underline{S}}_1)} \right\}. \quad (32)$$

The deviatoric stress \underline{S} associated with a stress tensor $\underline{\underline{\sigma}}$ is defined by

$$\underline{S} = \underline{\underline{\sigma}} - \frac{1}{3} \text{tr} \underline{\underline{\sigma}} \underline{I} \quad (33)$$

where $\text{tr} \underline{\underline{\sigma}}$ is the trace of the stress tensor $\underline{\underline{\sigma}}$ and \underline{I} the second order unit tensor.

The maximum value that the hydrostatic stress reaches during the loading cycle is on the other hand:

$$\sigma_{H,max} = \max_t \left\{ \frac{1}{3} \text{tr}(\underline{\underline{\sigma}}(t)) \right\}. \quad (34)$$

For a proportional cyclic loading, if one introduces the two extreme stress tensors $\underline{\underline{\sigma}}^A$ and $\underline{\underline{\sigma}}^B$ observed during the loading path, together with the stress range

$$\Delta\underline{\underline{\sigma}} = \underline{\underline{\sigma}}^B - \underline{\underline{\sigma}}^A \quad (35)$$

and its deviatoric part $\Delta\underline{S}$, the variation of the second invariant of the stress deviator reduces to

$$\sqrt{J_{2,a}} = \frac{1}{2} \max_t \sqrt{\frac{1}{2} \Delta\underline{S} : \Delta\underline{S}} = \frac{1}{2} \max_t \sqrt{\frac{1}{2} (\Delta s_{11}^2 + \Delta s_{22}^2 + \Delta s_{33}^2 + 2\Delta s_{12}^2 + 2\Delta s_{13}^2 + 2\Delta s_{23}^2)}. \quad (36)$$

The material constants a and b can be related to the limit t_{-1} of endurance in alternate torsion and to the limit s_{-1} of endurance in alternate tension-compression by

$$a = \frac{3t_{-1}}{s_{-1}} - \sqrt{3}, \quad b = t_{-1}. \quad (37)$$

3.2.3. Formulation of Crossland criterion with gradient effect

In particular, using as a basis the classical Crossland criterion Eq.(31) and the general framework for the development of a gradient dependent fatigue limit criterion Eq.(30), a new version can be written in the form:

$$\sqrt{J_{2,a}} + a\widetilde{\sigma_{H,max}} \leq b. \quad (38)$$

This formula takes into account the indicator of the influence of the gradient of the stress deviator which reflects the spatial non-uniform distribution of stress state.

In practice, [1] had proposed:

$$\sqrt{J_{2,a}} \sqrt{1 - \left(l_\tau \frac{\| \underline{\underline{Y}} \|_a}{\| \underline{\underline{S}} \|_a} \right)^{n_\tau}} + a\sigma_{H,max} \left(1 - \left(l_\sigma \frac{\| G \|}{\sigma_{H,max}} \right)^{n_\sigma} \right) - b < 0. \quad (39)$$

Here $\| \underline{\underline{Y}} \|_a$ is the full stress gradient and $\| G \|$ is used as an indicator of the influence of the normal stresses gradient.

$$\| G \| = \| \nabla \sigma_{H,max} \| = \sqrt{\left(\frac{\partial \sigma_{H,max}}{\partial x} \right)^2 + \left(\frac{\partial \sigma_{H,max}}{\partial y} \right)^2 + \left(\frac{\partial \sigma_{H,max}}{\partial z} \right)^2}. \quad (40)$$

3.3. Optimized Crossland Criterion formulation

The precedent Luu and al. formula has six materials parameters $a, b, l_\tau, l_\sigma, n_\tau, n_\sigma$ to be identified experimentally. The calibration can be complicated ; it does not lead to a unique set of parameters. Physical considerations, such as the length scales, have to be taken into account for choosing the optimized material constants. For practical application in an industrial context, it is essential to reduce the number of parameters. We therefore wish to investigate a simpler construction, departing from the classical Crossland criterion.

Surfaces with stresses decreasing in depth are, here and after, considered. Failure occurs at the point x_0 when, $(\sqrt{J_{2,a}} + a\sigma_{H,max} - b)(x_0) \geq 0$. To be more general and avoid singularity, this condition should be satisfied in some x_0 neighboring volume of size l_g , leading to a criterion given by:

$$\inf_{\substack{x \in B(x_0, l_g)}} (\sqrt{J_{2,a}} + a\sigma_{H,max} - b)(x) \geq 0. \quad (41)$$

To obtain a suitable expression, an expansion of Eq.(41) is performed in the neighborhood of x_0 . The sought formula should account for the beneficial effect of the stress gradient. Considering that the stress is decreasing in depth, a negative sign is associated with the norm of the gradient of stress tensor in to the proposed formula. In addition, the gradient term should not only affect hydrostatic stress but also shear stress.

An objective formulation based on the lowest possible value of $\sqrt{J_{2,a}}$ and of $\sigma_{H,max}$ in the neighborhood, is finally:

$$\sqrt{J_{2,a}} + a\sigma_{H,max} - l_g \| \nabla \sqrt{J_{2,a}} + a\nabla \sigma_{H,max} \| \leq b, \quad (42)$$

We keep the same material parameters a and b as before. l_g is a characteristic length to be optimized to match the experimental results. The approach has only one supplementary material constant whose calibration is easy.

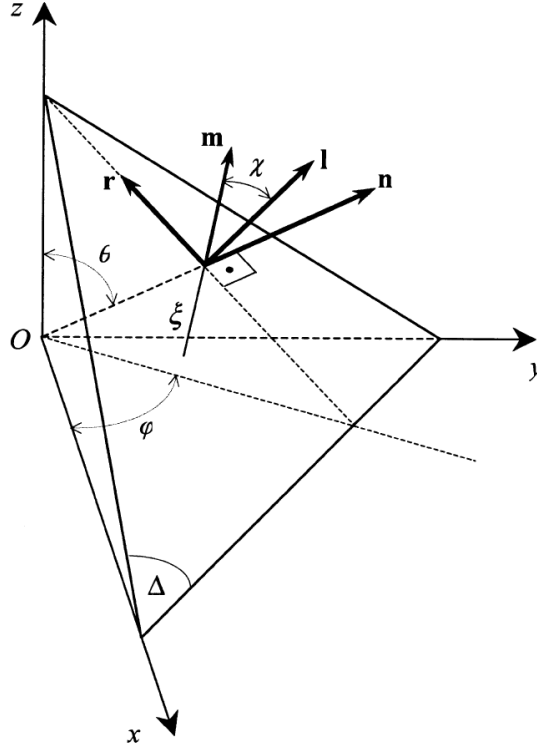


Fig. 10: Material plane Δ passing through point O of a body and its associated (n, l, r) frame.

3.4. Optimized Papadopoulos Criterion formulation

Papadopoulos[5] proposes to opt for a mean value of the accumulated plastic strain on all possible slip systems of representative elementary volume(REV). So he chose to use a average value of accumulated plastic deformation rather than looking at failure of a single crystal. A spherical coordinate system(Fig. 10) to guide the vector of normal in material plane, and the unit orientation vector r linked to a sliding direction of this plan is used to conduct the integration over all possible orientations.

At any point O of a body, a material plane Δ can be defined by its unit normal vector n . This vector n makes an angle θ with the z-axis of a $Oxyz$ frame attached to the body, and its projection on the xy plane makes an angle φ with axis x . For each plane Δ a new quantity is introduced as the quadratic mean value, over all the sliding directions of the considered plane, of the resolved shear stress amplitude and denoted as T_a . This shear stress quantity was first introduced in Papadopoulos [6] and was subsequently used by other researchers. The critical plane according to our proposal is that onto which $T_a(\varphi, \theta)$ achieves its maximum value. The fatigue limit criterion is written as:

$$\max T_a + \alpha_\infty \sigma_{h,max} \leq \gamma_\infty \quad (43)$$

where α_∞ and γ_∞ are material parameters to be determined[6].

$$\sigma_{h,max} = \max_t \left\{ \frac{1}{3} \operatorname{tr}(\underline{\underline{\sigma}}(t)) \right\}$$

The construction of T_a is based on the calculation of a local shear stress τ :

$$\begin{aligned} \tau = & [\sin\theta \cos\varphi \sigma_{xx} + \sin\theta \sin\varphi \sigma_{xy} + \cos\theta \sigma_{xz}](-\sin\varphi \cos\chi - \cos\theta \cos\varphi \sin\chi) + \\ & [\sin\theta \cos\varphi \sigma_{xy} + \sin\theta \sin\varphi \sigma_{yy} + \cos\theta \sigma_{yz}](\cos\varphi \cos\chi - \cos\theta \sin\varphi \sin\chi) + \\ & [\sin\theta \cos\varphi \sigma_{xz} + \sin\theta \sin\varphi \sigma_{yz} + \cos\theta \sigma_{zz}] \sin\theta \sin\chi \end{aligned} \quad (44)$$

It is clear that this shear stress is a function of φ , θ , χ and of time t in the case of variable loading, i.e. $\tau = \tau(\varphi, \theta, \chi, t)$. Upon fixing a pair of angles (φ, θ) (i.e. a plane Δ) and an angle χ (i.e. a line ξ on Δ), one can define the amplitude of the resolved shear stress τ_a , acting on Δ along ξ by the formula:

$$\tau_a(\varphi, \theta, \chi) = \frac{1}{2} [\max_{t \in P} \tau_a(\varphi, \theta, \chi, t) - \min_{t \in P} \tau_a(\varphi, \theta, \chi, t)] \quad (45)$$

Now, for a given plane Δ , i.e. for a fixed pair of angles (φ, θ) , the generalized shear stress amplitude T_a is defined as the L^2 average in the plane Δ of the amplitude of resolved shear stress:

$$T_a(\varphi, \theta) = 2 \sqrt{\frac{1}{\pi} \int_{x=0}^{\frac{\pi}{2}} \tau_a^2(\varphi, \theta, \chi) d\chi} \quad (46)$$

We note the fatigue limit in fully reversed torsion t_{-1} and the fatigue limit in fully reversed bending f_{-1} . From these two tests we get the parameters:

$$\begin{aligned} \gamma_{\infty} &= t_{-1}, \\ \alpha_{\infty} &= 3 \left(\frac{t_{-1}}{f_{-1}} - \frac{1}{2} \right). \end{aligned}$$

The Papadopoulos fatigue limit criterion achieves the form:

$$\max T_a + 3(t_{-1}/f_{-1} - 1/2) \sigma_{h,max} \leq t_{-1}. \quad (47)$$

Now, the Papadopoulos Criterion can be simply extended to cases with gradient effects by

$$\max T_a + \alpha_{\infty} \sigma_{H,max} - l_g \|\nabla \max T_a + \alpha_{\infty} \nabla \sigma_{H,max}\| \leq \gamma_{\infty}. \quad (48)$$

3.5. Optimized Dang Van Criterion formulation

The Dang Van criterion as presented in [4] is expressed as:

$$\max_{\vec{n}} \left\{ \max_t \{ \tau(\vec{n}, t) + a_D \sigma_H(t) \} \right\} \leq b_D. \quad (49)$$

Here, τ denotes the mesoscopic shear stress and is obtained from a mesoscopic stress tensor $\hat{\sigma}$ defined by:

$$\hat{\sigma}(t) = (\sigma(t) - s^*),$$

where s^* is the center of the smallest hypersphere circumscribed to the loading path in deviatoric stress space. It is obtained by solving a “min-max” problem as follows:

$$s^* = \arg \min_{s_1} \left\{ \max_t \|s(t) - s_1\| \right\}.$$

In the case of fully reversed loading, the values $s^* = 0$ can be directly deduced without solving the “min-max problem” as in general case.

The principal stress values of stress tensor $\tilde{\sigma}$ being denoted by $\hat{\sigma}_{III}(t) \leq \hat{\sigma}_{II}(t) \leq \hat{\sigma}_I(t)$, one gets the amplitude of shear stress by:

$$\tau(t) = \frac{1}{2} (\hat{\sigma}_I(t) - \hat{\sigma}_{III}(t)).$$

Moreover, $\sigma_H(t)$ denotes the hydrostatic stress as a function of the time. The material characteristic parameters a_D and b_D are finally given from traction compression and torsion fatigue limites by :

$$a_D = \frac{3t_{-1}}{s_{-1}} - \frac{3}{2};$$

$$b_D = t_{-1}.$$

Now, the Dang Van criterion can be extended to a graident dependent criterion by

$$\max_t \{ \tau(t) + a_D \sigma_H(t) \} - l_g \|\max_t \{ \nabla \tau(t) + a_D \nabla \sigma_H(t) \} \| \leq b_D. \quad (50)$$

3.6. Calibration of the criteria

In this section, two different uniaxial fatigue tests with stress gradient effects are used to calibrate the optimized gradient Crossland, Papadopoulos and DangVan criteria. An application to a biaxial test fatigue test shows the ability of the proposed approach to account for stress gradient in multiaxial cases.

3.6.1. Fully reversed 4-point bending and rotating cantilever bending fatigue tests

With Crossland criterion The model of 4-point bending is first considered. The bar made of steel has both ends fixed. The radius R is a variable ranging from 1mm to 30mm in order to challenge the fact "the smaller, the stronger". The length L of the bar is 100 mm.

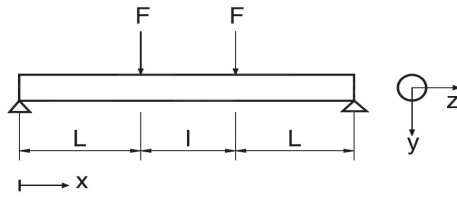


Fig. 11: 4-point bending test [13]

The bending moment is the same in the interval $L \leq x \leq L + l$ and equal to $M = FL$ (Fig. 11). For $L \leq x \leq L + l$ and $-R \leq y \leq R$, the bending stress σ is

$$\underline{\underline{\sigma}} = \sigma_{xx} \sin(wt) e_x \otimes e_x = \frac{FLy}{I} \sin(wt) e_x \otimes e_x \quad (51)$$

with $I = \pi R^4/4$. The maximum stress during the cyclic loading in the bar is thus $\sigma_{max} = \frac{FLy}{I}$, while the macroscopic stress range is $\Delta\underline{\underline{\sigma}}(t) = 2\sigma_{max} e_x \otimes e_x$, and the hydrostatics stress takes the value

$$\sigma_{H,max} = \max_t \left\{ \frac{1}{3} \text{tr}(\sigma(t)) \right\} = \frac{1}{3} \sigma_{max} = \frac{FLy}{3I}. \quad (52)$$

From the value of the deviatoric stress

$$\Delta\underline{\underline{\sigma}} = \underline{\underline{\sigma}} - \frac{1}{3} \text{tr}(\underline{\underline{\sigma}}) I = \begin{pmatrix} \frac{4}{3} \sigma_{max} & 0 & 0 \\ 0 & -\frac{2}{3} \sigma_{max} & 0 \\ 0 & 0 & -\frac{2}{3} \sigma_{max} \end{pmatrix}, \quad (53)$$

we can compute the second invariant of the stress deviator :

$$\sqrt{J_{2,a}} = \frac{1}{2\sqrt{2}} \sqrt{\Delta\underline{\underline{\sigma}} : \Delta\underline{\underline{\sigma}}} = \frac{\sigma_{max}}{\sqrt{3}} = \frac{FLy}{\sqrt{3}I}. \quad (54)$$

Then the gradient part is given by:

$$\nabla \sqrt{J_{2,a}} = \frac{\partial \sqrt{J_{2,a}}}{\partial x} e_x + \frac{\partial \sqrt{J_{2,a}}}{\partial y} e_y + \frac{\partial \sqrt{J_{2,a}}}{\partial z} e_z = \left(0, \frac{FL}{\sqrt{3}I}, 0 \right), \quad (55)$$

and

$$\nabla \sigma_{H,max} = \left(0, \frac{FL}{3I}, 0 \right). \quad (56)$$

The parameters a and b of the standard Crossland criterion, are obtained from fully reversed tension-compression fatigue limit s_{-1} and torsion fatigue limit t_{-1} using Eq.(37).

From Eq.(31), standard Crossland criterion without gradient effect (for radius R) is:

$$\sqrt{J_{2,a}} + a\sigma_{H,max} = \frac{FLR}{\sqrt{3}I} + \frac{aFLR}{3I} \leq b. \quad (57)$$

The gradient term here is given by:

$$\| \nabla \sqrt{J_{2,a}} + a\nabla\sigma_{H,max} \| = \frac{FL}{\sqrt{3}I} + \frac{aFL}{3I}. \quad (58)$$

By comparison we can see in 4-point bending test the difference between classical and modified Crossland criterion corresponds to the product of the characteristic length l_g by the term (58) associated to the decrease of the stress in depth. This value shows how much the modification affects the Crossland criterion. Crossland criterion with beneficial gradient term as shown in Eq.(42) is given by:

$$\begin{aligned} \sqrt{J_{2,a}} + a\sigma_{H,max} - l_g(\| \nabla \sqrt{J_{2,a}} + a\nabla\sigma_{H,max} \|) &= \\ \frac{FLR}{\sqrt{3}I} + \frac{aFLR}{3I} - l_g \left(\frac{FL}{\sqrt{3}I} + \frac{aFL}{3I} \right) &= \\ \frac{1}{\sqrt{3}}\sigma_{max} + \frac{a}{3}\sigma_{max} - l_g \left(\frac{1}{\sqrt{3}R}\sigma_{max} + \frac{a}{3R}\sigma_{max} \right) &\leq b, \end{aligned} \quad (59)$$

which is to say:

$$\sigma_{max} \leq \frac{b}{\frac{1}{\sqrt{3}} + \frac{a}{3} - l_g \left(\frac{1}{\sqrt{3}R} + \frac{a}{3R} \right)}. \quad (60)$$

The material parameters a and b are obtained using their classical expressions as Eq.(37) from tests free of stress gradient. The corresponding fatigue limit are denoted s_{ref} for the alternate tension-compression test, and $t_{ref} = b$ for the alternate torsion test. For a specimen of radius R the alternate bending fatigue limit is denoted $f_c(R)$. We can observe that:

$$f_c(R) = \frac{b}{\frac{1}{\sqrt{3}} + \frac{a}{3} - l_g \left(\frac{1}{\sqrt{3}R} + \frac{a}{3R} \right)} \geq s_{ref} = \frac{b}{\frac{1}{\sqrt{3}} + \frac{a}{3}}, \quad (61)$$

and that $f_c(R)$ tends to s_{ref} for large values of R .

With Papadopoulos criterion From 51, the resolved shear stress τ acting along a line ξ of a plane Δ is given by Eq.44, which in this case leads to:

$$\tau(\varphi, \theta, \chi, t) = \sigma_{xx} \sin(2\pi t/P) \sin\theta \cos\theta \sin\chi. \quad (62)$$

Clearly, for the worse case in χ , the resolved shear stress amplitude is equal to:

$$\tau_a(\varphi, \theta, \chi) = \sigma_{xx} |\sin\theta \cos\theta \sin\chi|. \quad (63)$$

The generalized shear stress amplitude T_a becomes:

$$T_a(\varphi, \theta) = 2 \sqrt{\frac{1}{\pi} \int_{\chi=0}^{\frac{\pi}{2}} (\sigma_{xx} |\sin\theta \cos\theta \sin\chi|)^2 d\chi} \quad (64)$$

The maximum value of T_a is obtained at $(\theta = \pi/4)$ and at $(\theta = 3\pi/4)$. It is equal to:

$$\max T_a = \sigma_{xx}/2 \quad (65)$$

The hydrostatic stress is given by:

$$\sigma_H(t) = \frac{1}{3} \sigma_{xx} \sin(2\pi t/P) \quad (66)$$

The maximum value of σ_H reached in a loading cycle is:

$$\sigma_{H,max} = \sigma_{xx}/3 \quad (67)$$

Papadopoulos criterion with beneficial gradient term as shown in Eq.(48) is then given by:

$$\begin{aligned} \max T_a + \alpha_\infty \sigma_{H,max} - l_g \parallel \nabla \max T_a + \alpha_\infty \sigma_{H,max} \parallel = \\ \frac{FLR}{2I} + \frac{\alpha_\infty FLR}{3I} - l_g \left(\frac{FL}{2I} + \frac{\alpha_\infty FL}{3I} \right) = \\ \frac{1}{2} \sigma_{max} + \frac{a}{3} \sigma_{max} - l_g \left(\frac{1}{2R} \sigma_{max} + \frac{a}{3R} \sigma_{max} \right) \leq \gamma_\infty = t_{ref}, \end{aligned} \quad (68)$$

which is to say:

$$\sigma_{max} \leq \frac{\gamma_\infty}{\frac{1}{2} + \frac{\alpha_\infty}{3} - l_g \left(\frac{1}{2R} + \frac{\alpha_\infty}{3R} \right)}. \quad (69)$$

For a specimen of radius R the alternate bending fatigue limit is denoted $f_p(R)$. We can observe that:

$$f_p(R) = \frac{\gamma_\infty}{\frac{1}{2} + \frac{\alpha_\infty}{3} - l_g \left(\frac{1}{2R} + \frac{\alpha_\infty}{3R} \right)} \geq s_{ref} = \frac{\gamma_\infty}{\frac{1}{2} + \frac{\alpha_\infty}{3}}. \quad (70)$$

With Dang Van criterion Under fully reversed loading we have:

$$\tau(t) = \frac{1}{2} (\sigma_{xx}(t) - 0)$$

From Eq.(50) we can deduce Dang Van criterion.

$$\begin{aligned} \max_t \{ \tau(t) + a_D \sigma_H(t) \} - l_g \parallel \nabla \tau(t) + a_D \nabla \sigma_H(t) \parallel = \\ \frac{FLR}{2I} + \frac{aFLR}{3I} - l_g \left(\frac{FL}{2I} + \frac{aFL}{3I} \right) = \\ \frac{1}{2} \sigma_{max} + \frac{a}{3} \sigma_{max} - l_g \left(\frac{1}{2R} \sigma_{max} + \frac{a}{3R} \sigma_{max} \right) \leq b_D = t_{ref}, \end{aligned} \quad (71)$$

which is to say:

$$\sigma_{max} \leq \frac{b}{\frac{1}{2} + \frac{a}{3} - l_g \left(\frac{1}{2R} + \frac{a}{3R} \right)}. \quad (72)$$

We can observe that the corresponding bending limit is thus

$$f_D(R) = \frac{b}{\frac{1}{2} + \frac{a}{3} - l_g \left(\frac{1}{2R} + \frac{a}{3R} \right)} \geq s_{ref} = \frac{b}{\frac{1}{2} + \frac{a}{3}}.$$

Comparison with experimental data The case of cantilever fully reversed bending corresponds to the four point bending test except that there, the bending moment is function of x . Thus, the maximum stress σ_{max} for a given section is a function of x . But, the y dimension of the beam is much smaller than its x dimension, which allows us to neglect gradients in x . All expressions of the four point bending case thus apply to this case.

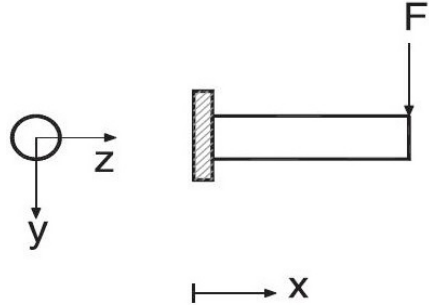


Fig. 12: Cantilever bending test [21]

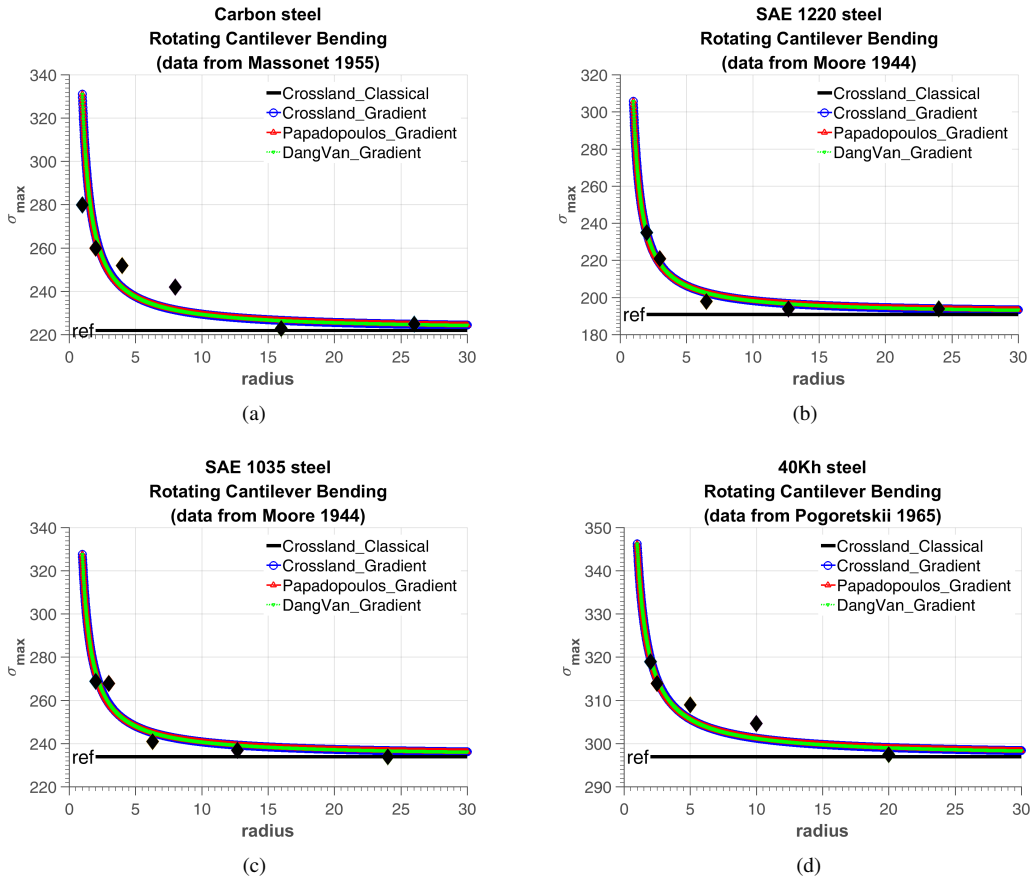


Fig. 13: Fatigue limits with gradient effect for different radii.

Eq.(61) with a et b calibrated from given S_{ref} and t_{ref} is used to estimate the characteristic length l_g in order to give the best correlation between simulated and experimental fatigue limit obtained in rotating cantilever bending tests for different materials and radii. The results are sketched in Fig.(13) and the

corresponding parameters are shown in Table.1.

Table 1: Length scales of different materials

	1220 steel	Carbon steel	1035 steel	40Kh steel
S_{ref} [MPa]	191	222	234	297
t_{ref} [MPa]	143	151	172	180
l_g [mm]	0.3755	0.3297	0.2861	0.1424

We can observe a very interesting phenomenon that the smaller fatigue limit is, the larger influence of gradient effect is.

3.6.2. Bending-torsion fatigue tests

With Crossland criterion The bending moment is a linear function of x , $M_b = -F(L-x)$. The twisting moment is denoted M_t . The stress σ_{xx} now varies along the depth (i.e. y-axis) and the length (i.e. x-axis) of the specimen, but as above we will neglect the gradient in x as compared to the gradient in y . The bending stress is given here by :

$$\sigma_a = \frac{-F(L-x)}{I} R = \frac{M_b}{I} y \quad \text{with} \quad I = \frac{\pi R^4}{4}, \quad (73)$$

while the twisting shear stress is given by $\tau_a = \frac{M_t}{J} y \quad \text{with} \quad J = \frac{\pi R^4}{2}$. The stress tensor $\underline{\underline{\sigma}}$ is then:

$$\underline{\underline{\sigma}}(t) = \begin{pmatrix} \sigma_a \sin(\omega t) & \tau_a \sin(\omega t) & 0 \\ \tau_a \sin(\omega t) & 0 & 0 \\ 0 & 0 & 0 \end{pmatrix}. \quad (74)$$

Its range tensor is:

$$\Delta \underline{\underline{\sigma}} = \begin{pmatrix} 2\sigma_a & 2\tau_a & 0 \\ 2\tau_a & 0 & 0 \\ 0 & 0 & 0 \end{pmatrix}, \quad (75)$$

with deviator

$$\underline{\underline{\Delta S}} = \Delta \underline{\underline{\sigma}} - \frac{1}{3} \text{tr} \Delta \underline{\underline{\sigma}} = \begin{pmatrix} \frac{4}{3}\sigma_a & 2\tau_a & 0 \\ 2\tau_a & -\frac{2}{3}\sigma_a & 0 \\ 0 & 0 & -\frac{2}{3}\sigma_a \end{pmatrix}. \quad (76)$$

The second invariant of the stress deviator is then:

$$\sqrt{J_{2,a}} = \frac{1}{2\sqrt{2}} \sqrt{\underline{\underline{\Delta S}} : \underline{\underline{\Delta S}}} = \sqrt{\frac{1}{3}\sigma_a^2 + \tau_a^2} = \sqrt{\frac{M_b^2}{3I^2} + \frac{M_t^2}{J^2}} y. \quad (77)$$

As for the hydrostatics stress, we have

$$\sigma_{H,max} = \max_t \left\{ \frac{1}{3} \text{tr}(\underline{\underline{\sigma}}(t)) \right\} = \frac{\sigma_a}{3} = \frac{M_b}{3I} y. \quad (78)$$

Then the gradient part has the value:

$$\begin{aligned}\nabla \sqrt{J_{2,a}} &= \frac{\partial \sqrt{J_{2,a}}}{\partial x} \underline{e}_x + \frac{\partial \sqrt{J_{2,a}}}{\partial y} \underline{e}_y + \frac{\partial \sqrt{J_{2,a}}}{\partial z} \underline{e}_z = \left(0, \sqrt{\frac{M_b^2}{3I^2} + \frac{M_t^2}{J^2}}, 0 \right) \\ &= \left(0, \frac{\sqrt{\frac{1}{3}\sigma_a^2 + \tau_a^2}}{y}, 0 \right),\end{aligned}\quad (79)$$

and

$$\nabla \sigma_{H,max} = \left(0, \frac{M_b}{3I}, 0 \right) = \left(0, \frac{\sigma_a}{3y}, 0 \right). \quad (80)$$

The parameters a and b of the standard Crossland criterion, are obtained from fully reversed tension-compression fatigue limit s_{ref} and torsion fatigue limit t_{ref} using Eq.(37).

From Eq.(31), standard Crossland criterion without gradient effect writes:

$$\sqrt{J_{2,a}} + a\sigma_{H,max} = \sqrt{\frac{\sigma_a^2}{3} + \tau_a^2} + \frac{\sigma_a}{3} \leq b. \quad (81)$$

The gradient term here is given by:

$$\| \nabla \sqrt{J_{2,a}} + a\nabla \sigma_{H,max} \| = \frac{\sqrt{\frac{\sigma_a^2}{3} + \tau_a^2}}{y} + \frac{a\sigma_a}{3y}. \quad (82)$$

Crossland criterion with beneficial gradient term as shown in Eq.(42) now writes

$$\begin{aligned}\sqrt{J_{2,a}} + a\sigma_{H,max} - l_g \| \nabla \sqrt{J_{2,a}} + a\nabla \sigma_{H,max} \| &= \\ \sqrt{\frac{\sigma_a^2}{3} + \tau_a^2} + \frac{a\sigma_a}{3} - l_g \left(\frac{\sqrt{\frac{\sigma_a^2}{3} + \tau_a^2}}{y} + \frac{a\sigma_a}{3y} \right) &\leq b.\end{aligned}\quad (83)$$

With Papadopoulos criterion We can find the resolved shear stress $\tau(\varphi, \theta, \chi, t)$ with Eq.(44):

$$\begin{aligned}\tau(\varphi, \theta, \chi, t) &= [\sin(\theta)\cos(\phi)\sigma_a \sin(\omega t) + \sin(\theta)\sin(\phi)\tau_a \sin(\omega t)] \\ &\quad [-\sin(\phi)\cos(\chi) - \cos(\theta)\cos(\phi)\sin(\chi)] + \\ &\quad [\sin(\theta)\cos(\phi)\tau_a \sin(\omega t)][\cos(\phi)\cos(\chi) - \cos(\theta)\sin(\phi)\sin(\chi)],\end{aligned}\quad (84)$$

Although the intermediate calculations are complicated, the result achieves the very simple form[3]. The generalized shear stress amplitude T_a is then:

$$\begin{aligned}T_a(\varphi, \theta) &= \sqrt{\frac{1}{\pi} \int_{x=0}^{\frac{\pi}{2}} \tau^2(\varphi, \theta, \chi) d\chi} = \sqrt{\frac{\sigma_a^2}{3} + \tau_a^2}. \\ \sigma_{H,max} &= \frac{1}{3}\sigma_a\end{aligned}$$

The modified Papadopoulos criterion from Eq.(48) is:

$$maxT_a + \alpha_\infty \sigma_{H,max} - l_g \| \nabla maxT_a + \alpha_\infty \sigma_{H,max} \| \leq \gamma_\infty,$$

From the above calculation and the linear dependance of the stress field as function of y , Papadopoulos criterion with beneficial gradient term reduces to

$$\max T_a + \alpha_\infty \sigma_{H,max} - l_g \parallel \nabla \max T_a + \alpha_\infty \sigma_{H,max} \parallel = \\ \sqrt{\frac{\sigma_a^2}{3} + \tau_a^2} + \frac{\alpha_\infty \sigma_a}{3} - l_g \left(\frac{\sqrt{\frac{\sigma_a^2}{3} + \tau_a^2}}{y} + \frac{\alpha_\infty \sigma_a}{3y} \right) \leq \gamma_\infty. \quad (85)$$

With Dang Van criterion The principle stresses in 2D tensor are expressed as:

$$\sigma_1 = \frac{\sigma_a}{2} + \sqrt{\left(\frac{\sigma_a}{2}\right)^2 + \tau_a^2} \\ \sigma_2 = \frac{\sigma_a}{2} - \sqrt{\left(\frac{\sigma_a}{2}\right)^2 + \tau_a^2}$$

With this one gets the amplitude of shear stress by:

$$\max_t \tau(t) = \frac{1}{2}(\sigma_1 - \sigma_2) = \sqrt{\left(\frac{\sigma_a}{2}\right)^2 + \tau_a^2}$$

Dang Van criterion with beneficial gradient term as shown in Eq.(86) now becomes :

$$\max_t \{\tau(t) + a_D \sigma_H(t)\} - l_g \parallel \nabla \tau(t) + a_D \nabla \sigma_H(t) \parallel = \\ \sqrt{\left(\frac{\sigma_a}{2}\right)^2 + \tau_a^2} + \frac{a_D \sigma_a}{3} - l_g \left(\frac{\sqrt{\left(\frac{\sigma_a}{2}\right)^2 + \tau_a^2}}{y} + \frac{a \sigma_a}{3y} \right) \leq b_D. \quad (86)$$

Comparison with experimental data This classical Crossland ellipse arc delimits in the $s_{ref} - t_{ref}$ plane the safe domain against fatigue failure. In the case of fully reversed in-phase tension-compression and torsion fatigue tests, it gives the "ellipse arc equation"[13] :

$$\left(\frac{\tau_a}{t_{ref}}\right)^2 + \left(\frac{2s_{ref}}{\sqrt{3}t_{ref}} - 1\right) \left(\frac{\sigma_a}{s_{ref}}\right)^2 + \left(2 - \frac{2s_{ref}}{\sqrt{3}t_{ref}}\right) \frac{\sigma_a}{s_{ref}} \leq 1 \quad (87)$$

However, if one tries to predict the behavior of the material in combined bending and torsion, which involves the gradients of normal and shear stresses, high discrepancies between predictions and experimental data will be found.

By introducing the values of $\sqrt{J_{2,a}}$ and $\sigma_{H,max}$ in the the classical Crossland criterion, along with the change of parameter α_∞ from $\left(\frac{3t_{-1}}{s_{-1}} - \sqrt{3}\right)$ to $\left(\frac{3t_{-1}}{f_{-1}} - \sqrt{3}\right)$ in Eq.(31), we obtain the "Papadopoulos ellipse arc" based on (t_{-1}, f_{-1}) in the plane of amplitudes σ_a and τ_a :

$$\left(\frac{\tau_a}{t_{-1}}\right)^2 + \left(\frac{2f_{-1}}{\sqrt{3}t_{-1}} - 1\right) \left(\frac{\sigma_a}{f_{-1}}\right)^2 + \left(2 - \frac{2f_{-1}}{\sqrt{3}t_{-1}}\right) \frac{\sigma_a}{f_{-1}} \leq 1 \quad (88)$$

Our proposal takes into account both gradients of hydrostatic stress and shear stress. Choosing the proper l_g (here $l_g = 2.5mm$) allows us to predict the experiments within the acceptable range as shown in Fig. 14 at the critical locations $y = R$. These results, represented in the σ_a, τ_a plane (the so called fatigue ellipse arc) illustrate that our proposal is quite satisfactory in biaxial case.

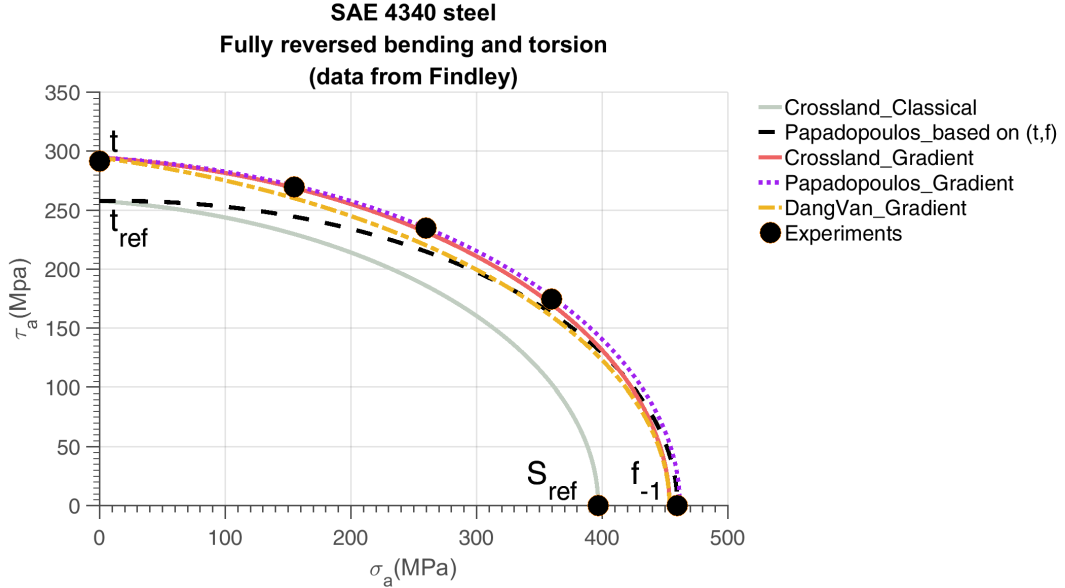


Fig. 14: Fully reversed combined bending-twisting fatigue limit data (Findley et al.[22], Papadopoulos and Panoskaltsis[21]) compared with updated values computed with gradient effects with $l_g = 2.5 \text{ mm}$.

3.7. Discussion

Remark 1 (Gradient terms). In this paper, the pure size effect has not been considered and only stress gradient effect is modeled. Whereas the latter is dominant rather than totally to the pure size effect as usually believed

Remark 2 (Material characteristic length scale l_g). We study here the fatigue limit of macroscopic specimens and components for which the crack initiation is generally detected by loss of stiffness corresponding to crack length which can reach a millimeter. We choose l_g ranging from 0.1 to 2.5mm(depending on crack nucleation definition). To verify the relevancy of this choice, we need more experimental data.

Remark 3 (Extensions to other load case). This new criteria is generalized to multiaxial cases to capture both well-known phenomena Smaller is Stronger and Higher Gradient is Stronger and thus can reproduce fatigue experimental data even at small scale.

3.8. Conclusion

The present study develops a simple formulation of gradient multi-axial fatigue criteria extending the classical HCF criteria. The objective is to model the surface gradient effects (yielding apparent size and loading effects), which is not included yet in classical mechanics but become important at small scale or in the presence of notches, by taking into account just the gradient effect. This is achieved by a simple and versatile technique, which we have validated on a few significative examples. This effect allows us to discriminate between a compression tension test combined with a torsion test and a bending twisting test. The extra cost is the apparition of a length scale l_g which has to be determined by adequate experiments at different sizes.

Nevertheless, in this work only simple fatigue tests have been examined. In these tests, the gradient has a beneficial effect on fatigue. However, cases where the effect can be presumably negative, especially under the circumstances of residual stresses, can be encountered. A reexamination and validation for complex loading could be perspective for this research direction.

4 Time varying load : the standard approach

Fatigue failure is a damage accumulation process in which material property deteriorates continuously under fatigue loading and the damage depends on the size of stress and strain. With the accumulation of fatigue damage, some accidents occur for these components. Research shows that a reliable lifetime prediction method is particularly important in the design, safety assessments, and optimization of engineering components and structures. Thus, it is important to formulate an accurate method to evaluate the fatigue damage accumulation and effectively predict the fatigue life of these components. The objective of this work is to contribute to the development life model that take into account the presence of complex variations of the stress tensor. We focus on Chaboche damage accumulation law in case of multiaxial high cycle fatigue. Heuristic formulations with different multiaxial fatigue criteria have been proposed. An application to an industrial structure is then performed.

4.1. The notion of damage in fatigue

In the case of fatigue, we usually employ the concept of the loading cycle instead of time to evaluate the evolution of damage and to measure the fatigue lifetime. The equations then depend on the load through globally defined quantities over a cycle, such as amplitude, maximum value, mean value. The growth equation of fatigue damage is therefore taken in the form:

$$\delta D = f(\dots)\delta N$$

$$\delta N = f\delta t$$

where δt is a time sampling of the history in a given number of time intervals $\delta t_1, \delta t_2, \dots, \delta t_i, \dots$ and f is the mean frequency of those cycles during the considered time step.

4.1.1. Linear and nonlinear accumulation of damage

Cumulative effects, whether linear or nonlinear, are of great importance in fatigue. The rule of linear accumulation is in fact a property of any linear or nonlinear differential equation with separable variables. One approach to variable load histories uses the concept of fraction of life(also referred to as cycle ratio) used up by an event. These fractions are added together; when their sum reaches 1.0 or 100 percent we expect failure. This is the most common measure of damage, and is the quantifying measure we use here.

The Palmgren-Miner linear rule as explained in [23] is based on the assumption that damage is accumulated additively when it is defined by the associated life ratio N_i/N_{F_i} where N_i is the number of cycles applied under a given load for which the number of cycles to fracture(under periodic conditions) would be N_{F_i} . The fracture criterion is:

$$\sum_i N_i/N_{F_i} = 1.$$

Therefore, in periodic tests, damage evolution is considered to be linear in that:

$$D = N/N_F.$$

For a test at two stress levels, the evolution is as shown schematically in Fig. 16. In fact, the linear accumulation rule can be applied even to a damage which evolves nonlinearly. For this it is sufficient that a one-to-one relationship between D and N/N_F exists, or even that the damage evolution curve be a unique function(independent of the applied cycle) of the life ratio N/N_F .

There are, therefore, two ways of defining a damage incremental law incorporating the linear accumulation rule. It can be linear of the form and shown in Fig. 15:

$$\delta D = \delta N/N_F(\dots),$$

where N_F is the number of cycles to failure defined by the chosen parametric data. The damage evolution

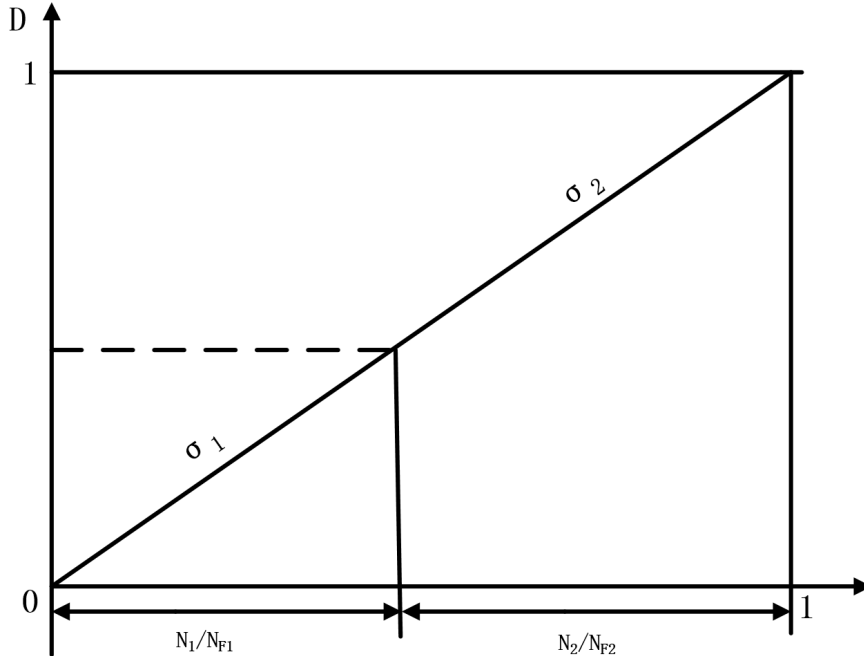


Fig. 15: Linear accumulation of damage with linear evolution

can be nonlinear such as:

$$\delta D = \frac{(1-D)^{-k}}{k+1} \frac{\delta N}{N_F(\dots)}.$$

Here in any case, the damage evolution curve as function of life ratio $\delta N/N_F$ is supposed to be independent of the local state of stress (Fig. 16).

In contrast, if the damage evolution curve, as a function of the life ratio N/N_F , depends on the applied loading we have the effect of nonlinear accumulation as shown in Fig. 17. There, D_1 represents the state of internal damage at the end of the first level σ_1 . Evolution at the second level σ_2 continues from the same state, and it is clear that the sum of the life ratio is less than 1. From the point of view of the damage law, this nonlinearity always corresponds to the case where the variables which represent the load σ and the damage variable D have coupled evolution.

The Palmgren-Miner linear accumulation law gives good results only for loads for which there is little variation in the amplitude and mean value of stress. The assumption of linear damage is open to many objections. For example, sequence and interaction of events may have major influences on life, the rate of damage accumulation may depend on the load amplitude, experimental evidence often indicates that $\sum_i N_i/N_{F_i} \neq 1$ for a low-to-high or a high-to-low loading sequence.

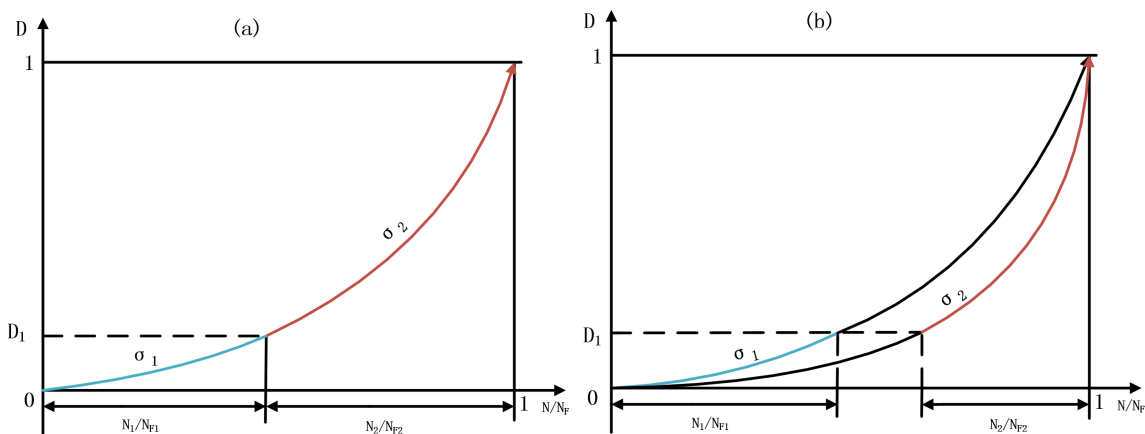


Fig. 16: Damage with nonlinear evolution and linear accumulation

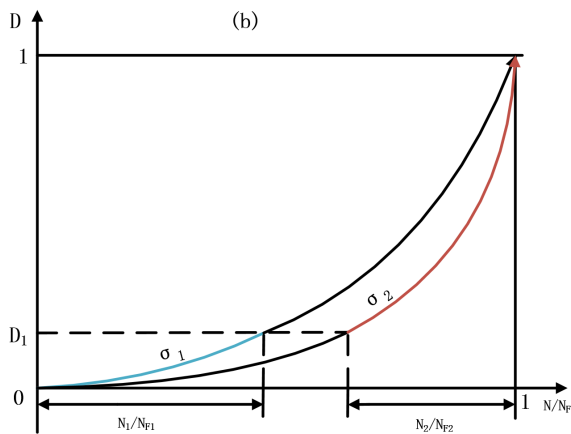


Fig. 17: Damage with nonlinear evolution and nonlinear accumulation

4.1.2. Classic Chaboche damage law

In periodic cyclic loadings, one way of writing a damage law which expresses the experimental results is to assume that the damage per cycle is a function of the maximum and the mean values of the stress:

$$\delta D / \delta N = f(\sigma_{Max}, \sigma_m).$$

In order to recover, after integration, one of the many forms proposed to represent the Wohler curves, we let:

$$\delta D / \delta N = \frac{\sigma_{Max} - \sigma_l(\sigma_m)}{\sigma_u - \sigma_{Max}} \left(\frac{\sigma_{Max} - \sigma_m}{B(\sigma_m)} \right)^\gamma. \quad (89)$$

with:

$\sigma_l(\sigma_m) = \sigma_m + s_{-1}(1 - b\sigma_m)$: mean stress component in the fatigue limit.

$B(\sigma_m) = B_0(1 - b\sigma_m)$: the mean stress component in the fatigue limit.

The number of cycles to failure is obtained by an obvious integration, with the condition:

$N = 0 \rightarrow D = 0$ (initial undamaged state)

$N = N_F \rightarrow D = 1$ (macro-crack initiation)

so that by integration Eq.(89) from $D = 0$ to $D = 1$ we get:

$$N_F = \frac{\sigma_u - \sigma_{Max}}{\sigma_{Max} - \sigma_l(\sigma_m)} \left(\frac{\sigma_{Max} - \sigma_m}{B(\sigma_m)} \right)^{-\gamma}. \quad (90)$$

Eq.(89) then writes:

$$\delta D = \delta N / N_F.$$

The constants are determined from conventional data: σ_u is usually known, s_{-1}, b fit the results on the fatigue limits with relation $\sigma_l(\sigma_m) = \sigma_m + s_{-1}(1 - b\sigma_m)$. Exponent γ is collaborated from the S-N curve for reversed conditions, by plotting σ_{Max} as function of $N_F(\sigma_{Max} - \sigma_l(\sigma_m)) / (\sigma_u - \sigma_{Max})$, as deduced from Eq.(90). Coefficient $B(\sigma_m)$ is obtained from one point of the S-N curve.

Uniaxial case

The equation studied below allows us to describe the effects of nonlinear accumulation in the case of non-periodic cyclic loads[24]. A simple way to introduce such effects in the damage growth equation consists in rendering the load and damage variables non-separable. For example, we may take:

$$\delta D = D^{\alpha(\sigma_{Max}, \sigma_m)} \left(\frac{\sigma_{Max} - \sigma_m}{C(\sigma_m)} \right)^\gamma \delta N$$

The exponent α depends on the loading (σ_{Max}, σ_m) , which results in non-separability.

$$\alpha(\sigma_{Max}, \sigma_m) = 1 - a \left\langle \frac{\sigma_{Max} - \sigma_l(\sigma_m)}{\sigma_u - \sigma_{Max}} \right\rangle$$

$$M(\sigma_m) = M_0(1 - b\sigma_m)$$

The exponent α represents the internal variables(for example the hardening state of the material), which depends on the loading (σ_{Max}, σ_m) , resulting in non-separability. α allows a non-linear damage cumulative rule as it is experimentally observed. a and γ are material parameters. M_0 represent the fatigue limit and the static fracture. The coefficients γ and M_0 are determined from these experimental Woehler's curves by plotting Eq.(93) and take one point from it.

The concept of effective stress applied to fatigue provides an indirect measure. The measured evolutions are extremely nonlinear. With this concept, damage can really be measured only in the last part of the lifetime, when microscopic initiations have already occurred (this is the phase of micro-propagation of defects). And these damage evolutions are extremely nonlinear. To reproduce this phenomenological aspect it is sufficient to make a change of variable by replacing D in the previous equation by:

$$1 - (1 - D)^{\gamma+1}.$$

The differential law can be written as:

$$\delta D = [1 - (1 - D)^{\gamma+1}]^{\alpha(\sigma_{Max}, \sigma_m)} \left[\frac{\sigma_{Max} - \sigma_m}{M(\sigma_m)} \right]^\gamma \delta N \quad (91)$$

This form is more complex, but its properties are identical to the properties of the previous equation, except for the current value of damage. Now we integrate it to see how damage D evolves with cycle numbers N and the influence of different parameters. By differential calculus, we get from Eq.(91):

$$\delta[1 - (1 - D)^{\gamma+1}]^{1-\alpha} = (1 - \alpha)(\gamma + 1) \left[\frac{\sigma_{Max} - \sigma_m}{M(\sigma_m)} \right]^\gamma \delta N \quad (92)$$

The number of cycles to failure, obtained by integrating D from 0 to 1 is:

$$N_F = \frac{1}{(\gamma + 1)(1 - \alpha)} \left(\frac{\sigma_{Max} - \sigma_m}{M(\sigma_m)} \right)^{-\gamma} \quad (93)$$

and we find that $M(\sigma_m) = C(\sigma_m)(\gamma + 1)^{1/\gamma}$. In differential form, the relation (94) writes from Eq.(92) and Eq.(93):

$$\delta[1 - (1 - D)^{\gamma+1}]^{1-\alpha} = \frac{\delta N}{N_F} \quad (94)$$

When we integrate Eq.(92) from 0 to D at constant loading conditions. The damage, expressed as a function of N/N_F is:

$$D = 1 - \left[1 - \left(\frac{N}{N_F} \right)^{\frac{1}{1-\alpha}} \right]^{\frac{1}{\gamma+1}}. \quad (95)$$

This expression is in good agreement with experimental results[23].

Multiaxial case

The applied stress and strain tensors are often multiaxial and present a complex path during a loading cycle. In the case of multiaxial loading fatigue, the Chaboche model is represented by the following equation:

$$\delta D = (1 - (1 - D)^{\gamma+1})^\alpha \left(\frac{\tilde{A}_{II}}{M(\sigma_H)} \right)^\gamma \delta N \quad (96)$$

Where the amplitude $\sigma_{Max} - \sigma_l(\sigma_m)$ is replaced by the deviatoric norm A_{II} and the average stress is replaced by the hydrostatic pressure. We should note that for an isotropic damage theory:

$$\tilde{A}_{II} = A_{II}/(1 - D)$$

$$\alpha = 1 - a \left\langle \frac{A_{II} - A_{II}^*(\sigma_H)}{\sigma_u - \sigma_{eqMax}} \right\rangle. \quad (97)$$

α represents the internal variables, characterizes the non-linearity of the damage evolution, defines the non-linear cumulation, and allows to take into account the mean stress effect and describes the damage occurrence of the material: as long as $\alpha < 1$, there is damage creation. The coefficient a gives the amount of fragility which is suggested by a given occurrence of fatigue limit violation.

A_{II} is the amplitude of octahedral shear stress given by:

$$A_{II} = \frac{1}{2} \max_t \sqrt{\frac{1}{2} \underline{\underline{\Delta s}} : \underline{\underline{\Delta s}}} = \sqrt{J_{2a}} = \frac{1}{2} \Delta \sigma_{eqmax}, \quad (98)$$

The quantity $A_{II}^*(\sigma_H)$ represents the infinite life fatigue limit. For example, the Sines fatigue limit criterion is formulated by the following equation:

$$A_{II}^*(\sigma_H) = s_{-1}(1 - 3b\sigma_H). \quad (99)$$

Above, s_{-1} and σ_u are respectively the fatigue limit at zero mean stress and the ultimate tensile stress. For steel, normally $s_{-1} \approx 0.48\sigma_u$.

The function $M(\sigma_H)$ in Eq.(132) quantifies the mean stress effect through Low Cycle Fatigue(LCF) loading range:

$$M(\sigma_H) = s_{-1} \left(1 - 3 \frac{\sigma_H}{\sigma_u} \right).$$

We can get the $D - N$ curve in Fig. 18 by integrating Eq.(132). This is in the case of constant loading conditions because we regard α and γ as invariable parameters.

$$N = \frac{(1 - (1 - D)^{\gamma+1})^{1-\alpha}}{(1 + \gamma)(1 - \alpha)} \left[\frac{A_{II}}{M(\sigma_H)} \right]^{-\gamma} \quad (100)$$

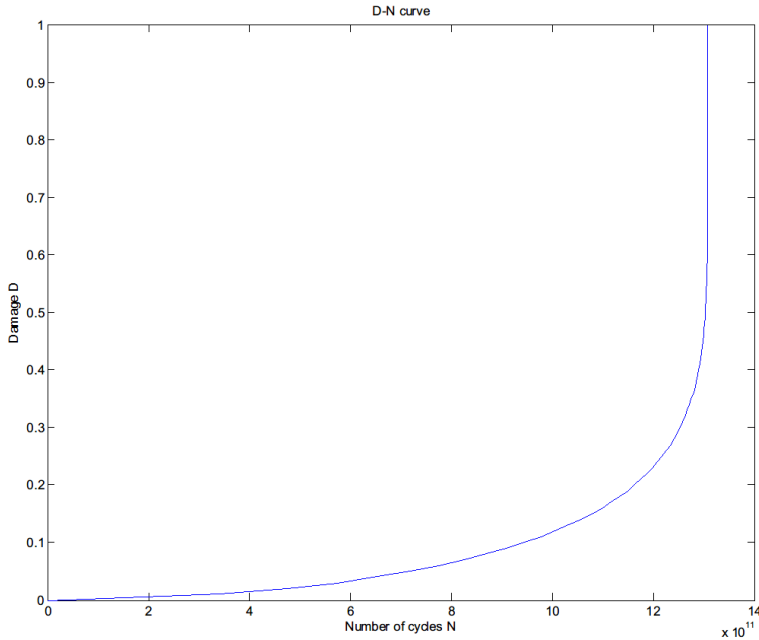


Fig. 18: Damage accumulation in terms of N in constant loading condition, with D and N are related by the evolution equation (100)

The number of cycles to failure, obtained at $D = 1$, is:

$$N_F = \frac{1}{(\gamma + 1)(1 - \alpha)} \left[\frac{\widetilde{A}_{II}}{M(\sigma_H)} \right]^{-\gamma} \quad (101)$$

It should be noted that in multiaxial case the effective stress amplitude is written as:

$$A_{II} = \frac{\tilde{A}_{II}}{(1 - D)}$$

In Eq.(101), γ , b and a are material parameters determined from fatigue tests.

In the case of multiaxial fatigue loading, an infinite life is obtained if the stress amplitude A_{II} respects:

$$A_{II} \leq A_{II}^*(\sigma_H) = s_{-1}(1 - 3b\sigma_H). \quad (102)$$

In terms of Sines criterion which Chaboche uses, it writes:

$$\sqrt{J_{2a}} + 3bs_{-1}\sigma_H - s_{-1} \leq 0. \quad (103)$$

σ_H is the mean hydrostatic stress defined by:

$$\sigma_H = \frac{1}{6}[\max \operatorname{tr}(\underline{\underline{\sigma}}(n)) + \min \operatorname{tr}(\underline{\underline{\sigma}}(n))], \quad (104)$$

The damage is expressed the same as in uniaxial case:

$$D = 1 - \left[1 - \left(\frac{N}{N_F} \right)^{\frac{1}{1-\alpha}} \right]^{\frac{1}{\gamma+1}}. \quad (105)$$

These theories account for the nonlinear nature of fatigue damage accumulation by using nonlinear relations such as Eq.(105) where the power α depends on the load level(see Fig. 19).

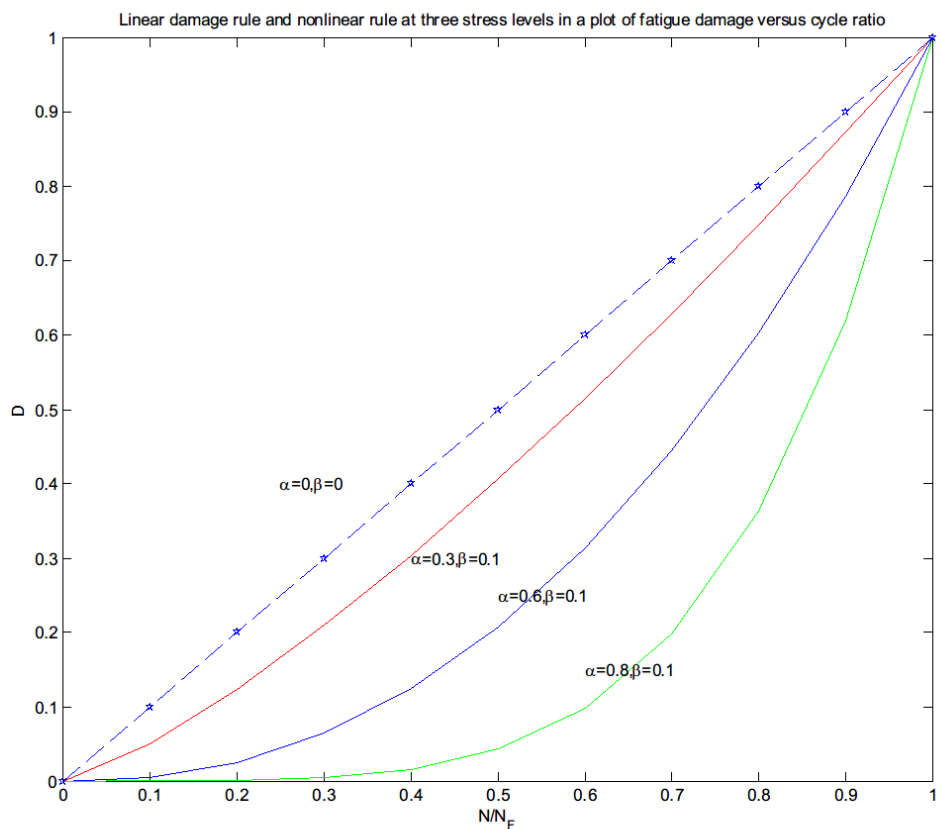
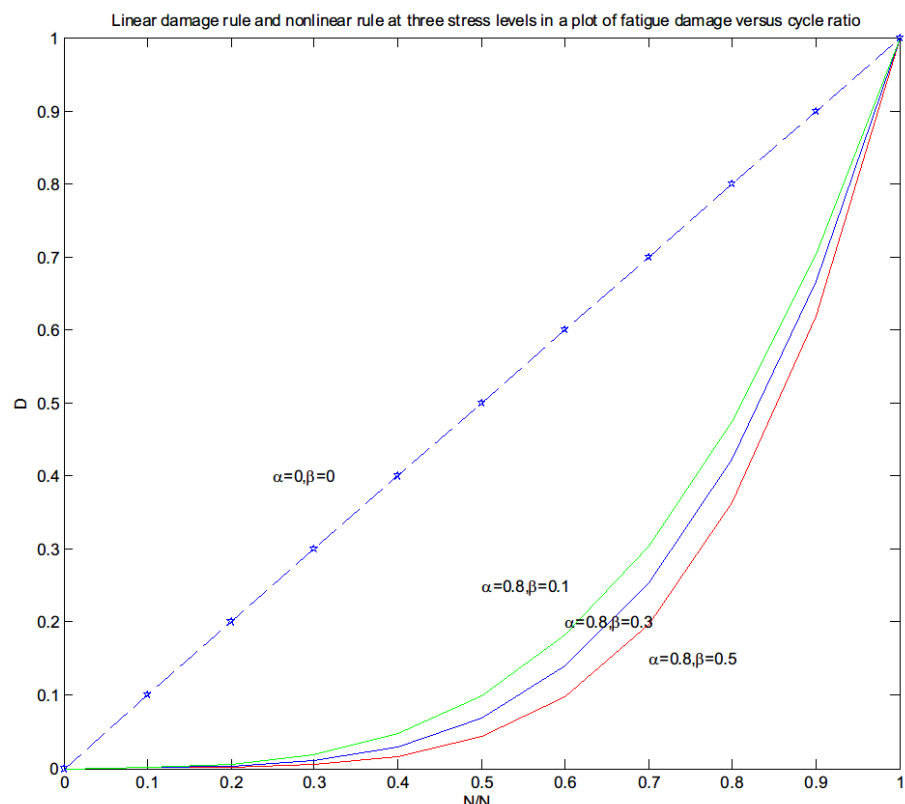


Fig. 19: Influence of function α in a plot of fatigue damage versus cycle ratio

Fig. 20: Influence of function γ in a plot of fatigue damage versus cycle ratio

4.2. Verification method of Chaboche law

Many fatigue damage accumulation models are based on the two level loading experiments which is one of the basic random loading analysis. To facilitate our verification of the law we use two-stress level loading, the specimen is firstly loaded at stress σ_1 for N_1 cycles and then at stress σ_2 for N_2 cycles until failure. We can then observe if the experimental results are satisfactory.

After N_1 cycles, we have from Eq.(105), a damage D_1 given by:

$$[1 - (1 - D_1)^{\gamma+1}]^{1-\alpha_1} = \frac{N_1}{N_{F1}} \quad (106)$$

By integrating Eq.(94) from $D = D_1$ to $D = 1$, we get:

$$1 - [1 - (1 - D_1)^{\gamma+1}]^{1-\alpha_2} = \frac{N_2}{N_{F2}} \quad (107)$$

Which yields:

$$1 - \frac{N_2}{N_{F2}} = 1 - [1 - (1 - D_1)^{\gamma+1}]^{1-\alpha_2} \quad (108)$$

From Eq.(106) and Eq.(108), after elimination of $[1 - (1 - D_1)^{\gamma+1}]$ we get:

$$\frac{N_2}{N_{F2}} = 1 - \left(\frac{N_1}{N_{F1}}\right)^{\frac{1-\alpha_2}{1-\alpha_1}} = 1 - \left(\frac{N_1}{N_{F1}}\right)^\eta \quad (109)$$

with

$$\eta = \frac{1 - \alpha_2}{1 - \alpha_1} = \frac{A_{II2} - A_{II}^*(P_{m2})}{A_{III} - A_{II}^*(P_{m1})} \frac{\sigma_u - \sigma_{eqMax1}}{\sigma_u - \sigma_{eqMax2}} = \frac{\sqrt{J_{2,a2}} - s_{-1}(1 - 3bP_{m2})}{\sqrt{J_{2,a1}} - s_{-1}(1 - 3bP_{m1})} \frac{\sigma_u - \max(2\sqrt{J_{2,a1}})}{\sigma_u - \max(2\sqrt{J_{2,a2}})} \quad (110)$$

In the case of high-low loading sequence($\sigma_1 > \sigma_2$):

$$\eta = \frac{1 - \alpha_2}{1 - \alpha_1} < 1; \frac{N_2}{N_{F2}} = 1 - \left(\frac{N_1}{N_{F1}}\right)^\eta < 1 - \frac{N_1}{N_{F1}}; \frac{N_1}{N_{F1}} + \frac{N_2}{N_{F2}} < 1$$

The cumulative damage under high-low loading sequence, as we deduced, has the addition of partial lives less than unit.

Similarly, the cumulative damage under low-high loading sequence has addition of partial lives more than 1.

$$\frac{N_1}{N_{F1}} + \frac{N_2}{N_{F2}} > 1$$

For constant two-level stress loading, $\alpha_1 = \alpha_2$, the Chaboche law returns to the Miner rule where:

$$\frac{N_1}{N_{F1}} + \frac{N_2}{N_{F2}} = 1$$

4.3. Chaboche law containing different criteria

4.3.1. Chaboche law with Crossland criterion

In the previous model we used Sines fatigue criterion constructing the damage criterion exponent α . Now we want to see Chaboche law with different criteria and compare the numerical results. Firstly, α represents the internal variables and contains the fatigue criterion, so we first change α to satisfy Crossland Criterion:

$$\alpha = 1 - a \left(\frac{\max_n \sqrt{J_{2a}(n)} + a_c P_{max}(n) - b_c}{\sigma_u - 2 \max_n \sqrt{J_{2a}(n)}} \right). \quad (111)$$

with

$$a_c = \frac{(t_{-1} - \frac{f_{-1}}{\sqrt{3}})}{\frac{f_{-1}}{3}}, \quad b_c = t_{-1}. \quad (112)$$

$$\eta_c = \frac{1 - \alpha_2}{1 - \alpha_1} = \frac{\sqrt{J_{2,a_2}} + a_c P_{M_2} - b_c}{\sqrt{J_{2,a_1}} + a_c P_{M_1} - b_c} \frac{\sigma_u - \max(2 \sqrt{J_{2,a_1}})}{\sigma_u - \max(2 \sqrt{J_{2,a_2}})} \quad (113)$$

In Eq.(100), the amplitude of octahedral shear stress A_{II} remain unchanged.

4.3.2. Chaboche law with Dang Van criterion

We change α to express it through Dang Van Criterion:

$$\alpha = 1 - a \left(\frac{\max_n \{\tau(n) + a_D P(n)\} - b_D}{\sigma_u - 2 \max \sqrt{J_{2a}}} \right). \quad (114)$$

with

$$\tau(n) = \frac{1}{2}(\hat{\sigma}_I(n) - \hat{\sigma}_{III}(n)) \quad (115)$$

$$a_D = \frac{3t_{-1}}{f_{-1}} - \frac{3}{2}, \quad b_D = t_{-1}.$$

$$\eta_D = \frac{1 - \alpha_2}{1 - \alpha_1} = \frac{\max_t \{\tau_2(n) + a_D P_2(n)\} - b_D}{\max_t \{\tau_1(n) + a_D P_1(n)\} - b_D} \frac{\sigma_u - \max(2 \sqrt{J_{2a_1}})}{\sigma_u - \max(2 \sqrt{J_{2a_2}})} \quad (116)$$

In Eq.(100), we proposed to change A_{II} to $\max\tau(n)$:

$$N_F = \frac{1}{(\gamma + 1)(1 - \alpha)} \left[\frac{\max\tau(n)}{M(\sigma_H)} \right]^{-\gamma} \quad (117)$$

4.4. Numerical testing on different loading patterns

The fatigue limit with different criteria are distinctive. We compare different criteria in a $A_{II} - N_F$ figure as predicted in Eq.(101). Here γ , b and a are material parameters determined from fatigue tests.

In this case we have

$$N_F = \frac{1}{(\gamma + 1)(1 - \alpha)} \left[\frac{A_{II}}{M(\sigma_H)} \right]^{-\gamma},$$

$$M(\sigma_H) = s_{-1} (1 - 3\sigma_H/\sigma_u).$$

For Sines and Crossland criteria:

$$A_{II} = \sqrt{J_{2a}} = \frac{1}{2} \max_t \sqrt{\frac{1}{2}(\Delta s_{11}^2 + \Delta s_{22}^2 + \Delta s_{33}^2 + 2\Delta s_{12}^2 + 2\Delta s_{13}^2 + 2\Delta s_{23}^2)}.$$

For Dang Van criterion:

$$A_{II} = \max\tau(n).$$

4.4.1. Test on pure rotation

From the fatigue zone we select $r = 0.1$ as the radius to study. We select here:

$$s_{-1} = f_{-1} = 0.8 \text{ MPa},$$

$$\sigma_u = 1.67 \text{ MPa}$$

$$\gamma = 6$$

$A_{II} - N_F$ figure is shown in Fig. 21.

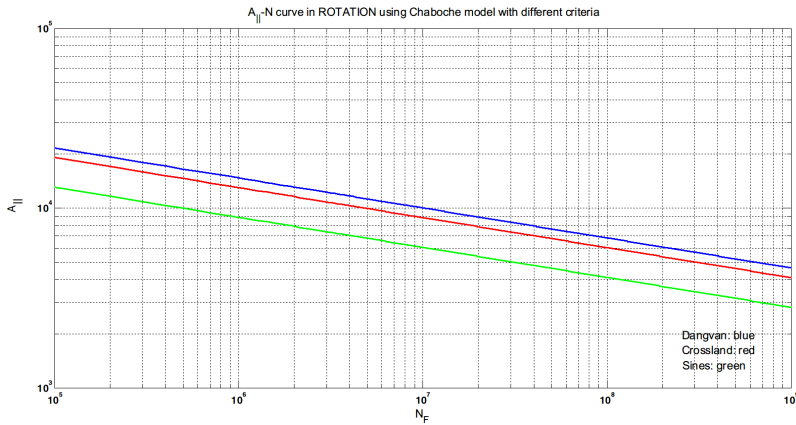


Fig. 21: $A_{II} - N_F$ curve in rotation at $r=0.1$

In pure rotation, we assume the first and second rotating speed are respectively $w_1 = 20 \text{ rpm}$ and $w_2 = 15 \text{ rpm}$.

$$A_{II1} = \sqrt{J_{2,a_1}} = 7.7606E5 \text{ Pa}$$

$$A_{II2} = \sqrt{J_{2,a_2}} = 4.3653E5 \text{ Pa}$$

$$P_{m_1} = 8.8342E5 \text{ Pa}$$

$$P_{m_2} = 4.9693E5 \text{ Pa}$$

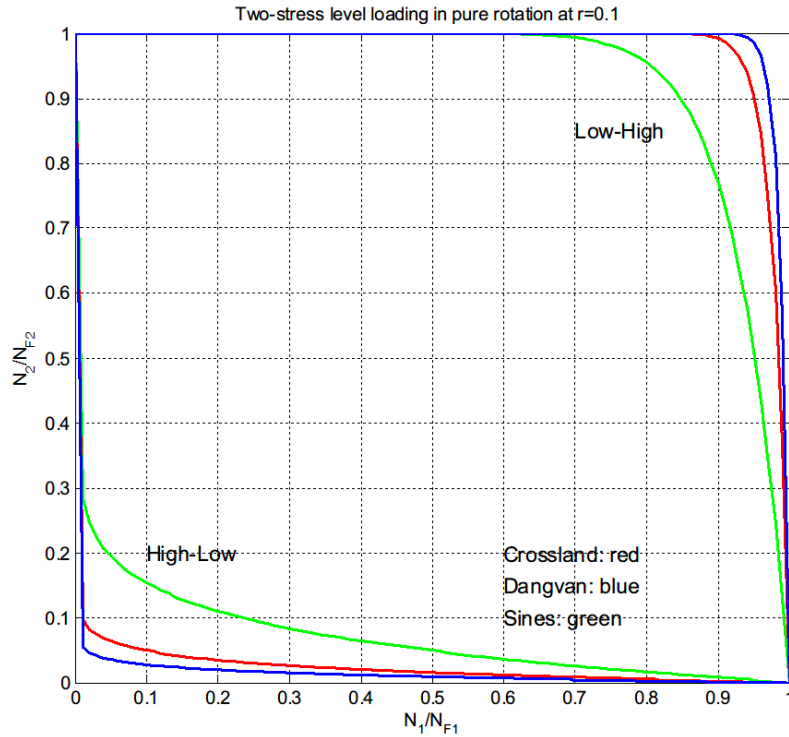
Substituting the above to Eq.(110) we can get η in High-Low sequence:

$$\eta_1 = 0.0721,$$

in Low-High sequence:

$$\eta_2 = 13.8654.$$

The predicted results are shown in Fig. 22.

Fig. 22: Two-stress level loading in pure rotation at $r=0.1$

4.4.2. Test on 4-point bending

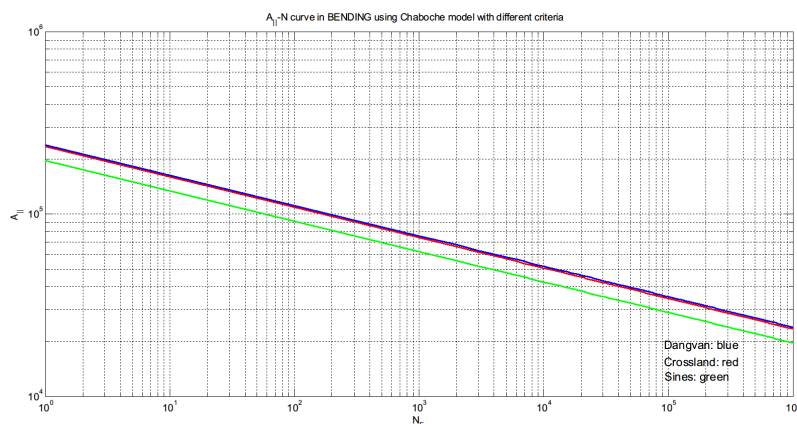
From the fatigue zone we select $y = 3$ to study. We select here:

$$s_{-1} = f_{-1} = 0.8 \text{ MPa},$$

$$\sigma_u = 1.67 \text{ MPa}$$

$$\gamma = 6$$

The $A_{II} - N_F$ figure is shown in Fig. 23.

Fig. 23: $A_{II} - N_F$ curve in 4-point bending at $y=3$

In 4-point bending, we assume the first and second loading are respectively $F_1 = 1E6N$ and $F_2 = 0.8E6N$.

$$\sqrt{J_{2a_1}} = 7.2194E5Pa$$

$$\sqrt{J_{2a_2}} = 5.7755E5Pa$$

$$P_{m_1} = 3.9298E5Pa$$

$$P_{m_2} = 3.1438E5Pa$$

Substituting the above to Eq.(110) we can get η in High-Low sequence:

$$\eta_1 = 0.3174,$$

in Low-High sequence:

$$\eta_2 = 3.1510.$$

The predicted results are shown in Fig. 24.

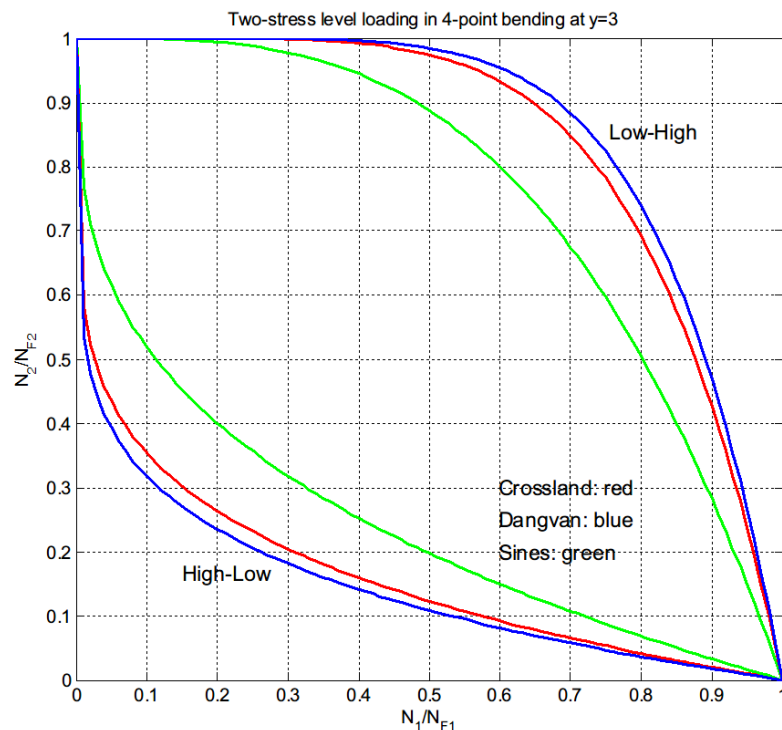


Fig. 24: Two-stress level loading in 4-point bending at $y=3$

4.4.3. Test on rotative bending

From the fatigue zone we select $r = 0.5$ as the radius to study. The $A_{II} - N_F$ figure is shown in Fig. 25.

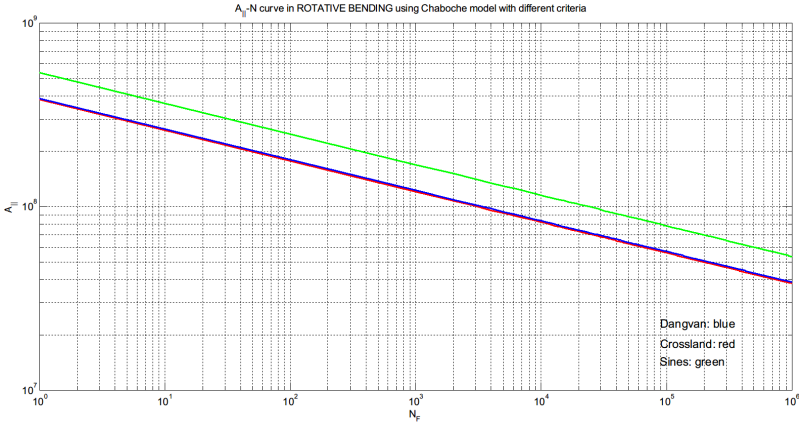


Fig. 25: $A_{II} - N_F$ curve in rotative bending at $r=3$

In rotative bending, we assume the rotating speed are $w = 5\text{ rpm}$. The applied force are respectively $F = 9E5N$ and $F = 3E5N$. We select:

$$s_{-1} = f_{-1} = 400\text{ MPa}, \sigma_u = 1000\text{ MPa}$$

$$\sqrt{J_{2a_1}} = 7.0226E8\text{ Pa}$$

$$\sqrt{J_{2a_2}} = 6.6454E8\text{ Pa}$$

$$P_{m_1} = 6.8921E8\text{ Pa}$$

$$P_{m_2} = 7.1700E8\text{ Pa}$$

Substituting the above to Eq.(110) we can get η in High-Low sequence:

$$\eta_1 = 0.7170,$$

in Low-High sequence:

$$\eta_2 = 1.3947.$$

The predicted results are shown in Fig. 26.

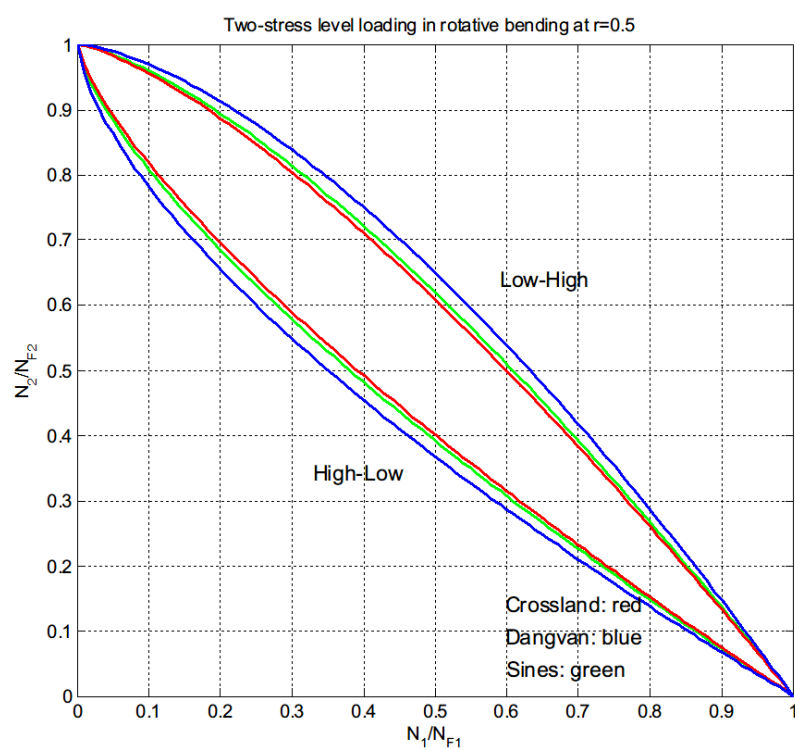


Fig. 26: Two-stress level loading in rotative bending at $r=0.5$

5 Handling general loadings

What makes automobile fatigue so difficult to predict is that, unlike standard tests done in a laboratory, an automobile's structure has to endure a complex, mostly random, set of static as well as cyclical stresses when in service, such as in Fig. 27 which could represent load data from testing or measurement, extracting the cyclic information can be challenging.

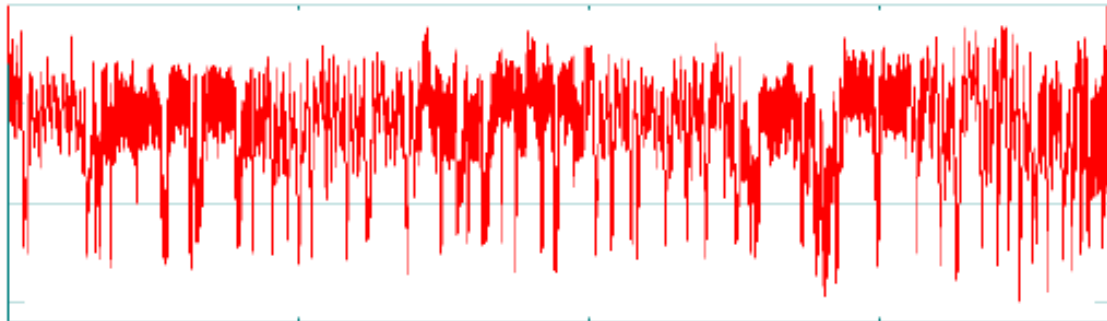


Fig. 27: Complex Cyclic Loading

5.1. Cycle Counting Method

The object of all cycle counting methods is to compare the effect of variable amplitude load histories to fatigue data and curves obtained with simple constant amplitude load cycles. Rainflow counting is a process to obtain cyclic data of complex loading. Its name comes from the original description from the Japanese researchers Matsuishi and Endo where they describe the process in terms of rain falling off a pagoda style roof. A more insightful description based on cyclic plasticity is usually used to explain the method.

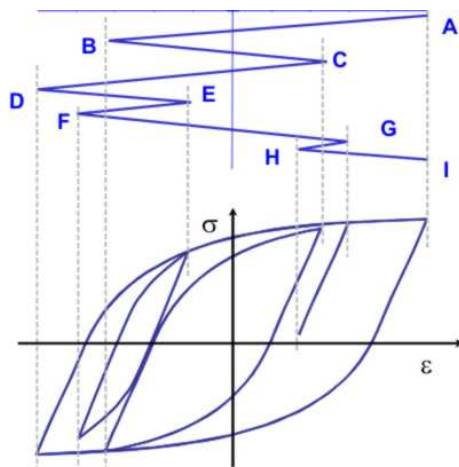


Fig. 28: Complex Cyclic Loading

In Fig. 28 a simple loading history (points A - I) is plotted vertically so that it resembles a Japanese pagoda. The resulting deformation, stresses and strains, is plotted directly below the loading history. In the lower part of the figure, four cycles are easily identified. One large overall cycle, one intermediate cycle in the center of the plot, and two smaller cycles. Each cycle has its own strain range and mean stress. From a deformation viewpoint the process proceeds as follows. Start at A, the maximum strain, and unload the material to B. Then reload to point C and unload to D. When the material reaches the strain at point B during

the unloading from C to D the material remembers its prior deformation and deforms along a path from A to D as if the event C-D never happened. This is better illustrated in the next part of the loading. Load from D to E and unload to F. Now load from F to G. When the material reaches the strain at point E during the loading from F to G the material remembers its prior deformation and deforms along a path from D to G as if the event E-F never happened. The same process occurs for G-H.

Rainflow counting will identify four cycles, A-D-I, B-C-B, E-F-E and G-H-G. Rainflow counting identifies the major load excursions, for example D to I, and treats subcycles like E-F and G-H as interruptions to the overall loading event D-I.

The five-step procedure to extract the cyclic data is summarized as follows:

1. Determine the peaks and valleys of the stress/strain during cycling, and reorder to start from the absolute maximum (Fig. 29).
2. Visualize as draining water starting at the deepest valley (Fig. 30).
3. Measure total depth drained (stress range) and mean depth (mean stress), (Fig. 30), and the number of these cycles in the load history.
4. Continue by draining the next lowest (Fig. 31) and repeat until all valleys are drained. A Rainflow cycle is counted if the second segment is vertically shorter than the first and the third segments(i.e. 6-7 is smaller than 5-6 and 7-8).
5. Use the damage rule to obtain the life from all cycles.

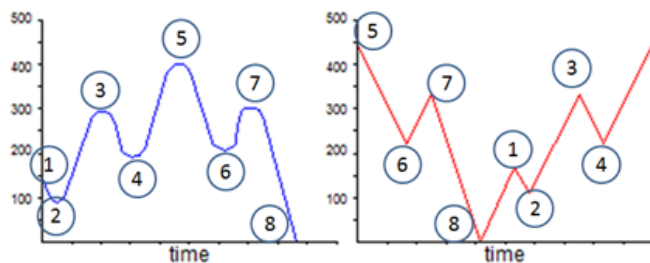


Fig. 29: Reorder to Start from Absolute Maximum

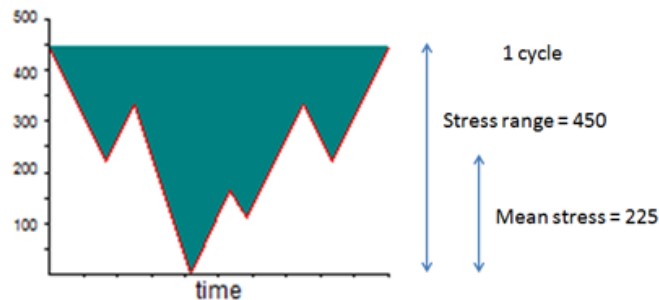


Fig. 30: Imagine Filling with Water and Extract Stress Range and Mean Stress

Once all the cycles have been categorized, the Palmgren-Miner Rule is applied. Even though the linear damage rule ignores sequence effects, it is most widely used because of its simplicity and the fact that though many nonlinear damage models have been developed, unfortunately none can encompass many of the complicating factors encountered during complex variable amplitude loading. As an example, for this case assuming mean stress is ignored:

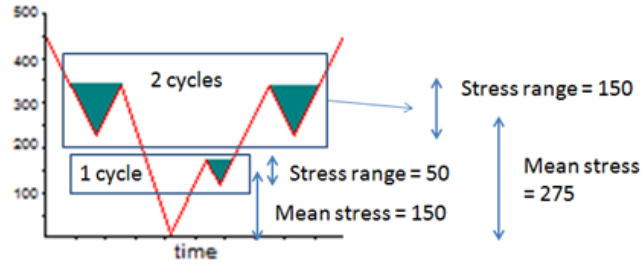


Fig. 31: Drain Water Starting at Lowest Valley and Repeat Cycle Extraction

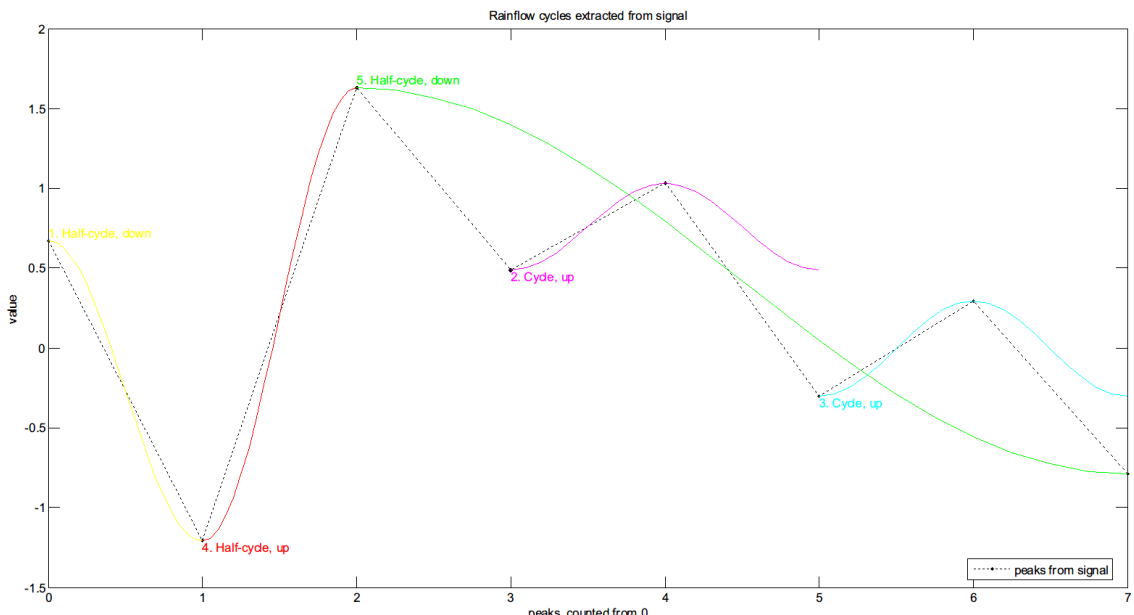


Fig. 32: Rainflow counting method demonstration

$$\sum_i \frac{N_i}{N_{F_i}} = \frac{1}{N_{F_{450}}} + \frac{1}{N_{F_{200}}} + \frac{1}{N_{F_{50}}} + \dots = 1.$$

where n is replaced with the number of actual cycles of its corresponding type in the load history, for instance $N_{F_{450}}$ represents the life obtained from the $S - N$ data for a stress range of 450 MPa . From this equation, the number of total cycles through the entire load history can be found.

The rainflow procedure can be automated so that cyclic content of complex loading can be extracted efficiently. For example, fatigue computer codes such as *nCodeDesignLife* will accept files of test data, or the input of multiple load steps from a static or transient finite element analysis, and use the rainflow approach to automatically extract the cyclic data. In addition, *DesignLife* automates the Palmgren-Miner Damage Rule calculation to determine number of cycles to failure, with the term cycle here defined as one pass through the entire time history. A computer program that accomplishes rainflow cycle counting applied to a complex history such as that in Fig. 33 results in a table of ranges and means shown in Fig. 34.

5.2. Multiaxial loading: existing models and limitations(Roux)

In HCF, the material undergoes elastic deformation at the macroscopic level; plastic deformation occurs only near a stress concentration area, if there is.

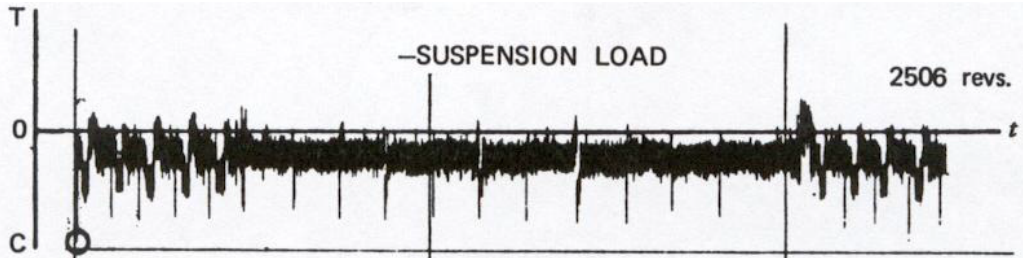


Fig. 33: Suspension load

Stress Range (MPa)	Mean Stress (MPa)														
	-500	-450	-400	-350	-300	-250	-200	-150	-100	-50	0	50	100	150	
200	8	16	24	8	6	66	358	104	6	10	6	6	4	2	
250	2	16	46	10	4	72	564	118	20	10	10	2	2	6	
300	2	8	22	6		36	312	90	14	8	4				
350		4	6			14	148	36	20	6	2				
400		2	10	6	4	64	12	10	6						
450			4			2	20	10	4				2		
500			2	2			8	12					4		
550				4	2		8	2				2			
600				2				2							
650				2	4	4	2				2				
700				4	2										
750			2												
800				2											
850				4	2										
900				4	4										
950				2	4	2									
1000			2			2									
1050						2									
1100															
1150			2												
1200															
1250															
1300															
1350					2										

Fig. 34: Example of the Number of cycles at Various Stress Ranges and Mean Stress Combinations from the Suspension Load History in Fig. 33

Discussion

The Chaboche law is based on this assumption: fatigue damage occurs and accumulates only when the loading stress is higher than its fatigue limit. However, Eq.(132) neglects the damage contribution of the loading stress which is lower than the fatigue limit. According to some experimental results such as: Lu and Zheng [25] [26] [27], Sinclair [28], and Makajima et al. [29], it has shown that the damage of low amplitude loads is one of the main reasons for prediction errors.

Impurities in the material affect the fatigue life. So does the material's hardness, and especially its surface condition. How the components were heat-treated in the factory is another factor. The operating temperature makes a difference, too. Worse still is the structural component's shape: notches and sharp corners create concentrations of stress that can initiate cracks. Thus further studies should be carried out concerning these factors.

5.3. Multiscale energy dissipation approach

The object of this work is to propose an energy based fatigue approach which takes into account impurities and hardness in the material which affect the fatigue life while handling multidimensional time varying loading histories.

Our fundamental thought is to assume that the local dissipated energy at small scale governs fatigue at failure. The proposal of our model is to consider a plastic behavior at the mesoscopic scale with a dependence of the yield function not only on the deviatoric part of the stress but also on the hydro static part. A kinematic hardening under the assumptions of associative plasticity is also considered. We follow the Dang Van paradigm. The structure is elastic at the macroscopic scale. At each material points, there is a stochastic distribution of weak points which will undergo strong plastic yielding, which contribute to energy dissipation without affecting the overall macroscopic stress.

Instead of using the number of cycles, we use the concept of loading time. To elaborate real life loading history more accurately, mean stress effect is taken into account in mesoscopic yield function and non-linear damage accumulation law are also considered in our model. Fatigue will then be determined from the plastic shakedown cycle and from a phenomenological fatigue law linking lifetime and accumulated mesoscopic plastic dissipation.

5.4. Kinematic Hardening Models

5.4.1. Linear Kinematic Hardening

A hardening rule is needed to describe the behavior of the material once it is plastically deformed or yielded. One possible hardening rule is the isotropic rule, which assumes that strain hardening corresponds to an enlargement of the yield surface (i.e. an increase in yield stress) without change of shape or position in the stress space. Another is the kinematic rule, which assumes that strain hardening shifts the yield surface without changing its size or shape.

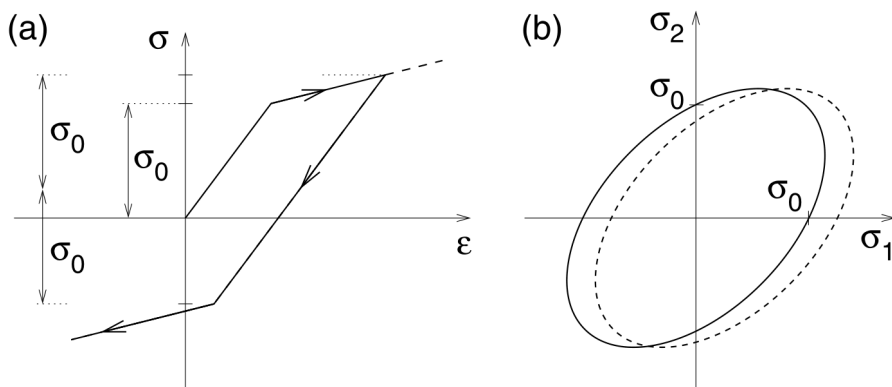


Fig. 35: Kinematic hardening: a) uniaxial stress-strain diagram, b) evolution of the yield surface in the biaxial stress plane

Kinematic hardening rules are necessary, especially for the case of unloading and cyclic loading. In Kinematic Hardening the current loading surface is assumed not to expand but to move as a rigid body within the stress space (Fig. 35(b)). The use of kinematic hardening is, for example, necessary to model the so-called Bauschinger effect (Bauschinger, 1881). This effect is often observed in metals subjected to cyclic loading. Even if the magnitudes of the yield stress in tension and in compression are initially the same, this is no longer the case when the material is preloaded into the plastic range and then unloaded. For example, after previous yielding in tension, yielding in compression may start at a stress level lower than the initial yield stress (Fig. 35(a)).

Kinematic hardening leads to a translation of the loading surface, i.e. to a shift of the origin of the initial yield surface. If the initial yield surface is described by a yield function of the form

$$f(\sigma) = F(\sigma) - \sigma_0$$

the shifted surface is obviously described by

$$f(\sigma, \sigma_b) = F(\sigma - \sigma_b) - \sigma_0$$

where σ_b is the so-called backstress that represents the center of the shifted elastic domain and plays the role of a tensorial hardening variable. Now we need a kinematic hardening law that governs the evolution of the back stress. Melan (1938b) proposed a law of the form

$$\sigma_b = \bar{H}_K \dot{\varepsilon}_p \quad (118)$$

where $\dot{\varepsilon}_p$ is the rate of effective plastic strain. According to which the rate of the back stress is proportional to the plastic strain rate. It is a macroscopic variable representing the dislocation sub-structure resistance to deformation. The proportionality factor \bar{H}_K is directly related to the plastic modulus and is derived from a simple monotonic uniaxial curve. The linear hardening law Eq.(118) is often credited to Prager (1955, 1956); we will call it the MelanPrager hardening rule.

5.4.2. Non-linear Kinematic Hardening

To describe cyclic plasticity, one of the famous model is the non-linear kinematic hardening model formulated by Armstrong and Frederick. It is based on a physical mechanism of strain hardening and dynamic recovery and is capable of simulating the multiaxial Bauschinger effect (movement of the yield surface in the stress space). Therefore, the model has been examined and implemented in commercial software and finite element analysis.

The Armstrong-Frederick model (AF) is a modification of the MelanPrager linear kinematic hardening model. The only modification of this simple model is the "recall" term which changes the evolution law for the symmetric backstress tensor σ_b from a classical linear kinematic hardening law (MelanPrager) to a nonlinear kinematic hardening law. The term is proportional to the current back stress multiplied by the norm of the plastic strain rate. According to the Armstrong-Frederick rule, the evolution of the back stress is governed by the differential equation:

$$\dot{\sigma}_b = \underbrace{\bar{H}_K \dot{\varepsilon}_p}_{lin.kin.hardening} - \underbrace{\gamma \dot{p} \sigma_b}_{recall-term,nonlinearhardening} \quad (119)$$

where \dot{p} is the accumulated plastic strain rate given as $\sqrt{\frac{2}{3} \|\dot{\varepsilon}_p\|^2}$. The constants \bar{H}_K and γ are determined from uniaxial tests. At the onset of yielding, the back stress is still zero and Eq.(119) gives the same response as the linear hardening law Eq.(118). As the back stress develops, the additional term becomes activated and slows down the rate at which the back stress grows (i.e. reduces the tangent plastic modulus).

5.5. Weakening scales and yield function

5.5.1. The concept of weakening scales

We follow the Dan Van paradigm. The structure is elastic at the macroscopic scale. At each material points, there is a stochastic distribution of weak points which will undergo strong plastic yielding, without contributing to the overall macroscopic stress. From a microscopic point of view, there is a distribution of weakening scales, namely $s \in [1, \infty)$. Let S_{max} be the macroscopic stress intensity at present time. Let σ_y be the yield limit before weakening. Then we imagine that for a given scale s :

- either $1 \leq s \leq \sigma_y/S_{max}$, then $S_{max} \leq \sigma_y/s$, the material stays in the elastic regime and there is no energy dissipation at this scale.
- or $\sigma_y/S_{max} \leq s \leq \infty$, then $S_{max} \geq \sigma_y/s$, the material is in the plastic regime and there is dissipated energy at scale s , contributing to the fatigue limit, which evolve through kinematic hardening.

In more details, at each scale s of a plastic evolution process there is a weakened yield limit σ_y/s , zero initial plastic strain $\underline{\varepsilon}_p$ and zero initial backstress $\underline{\sigma}_b$ at initial time t_0 .

5.5.2. Distribution of weakening scales

We assume the weakening scales have a probability distribution of power law:

$$P(s) = Cs^{-\beta},$$

where β is a material constant and C is hardening constant. The choice of a power law has two reasons: on one hand, this type of distribution corresponds to a scale invariant process, on the other hand it leads in cyclic loading to a prediction of a number of cycles to life limit as a power law function of the stress intensity. More general laws can also be proposed.

The integrated probability ranging from macroscopic to microscopic stress is unity. From this we can conclude:

$$\int_1^\infty P(s)ds = \left[\frac{Cs^{1-\beta}}{1-\beta} \right]_1^\infty = 0 - \frac{C}{1-\beta} = 1.$$

Then we know $C = \beta - 1$, so the distribution is given by:

$$P(s) = Cs^{-\beta} = (\beta - 1)s^{-\beta}$$

and it is shown in Fig. 36.

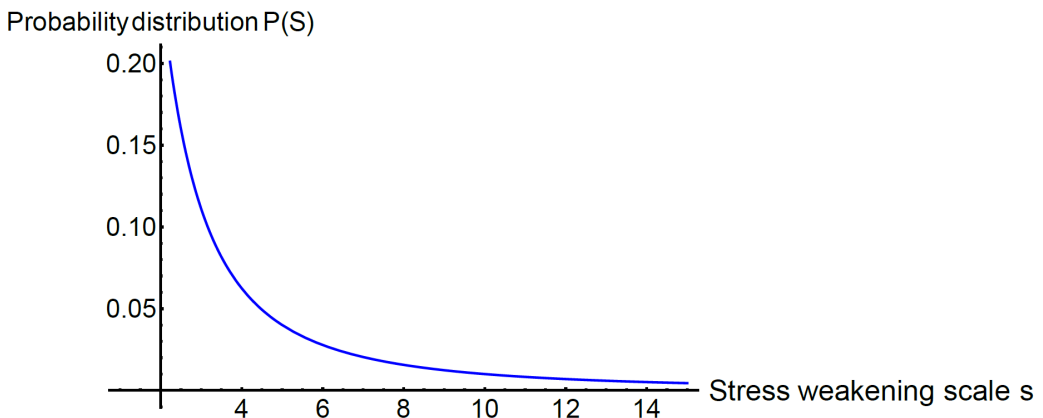


Fig. 36: Weakening scales s probability distribution curve

5.5.3. Yield function with mean stress effect

Positive mean stress clearly reduces the fatigue life of the material. In design evaluation of multiaxial fatigue with mean stress, a simplified, conservative relation between mean stress and equivalent alternating stress is necessary. We can improve the model by modifying the yield function σ_y and the localization tensor.

Christensen approach We can improve the model by modifying the yield function σ_y and the localization tensor. There are several different models of yield function (Johnson Cook model if there is strain hardening, Christensen for mean stress effect), or we could integrate yield function with damage. Moreover, Sylvain Calloch at ENSTA Bretagne may have physical evidence and interpretation on the thermal dissipation in fatigue loading.

The yield function that was given by Christensen[30] integrates measures of damage, as well as intrinsic yield strength and concept of transitions. The derived yield function formalism resulted in the form as:

$$\frac{\alpha K}{\sqrt{3}}\sigma_{kk} + \frac{(1+\alpha)^2}{2}s_{ij}s_{ij} \leq \frac{K^2}{(1+\alpha)}, \quad (120)$$

where α changes the shape of the yield function, thus it is called the shape parameter.

$$\alpha = \frac{|\sigma_{11}^C|}{\sigma_{11}^T} - 1,$$

the new parameter K is called the ideal or intrinsic strength which uniformly expands or contrasts the yield function, thus is is called the scale parameter:

$$K = \frac{(\sigma_{11}^C)^2}{\sqrt{3}\sigma_{11}^T}.$$

The intrinsic strength would occur if there were no damage or microstructure disturbance. σ_{11}^C and σ_{11}^T are respectively compressive and tensile yield stress in uniaxial states ($|\sigma_{11}^C| \geq \sigma_{11}^T$, for ductile materials, $\frac{1}{2} \leq \frac{|\sigma_{11}^C|}{\sigma_{11}^T} \leq 1$). The yield stress in uniaxial and shear states are give by:

$$\begin{aligned} \sigma_{11}^C &= \frac{-\sqrt{3}K}{(1+\alpha)} \\ \sigma_{12}^Y &= \frac{K}{(1+\alpha)^{3/2}} \\ \sigma_{11}^T &= \frac{\sqrt{3}K}{(1+\alpha)^2}. \end{aligned} \quad (121)$$

At $\alpha = 0$, relations Eq.(120) and Eq.(121) show the behavior to be that of purely Mises type. This is taken to be the ideal condition where the intrinsic strength K solely determines the yield strength. As the shape parameter increases beyond the value $\alpha = 1$, the yield function behaves in accordance with a state of increasing crack density or any other physical weakening. The term fracture, as used here for behavior at or near $\alpha = 1$, actually corresponds to fracture mechanics for non-interacting cracks. Beyond this range near $\alpha = 1$ or $\alpha \rightarrow \infty$ has simply been called yield or failure. Parameter α could be easily viewed as a damage measure or microstructure parameter since it represents microstructure changes on any scale that causes deviation from the ideal state.

It is concluded a decrease in mean stress σ_{kk} reduces the effective value of α . That is, moving the behavior toward ductile case. Alternatively, increasing the mean stress moves α toward larger values, which is taken to be that of brittle behavior.

The fully expanded form of the yield function Eq.(120) is:

$$\begin{aligned} & \frac{\alpha K}{\sqrt{3}}(\sigma_{11} + \sigma_{22} + \sigma_{33}) \\ & + (1+\alpha)^2 \left[\frac{(\sigma_{11} - \sigma_{22})^2 + (\sigma_{22} - \sigma_{33})^2 + (\sigma_{33} - \sigma_{11})^2}{6} + (\sigma_{12}^2 + \sigma_{23}^2 + \sigma_{31}^2) \right] \\ & \leq \frac{K^2}{(1+\alpha)}. \end{aligned} \quad (122)$$

The most compact form of Eq.(120) is:

$$\frac{1}{2} s_{ij} s_{ij} \leq \eta K^2, \quad (123)$$

where η is a nondimensional scaling factor on K^2 , determined by mean normal stress.

$$\eta = \frac{1 - \frac{\alpha(1+\alpha)}{\sqrt{3}K} \sigma_{kk}}{(1+\alpha)^3} < 1$$

The mean stress σ_{kk} has a positive relationship with the shape parameter α . We suppose the material endures transition from ductile to brittle when α reaches 1. That means α has a very similar physical meaning with the damage parameter D .

The Gerber parabola Several models are available addressing the influence of tensile mean stress on fatigue life. Among these are the Gerber (Germany, 1874), Goodman (England, 1899), and Soderberg (USA, 1930) models. The modified Goodman criterion is often used as a design criterion because it is more conservative than the Gerber criterion. The use of the Gerber criterion in the determination of member size is generally more computationally intensive and so rather unattractive for many designers.

The effect of mean stress on the fatigue strength is commonly presented in Haigh diagrams as shown in Fig. 37, where S_a/S_f is plotted against S_m/S_u . So is the fatigue strength at a given life under fully reversed ($S_m = 0, R = -1$) conditions. S_u is the ultimate tensile strength. S_f is the reversed fatigue strength. The data points thus represent combinations of S_a and S_m giving that life. The results were obtained for small unnotched specimens, tested at various tensile mean stresses. The straight lines are the modified Goodman and the Soderberg lines, and the curved line is the Gerber parabola. These are empirical relationships that are represented by the following equations:

$$\text{Modified Goodman: } S_a/S_f + S_m/S_u = 1$$

$$\text{Gerber: } S_a/S_f + (S_m/S_u)^2 = 1$$

$$\text{Soderberg: } S_a/S_f + S_m/S_u = 1$$

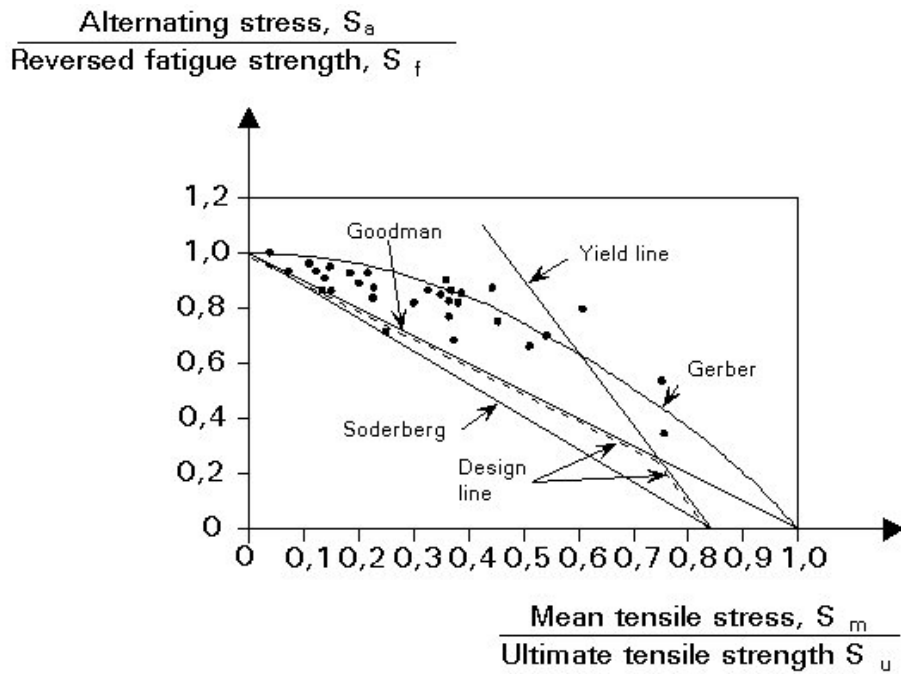


Fig. 37: Haigh diagram showing test data points for the effect of mean stress, and the Gerber, modified Goodman and Soderberg relations.

The idea is to consider as in Maitournam and Krebs[31] that the yield limit σ_y can be reduced in presence of positive mean stress. The mesoscopic yield function can therefore be written as:

$$f(s) = \|\underline{\underline{S}}(s) - \underline{\underline{b}}(s)\| + (\lambda \Sigma_H - \sigma_y) / s \leq 0 \quad (124)$$

with $\underline{\underline{S}}$ denoting the deviatoric part of the stress tensor at microscale, and $\underline{\underline{b}}(s)$ the corresponding backstress at the same scale. The material remain in elastic regime when $f < 0$ and in plastic regime when $f = 0$.

5.5.4. Local plastic model

First we should describe the mesoscopic stress state. The model considers a plastic behavior at the mesoscopic scale. The mesoscopic evolution equations are thus:

$$\underline{\dot{\Sigma}}(s, M, t) = \text{dev}\underline{\dot{\Sigma}}(M, t) - \frac{E}{1 + \gamma} \underline{\dot{\varepsilon}}^p(s, M, t), \quad (125)$$

which defines a Taylor-Lin scale transition model with unit localization tensor[32].

$$\underline{\dot{b}}(s, M, t) = \frac{kE}{E - k} \underline{\dot{\varepsilon}}^p(s, M, t), \quad (126)$$

which is our isotropic kinematic hardening model.

$$\underline{\dot{\varepsilon}}^p(s, M, t) = \gamma \frac{\partial f(s, M, t)}{\partial \underline{S}}, \quad (127)$$

which is the associated plastic flow rule assuming $\gamma = 0$ when $f < 0$ and $\gamma \geq 0$ when $f = 0$.

Here E denotes the Young's modulus and k the hardening parameter. The local dissipated energy rate per volume at weakening scales s is given by the local entropy dissipation:

$$\dot{w}(s, M, t) = (\underline{S} - \underline{b})(s, M, t) : \underline{\dot{\varepsilon}}^p(s, M, t). \quad (128)$$

5.5.5. Energy dissipation in shear cycle with mean stress

Calibration on 39NiCrMo3 steel Monotonic properties of the 39NiCrMo3 steel:

Young modulus $E = 206000 \text{ MPa}$

Tensile strength $\sigma_u = 856 \text{ MPa}$

Tensile yield strength $\sigma_y = 625 \text{ MPa}$

Table 2: Torsion test results on the 39NiCrMo3 steel

$\tau_m = 0$		$\tau_m = 45 \text{ MPa}$		$\tau_m = 90 \text{ MPa}$	
τ_a	N_f	τ_a	N_f	τ_a	N_f
255	5,00E+06	240	5,00E+06	240	5,00E+06
255	5,00E+06	255	5,00E+06	240	5,00E+06
255	5,00E+06	255	5,00E+06	240	5,00E+06
255	5,00E+06	255	3,54E+06	240	5,00E+06
255	5,00E+06	255	5,00E+06	255	2,29E+06
270	2410000	255	5,00E+06	255	5,00E+06
270	1076000	255	5,00E+06	255	2,53E+06
270	1720000	255	5,00E+06	255	2,95E+06
270	1263000	270	2516000	255	5,00E+06
270	5,00E+06	270	1397000	255	3,85E+06
270	1,58E+06	270	7,24E+05	255	3,21E+06
285	697000	270	2,55E+06	270	6,55E+05
285	2,89E+05	270	2,05E+06	270	1,06E+06

The results are plotted in Fig. 38. Collaborated parameters are shown in Table. 3.

5.6. Construction of an energy based fatigue approach

In a preliminary step, we will consider a simple macroscopic loading history $\underline{\Sigma}(M, t)$ which is uniaxial and time periodic of deviatoric amplitude S_{max} , and a Von Mises flow rule to see if we get a prediction of local failure for a number of cycles N_F varying as $\Sigma^{-\beta}$.

In uniaxial cyclic loading, there will be 3 kinds of loading patterns, as is shown in Fig. 39:

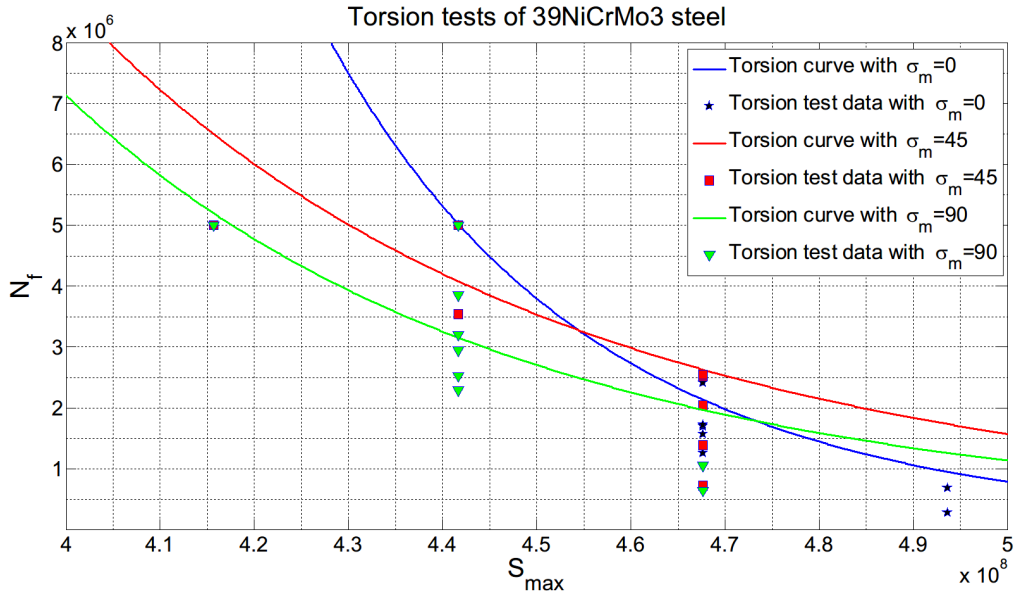


Fig. 38: Torsion test with mean stress

Table 3: Parameter comparison of SM45C

	Yield stress(MPa)	W_F	β	k	λ
$\tau_m = 0 MPa$	625	1.336E10	13.92	0.3404	0
$\tau_m = 45 MPa$	625	5.102E11	6.671	0.506	1.734
$\tau_m = 90 MPa$	625	4.907E12	7.221	0.9293	3.003

1. Elastic regime, in phase 2 and 4, where $\underline{\dot{\varepsilon}}^p(s, M, t) = 0$, and $|\underline{S} - \underline{b}| < (\sigma_y - \lambda \Sigma_H) / s$.
2. Plastic regime according to plastic flow rule, with increasing plastic deformation, in phase 5 and 1, where $\underline{\dot{\varepsilon}}^p(s, M, t) = \gamma \frac{\underline{S}(s) - \underline{b}(s)}{\|\underline{S}(s) - \underline{b}(s)\|} > 0$ with $\gamma = (dev \dot{\Sigma}) \left(\frac{kE}{E-k} + \frac{E}{1+\nu} \right)^{-1}$, with $\underline{S} - \underline{b} = (\sigma_y - \lambda \Sigma_H) / s$ and $\dot{\underline{S}} - \dot{\underline{b}} = 0$.
3. Plastic regime in the other direction, in phase 3, there is $\underline{\dot{\varepsilon}}^p(s, M, t) < 0$, then $\underline{S} - \underline{b} = -(\sigma_y - \lambda \Sigma_H) / s$ and $\dot{\underline{S}} - \dot{\underline{b}} = 0$

Phase 1: The deviatoric stress amplitude increases from σ_y / s to S_{max} .

The material is in local plastic regime, then $\dot{\varepsilon}^p > 0$ and $\dot{\sigma} - \dot{b} = 0 \Rightarrow \dot{\Sigma} - \frac{E}{1+\nu} \dot{\varepsilon}^p = \frac{kE}{E-k} \dot{\varepsilon}^p \Rightarrow$

$$\dot{\varepsilon}^p = \frac{(E-k)(1+\nu)}{E(E+k\nu)} \dot{\Sigma}.$$

$$\Rightarrow \dot{\varepsilon}^p \text{ varies from 0 to } \frac{(E-k)(1+\nu)(S_{max} - \sigma_y / s)}{E(E+k\nu)}.$$

From Taylor-Lin scale transition model:

$$\dot{\sigma} = \dot{\Sigma} - \frac{E}{1+\nu} \dot{\varepsilon}_p = \dot{\Sigma} - \frac{E-k}{E-\nu k} \dot{\Sigma} = \frac{k(1-\nu)}{E-k\nu} \dot{\Sigma}.$$

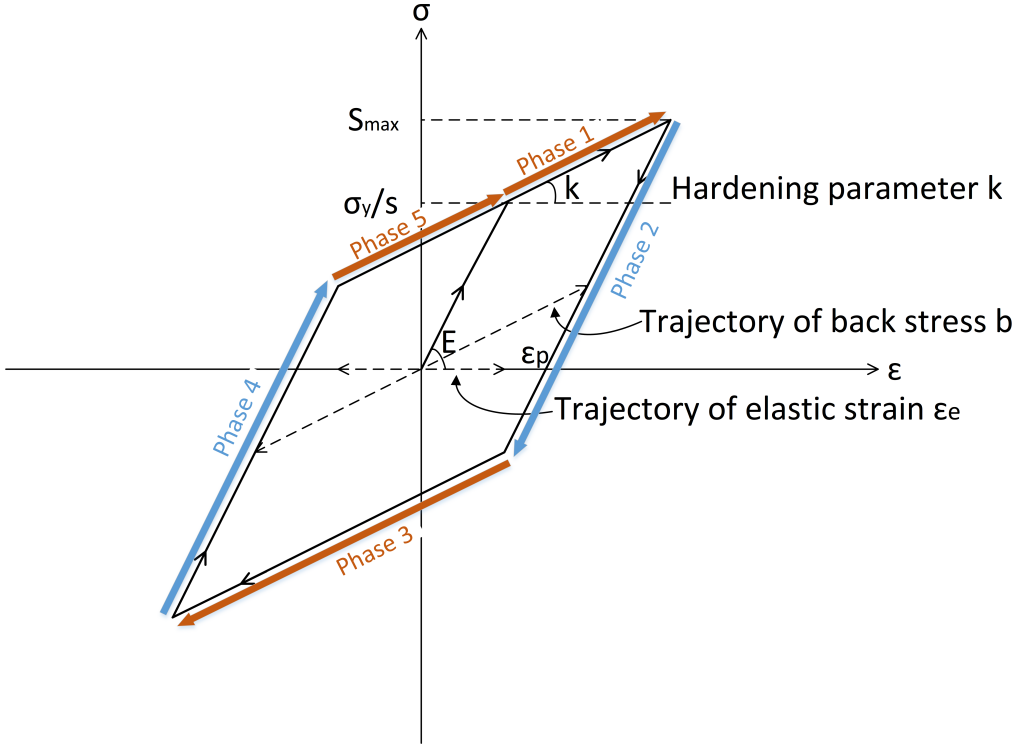


Fig. 39: Uniaxial load with plastic dissipation

$$\Rightarrow \sigma \text{ varies from } \sigma_y/s \text{ to } \sigma_y/s + \frac{k(1-\nu)(S_{max} - \sigma_y/s)}{E - k\nu}.$$

$$\dot{b} = \dot{\Sigma} - \frac{E}{1+\nu} \dot{\varepsilon}_p = \dot{\Sigma} - \frac{E-k}{E-k\nu} \dot{\Sigma} = \frac{k(1-\nu)}{E-k\nu} \dot{\Sigma}.$$

$$\Rightarrow b \text{ varies from } 0 \text{ to } \frac{k(1-\nu)(S_{max} - \sigma_y/s)}{E - k\nu}.$$

So the energy dissipation rate is:

$$(\sigma - b) \dot{\varepsilon}^p = \frac{\sigma_y}{s} \dot{\varepsilon}^p = \frac{\sigma_y}{s} \frac{(E-k)(1+\nu)}{E(E+k\nu)} \dot{\Sigma}.$$

The energy dissipation is:

$$(\sigma - b) \Delta \varepsilon^p = \frac{\sigma_y}{s} \frac{(E-k)(1+\nu)(S_{max} - \sigma_y/s)}{E(E+k\nu)}.$$

Phase 2: The deviatoric stress amplitude decreases from S_{max} to $S_{max} - 2\sigma_y/s$. The material is in local elastic regime, then $\dot{\varepsilon}^p = 0$ and $\dot{\sigma} - \dot{b} = 0 \Rightarrow$

$$\dot{b} = 0, \dot{\sigma} = \dot{\Sigma} - \frac{E}{1+\nu} \dot{\varepsilon}_p = \dot{\Sigma}.$$

$$\sigma \text{ varies from } \sigma_y/s + \frac{k(1-\nu)(S_{max} - \sigma_y/s)}{E - k\nu} \text{ to } -\sigma_y/s + \frac{k(1-\nu)(S_{max} - \sigma_y/s)}{E - k\nu}.$$

$$\sigma - b \text{ varies from } \sigma_y/s \text{ to } -\sigma_y/s.$$

The energy dissipation rate is:

$$(\sigma - b)\dot{\varepsilon}^p = 0.$$

Phase 3: The deviatoric stress amplitude decreases from $S_{max} - 2\sigma_y/s$ to $-S_{max}$. The material is in local plastic regime, then $\dot{\varepsilon}^p > 0$ and $\dot{\sigma} - \dot{b} = 0 \Rightarrow$

$$\dot{\varepsilon}^p = \frac{(E - k)(1 + \nu)}{E(E + k\nu)} \dot{\Sigma}$$

as opposite to phase 1 for $\dot{\Sigma} < 0$.

$$\Rightarrow \varepsilon^p \text{ varies from } \frac{(E - k)(1 + \nu)(S_{max} - \sigma_y/s)}{E(E + k\nu)} \text{ to } \frac{(E - k)(1 + \nu)(S_{max} - \sigma_y/s - S_{max} - (S_{max} - 2\sigma_y/s))}{E(E + k\nu)} = -\frac{(E - k)(1 + \nu)(S_{max} - \sigma_y/s)}{E(E + k\nu)}.$$

From Taylor-Lin scale transition model:

$$\begin{aligned} \dot{\sigma} &= \dot{\Sigma} - \frac{E}{1 + \nu} \dot{\varepsilon}_p = \dot{\Sigma} - \frac{E - k}{E - \nu k} \dot{\Sigma} = \frac{k(1 - \nu)}{E - \nu k} \dot{\Sigma}. \\ \Rightarrow \sigma &\text{ varies from } -\sigma_y/s + \frac{k(1 - \nu)(S_{max} - \sigma_y/s)}{E - \nu k} \text{ to } -\sigma_y/s - \frac{k(1 - \nu)(S_{max} - \sigma_y/s)}{E - \nu k}. \\ \dot{b} &= \dot{\Sigma} - \frac{E}{1 + \nu} \dot{\varepsilon}_p = \dot{\Sigma} - \frac{E - k}{E - \nu k} \dot{\Sigma} = \frac{k(1 - \nu)}{E - \nu k} \dot{\Sigma}. \\ \Rightarrow b &\text{ varies from } \frac{k(1 - \nu)(S_{max} - \sigma_y/s)}{E - \nu k} \text{ to } -\frac{k(1 - \nu)(S_{max} - \sigma_y/s)}{E - \nu k}. \end{aligned}$$

So the energy dissipation rate is:

$$(\sigma - b)\dot{\varepsilon}^p = -\frac{\sigma_y}{s} \dot{\varepsilon}^p = -\frac{\sigma_y}{s} \frac{(E - k)(1 + \nu)}{E(E + k\nu)} \dot{\Sigma}.$$

The energy dissipation is:

$$(\sigma - b)\Delta\varepsilon^p = -\frac{\sigma_y}{s} \frac{(E - k)(1 + \nu)(-2S_{max} + 2\sigma_y/s)}{E(E + k\nu)} = \frac{2\sigma_y}{s} \frac{(E - k)(1 + \nu)(S_{max} - \sigma_y/s)}{E(E + k\nu)}.$$

Phase 4: The deviatoric stress amplitude increases from $-S_{max}$ to $-S_{max} + 2\sigma_y/s$. The material is in local elastic regime, then $\dot{\varepsilon}^p = 0$ and $\dot{\sigma} - \dot{b} = 0 \Rightarrow$

$$\dot{b} = 0, \dot{\sigma} = \dot{\Sigma} - \frac{E}{1 + \nu} \dot{\varepsilon}_p = \dot{\Sigma}.$$

$$\sigma \text{ varies from } -\sigma_y/s - \frac{k(1 - \nu)(S_{max} - \sigma_y/s)}{E - \nu k} \text{ to } \sigma_y/s - \frac{k(1 - \nu)(S_{max} - \sigma_y/s)}{E - \nu k}.$$

$\sigma - b$ varies from $-\sigma_y/s$ to σ_y/s .

So the energy dissipation rate is:

$$(\sigma - b)\dot{\varepsilon}^p = 0.$$

Phase 5: The deviatoric stress amplitude increases from $-S_{max} + 2\sigma_y/s$ to σ_y/s . The material is in local plastic regime, then $\dot{\varepsilon}^p > 0$ and $\dot{\sigma} - \dot{b} = 0 \Rightarrow$

$$\dot{\varepsilon}^p = \frac{(E - k)(1 + \nu)}{E(E + k\nu)} \dot{\Sigma}$$

as in phase 1.

$$\Rightarrow \dot{\varepsilon}^p \text{ varies from } -\frac{(E-k)(1+\nu)(S_{max}-\sigma_y/s)}{E(E+k\nu)} \text{ to } 0.$$

$$\dot{\sigma} = \dot{\Sigma} - \frac{E}{1+\nu} \dot{\varepsilon}_p = \dot{\Sigma} - \frac{E-k}{E-\nu k} \dot{\Sigma} = \frac{k(1-\nu)}{E-k\nu} \dot{\Sigma}.$$

$$\Rightarrow \sigma \text{ varies from } \sigma_y/s - \frac{k(1-\nu)(S_{max}-\sigma_y/s)}{E-k\nu} \text{ to } \sigma_y/s.$$

$$\dot{b} = \dot{\Sigma} - \frac{E}{1+\nu} \dot{\varepsilon}_p = \dot{\Sigma} - \frac{E-k}{E-\nu k} \dot{\Sigma} = \frac{k(1-\nu)}{E-k\nu} \dot{\Sigma}.$$

$$\Rightarrow b \text{ varies from } -\frac{k(1-\nu)(S_{max}-\sigma_y/s)}{E-k\nu} \text{ to } 0.$$

So the energy dissipation rate is:

$$(\sigma - b) \dot{\varepsilon}^p = \frac{\sigma_y}{s} \dot{\varepsilon}^p = \frac{\sigma_y}{s} \frac{(E-k)(1+\nu)}{E(E+k\nu)} \dot{\Sigma}.$$

The energy dissipation is:

$$(\sigma - b) \Delta \varepsilon^p = \frac{\sigma_y}{s} \frac{(E-k)(1+\nu)(S_{max}-\sigma_y/s)}{E(E+k\nu)}.$$

From the three phase analysis in local plastic regime, the dissipated energy is like $dW(\text{phase1}) = \frac{1}{2} dW(\text{phase3}) = dW(\text{phase5})$ and the dissipation rate is like $d\dot{W}(\text{phase1}) = d\dot{W}(\text{phase3}) = d\dot{W}(\text{phase5})$.

$$d\dot{W} = \frac{(E-k)(1+\nu)}{E(E-k\nu)} \left(\frac{\sigma_y}{s} \right) |\dot{\Sigma}| \quad (129)$$

We can then calculate the local dissipated energy W at point M during one cycle by cumulating the input of all sub-scales with their probabilities [33].

$$\begin{aligned} W_{\text{cyc}} &= 4 \int_{(\sigma_y - \lambda \Sigma_H)/S_{max}}^{\infty} dW(s, M, t) P(s) ds \\ &= 4 \int_{(\sigma_y - \lambda \Sigma_H)/S_{max}}^{\infty} \frac{(E-k)(1+\nu)}{E(E+k\nu)} \frac{\sigma_y - \lambda \Sigma_H}{s} \left(S_{max} - \frac{\sigma_y - \lambda \Sigma_H}{s} \right) (\beta - 1) s^{-\beta} ds \\ &= \frac{4(E-k)(1+\nu)(\beta-1)}{E(E+k\nu)\beta(\beta+1)} \frac{S_{max}^{\beta+1}}{\left(\sigma_y - \lambda \Sigma_H \right)^{\beta-1}}. \end{aligned} \quad (130)$$

If the dissipated energy accumulates linearly until a failure value W_F , we can get directly the time to failure from Eq.(131):

$$T_{\text{fail}} = N_F t_{\text{cyc}} = \frac{W_F}{W_{\text{cyc}}} t_{\text{cyc}} = C(S_{max})^{-\beta-1}. \quad (131)$$

From Eq.(130), we then obtain that the model predicts as expected a power law dependence in function of S_{max} . However, experiments shows that the damage or the energy accumulation of a material evolves non-linearly in time. We should introduce below a method to handle such a nonlinearity.

5.7. Nonlinearity of damage accumulation

5.7.1. Energy approach with Chaboche law

The Chaboche law[23] is essentially a damage incremental law for cyclic loading of stress intensity σ with a deviatoric part A_{II} and hydrostatic part Σ_H , defining the damage increase by:

$$\delta D = (1 - (1 - D)^{\gamma+1})^\alpha \left(\frac{A_{II}/(1 - D)}{M(\Sigma_H)} \right)^\gamma \delta N \quad (132)$$

which writes equivalently as Eq.(133)

$$\delta[1 - (1 - D)^{\gamma+1}]^{1-\alpha} = (1 - \alpha)(\gamma + 1) \left(\frac{A_{II}}{M(\Sigma_H)} \right)^\gamma \delta N = \frac{\delta N}{N_F(\sigma)}. \quad (133)$$

Here $N_F(\sigma)$ denotes the number of cycles at intensity σ to failure as obtained by integration of Eq.(133) from $D = 0$ to $D = 1$.

In our model, in case of a simple uniaxial cyclic loading, we propose to replace $\frac{1}{N_F(\sigma)}$ which is the relative unit increment of cycles by $\frac{W_{cyc}}{W_F}$, yielding the nonlinear damage incremental law:

$$\delta[1 - (1 - D)^{\gamma+1}]^{1-\alpha} = \frac{W_{cyc}}{W_F} \delta N. \quad (134)$$

This is a nonlinear law but used with a constant α , there will be no sequence effect. In other words, when applying two successive cycles of different intensities, the failure will occur at the same number of cycles whatever the order of the loading(high then low versus low then high).

5.7.2. Generalized damage accumulation

Formula (133) is a general accumulation law which can be applied for any cyclic loading sequence provided that we can identify the multiscale value of the dissipated energy per cycle.

But the notion of cycle itself may be hard to identify for general loadings. The idea is then to replace the relative increment of dissipated energy per cycle by the relative increment of dissipated energy per unit time, yielding:

$$\delta[1 - (1 - D)^{\gamma+1}]^{1-\alpha} = \frac{\dot{W}}{W_F} \delta t. \quad (135)$$

In a general loading case, \dot{W} is to be computed. By integrating Eq.(128) over all microscales, we get:

$$\dot{W}(M, t) = \int_{s=1}^{\infty} \dot{w}(s, M, t) P(s) ds = \int_{s=1}^{\infty} (\underline{S} - \underline{b})(s, M, t) : \underline{\dot{\varepsilon}}^p(s, M, t) P(s) ds. \quad (136)$$

The evolution of \underline{S} , \underline{b} and $\underline{\dot{\varepsilon}}^p$ are given in section 1.4. Equation (135) and (136) are therefore our proposed damage law.

6 Numerical implementation and validation

6.1. Integration rules for \dot{W} and δD

Our first approach takes one cycle as unit time. We compute analytically the energy dissipation at each scale during this cycle. The method is valid for simple loading history and which includes the integration on all weakening scales. The damage D is accumulated after each cycle.

However, there are certain limitations of this method. Firstly we need a load history decomposition in cycles. Secondly in real life the perfect close loop cycle is hardly applicable.

Thus we propose in Eq.(135) a more general method which can be integrated by a step by step strategy. We compute numerically the dissipation at different scales using an implicit Euler time integration of the

constitutive laws of section 1.4. After which we make a numerical integration on different scales. Then we can update the damage and go to next time step.

Instead of doing the scale integration directly which can be difficult for complex loading, the Gaussian Quadrature rule with Legendre points is used to give the value of local dissipated energy rate.

To use the Gaussian quadrature rule the limit range of integral must be from -1 to 1 , while the total dissipated energy is expressed by integrating all the weakening scale s ranging from 1 to infinity with their occurrence probabilities:

$$\dot{W} = \int_1^\infty \dot{w}(s)(\beta - 1)(s)^{-\beta} ds.$$

To change the limit range of integral from $[1, \infty]$ to $[1, 0]$ we take as new integration variable $u(s) = s^{-p}$ with $p = \beta - 1$, yielding $u(1) = 1$ and $u(\infty) = 0$ with

$$du = -ps^{-p-1} ds$$

that is

$$du = (-\beta + 1)s^{-\beta} ds = (-\beta + 1)u^{\frac{1}{1-\beta}} du.$$

Therefore the dissipated energy summed on all scales is:

$$\begin{aligned} \dot{W} &= \int_1^\infty \dot{w}(s)(\beta - 1)(s)^{-\beta} ds \\ &= \int_1^0 \dot{w}\left(u^{\frac{1}{1-\beta}}\right)(\beta - 1)\frac{1}{-\beta + 1} du \\ &= \int_0^1 \dot{w}\left(u^{\frac{1}{1-\beta}}\right)(\beta - 1)\frac{1}{\beta - 1} du \\ &= \int_0^1 \dot{w}\left(u^{\frac{1}{1-\beta}}\right) du \\ &= \frac{1}{2} \int_{-1}^1 \dot{w}\left[\left(\frac{x+1}{2}\right)^{\frac{1}{1-\beta}}\right] dx \end{aligned} \quad (137)$$

if we set $u = \frac{x+1}{2}$.

So the dissipated energy rate integrated over all scales takes the form of Eq.(138):

$$\dot{W} = \frac{1}{2} \int_{-1}^1 \dot{w}\left[\left(\frac{x+1}{2}\right)^{\frac{1}{1-\beta}}, t\right] dx \approx \frac{1}{2} \sum_i \omega_i \dot{w}\left[\left(\frac{x_i+1}{2}\right)^{\frac{1}{1-\beta}}, t\right], \quad (138)$$

where ω_i and x_i are respectively the weights and nodes of the Gauss Legendre integration rule used for the numerical integration. In this work, we used 25 points[34]. After changing the integration limit, $\left(\frac{x+1}{2}\right)^{\frac{1}{1-\beta}}$ represents the scale s . The values are shown in Table.4.

After changing the integration limit, $\left(\frac{x+1}{2}\right)^{\frac{1}{1-\beta}}$ represents the weakening scale s .

Damage accumulation is deduced from Eq.(135):

$$g_{n+1} = g_n + \frac{\dot{W}dt}{W_F} \quad (139)$$

with $g_n = [1 - (1 - D_n)^{\gamma+1}]^{1-\alpha}$.

We upgrade the damage step by step following Eq.(139). When D reaches one, the material fails.

Table 4: Weighting factors ω , function arguments x used in Gauss Quadrature Formulas and equivalent scales s' .

Scales x_i	Scales s'_i	Scale weighting factors ω_i
-0.99555697	21.21658	0.011393799
-0.976663921	9.257656	0.026354987
-0.942974571	5.922168	0.040939157
-0.894991998	4.364192	0.054904696
-0.833442629	3.465238	0.068038334
-0.759259263	2.882307	0.0801407
-0.673566368	2.475241	0.091028262
-0.57766293	2.176133	0.100535949
-0.473002731	1.948098	0.108519624
-0.361172306	1.769388	0.114858259
-0.243866884	1.626357	0.119455764
-0.122864693	1.510017	0.122242443
0	1.414214	0.123176054
0.122864693	1.334601	0.122242443
0.243866884	1.268026	0.119455764
0.361172306	1.212156	0.114858259
0.473002731	1.165234	0.108519624
0.57766293	1.125921	0.100535949
0.673566368	1.093185	0.091028262
0.759259263	1.066228	0.0801407
0.833442629	1.044435	0.068038334
0.894991998	1.027333	0.054904696
0.942974571	1.014569	0.040939157
0.976663921	1.005886	0.026354987
0.99555697	1.001113	0.011393799

6.2. Regime determination under multiple scales

The material could be both in elastic and plastic regime under different scales. To be more elaborate, we reuse the fundamental equations in different regimes. At scale s , we have a dissipation rate given by:

$$\dot{w}(s) = \left(\underline{\underline{S}} - \underline{\underline{b}} \right) : \dot{\underline{\underline{\varepsilon}}}^p,$$

which differs between plastic and elastic regime.

Elastic regime:

There we have $\dot{\underline{\underline{\varepsilon}}}^p = 0$, $\dot{\underline{\underline{b}}} = 0$ and $\dot{\underline{\underline{S}}} = \text{dev} \dot{\underline{\underline{\Sigma}}}$, so

$$\dot{\underline{\underline{S}}} - \dot{\underline{\underline{b}}} = \text{dev} \dot{\underline{\underline{\Sigma}}},$$

yielding

$$\left(\underline{\underline{S}} - \underline{\underline{b}} \right) (t + dt) = \left(\underline{\underline{S}} - \underline{\underline{b}} \right) (t) + \text{dev} \dot{\underline{\underline{\Sigma}}} dt := \left(\underline{\underline{S}} - \underline{\underline{b}} \right)_{\text{trial}} (s, t + dt). \quad (140)$$

We are in elastic regime at scale s as long as we satisfy

$$\left(\underline{\underline{S}} - \underline{\underline{b}} \right) (t + dt) \leq \left(\sigma_y - \lambda \Sigma_H \right) / s.$$

Plastic regime:

When we leave elastic regime at scale s , we have:

$$\left\{ \begin{array}{ll} \underline{\dot{\varepsilon}}^p = \gamma \frac{\underline{S} - \underline{b}}{\|\underline{S} - \underline{b}\|}, \gamma > 0, & \text{plastic flow,} \\ \|\underline{S} - \underline{b}\| = (\sigma_y - \lambda \Sigma_H) / s, & \text{yield limit,} \end{array} \right. \quad (141)$$

$$\left\{ \begin{array}{ll} (\underline{S} - \underline{b}) : (\dot{\underline{S}} - \dot{\underline{b}}) = 0, & \text{yield limit time invariance,} \end{array} \right. \quad (143)$$

$$\dot{\underline{b}} = \frac{kE}{E - k} \dot{\underline{\varepsilon}}^p, \quad \text{kinematic hardening rule,} \quad (144)$$

$$\dot{\underline{S}} = \text{dev} \dot{\underline{\Sigma}} - \frac{E}{1 + \nu} \dot{\underline{\varepsilon}}^p, \quad \text{localisation rule.} \quad (145)$$

In all cases, at a certain scale s_i , after elimination of $\dot{\underline{\varepsilon}}^p$, there are

$$\dot{\underline{S}} - \dot{\underline{b}} = \text{dev} \dot{\underline{\Sigma}} - E\gamma \left(\frac{1}{1 + \nu} + \frac{k}{E - k} \right) \frac{\underline{S} - \underline{b}}{\|\underline{S} - \underline{b}\|}.$$

If we are at yield limit at $(t+dt)$, we get on the other hand:

$$\begin{aligned} (\underline{S} - \underline{b})(t + dt) &= (\underline{S} - \underline{b})(t) + (\dot{\underline{S}} - \dot{\underline{b}})dt, \\ \left\| (\underline{S} - \underline{b})(t + dt) \right\| &= (\sigma_y - \lambda \sigma_m) / s_i. \end{aligned} \quad (146)$$

Replacing $(\dot{\underline{S}} - \dot{\underline{b}})$ in the integration by its expression we get:

$$(\underline{S} - \underline{b})(t + dt) = (\underline{S} - \underline{b})(t) + \text{dev} \dot{\underline{\Sigma}} dt - E\gamma dt \left(\frac{1}{1 + \nu} + \frac{k}{E - k} \right) \frac{(\underline{S} - \underline{b})(t + dt)}{\|\underline{S} - \underline{b}\|(t + dt)} \quad (147)$$

Putting all terms with $(\underline{S} - \underline{b})(t + dt)$ on the left hand side, we get:

$$(\underline{S} - \underline{b})(t + dt)(1 + \eta) = (\underline{S} - \underline{b})(t) + \text{dev} \dot{\underline{\Sigma}} dt = (\underline{S} - \underline{b})_{\text{trial}}(t + dt) \quad (148)$$

with

$$\eta = \frac{E\gamma dt}{\|\underline{S} - \underline{b}\|(t + dt)} \left(\frac{1}{1 + \nu} + \frac{k}{E - k} \right). \quad (149)$$

To see whether the structure is in elastic or plastic regime at each time step, we use $(\underline{S} - \underline{b})_{\text{trial}}(t + dt)$ to compare with the yield stress at the same scale s_i , thus to give a value to $(\underline{S} - \underline{b})(t + dt)$.

Since $(\underline{S} - \underline{b})(t + dt)$ is in the same direction as $(\underline{S} - \underline{b})_{\text{trial}}(t + dt)$, we have

$$(\underline{S} - \underline{b})(t + dt) = (\sigma_y - \lambda \sigma_m) / s \frac{(\underline{S} - \underline{b})_{\text{trial}}(t + dt)}{\|\underline{S} - \underline{b}\|_{\text{trial}}(t + dt)} \quad (150)$$

We now compare Eq.(148) and Eq.(150), the only solution is to have:

$$1 + \eta = \frac{\|\underline{S} - \underline{b}\|_{trial}}{(\sigma_y - \lambda\sigma_m)/s} \quad (151)$$

that is:

$$\eta = \frac{\|\underline{S} - \underline{b}\|_{trial}}{(\sigma_y - \lambda\sigma_m)/s} - 1 \quad (152)$$

which is positive in plastic regime.

$$(\underline{S} - \underline{b})(s, t + dt) = \frac{(\underline{S} - \underline{b})_{trial}(s, t + dt)}{1 + \eta}, \quad (153)$$

with

$$\eta = \max \left\{ \underbrace{0}_{\text{elastic regime}}, \underbrace{\frac{\|\underline{S} - \underline{b}\|_{trial}}{(\sigma_y - \lambda\Sigma_H)/s} - 1}_{\text{plastic regime when this number is positive}} \right\},$$

$$(\underline{S} - \underline{b})_{trial}(s, t + dt) = (\underline{S} - \underline{b})(s, t) + \text{dev} \dot{\Sigma}(t) dt.$$

That is to say, when the structure is in elastic regime at time t and scale s , we have $(\underline{S} - \underline{b})(s, t) = (\underline{S} - \underline{b})_{trial}(s, t)$. Otherwise, if the norm of $(\underline{S} - \underline{b})_{trial}(s, t)$ is greater than the local yield limit $(\sigma_y - \lambda\Sigma_H)/s$, $(\underline{S} - \underline{b})(s, t)$ will be projected on the yield limit.

Knowing the distinction between elastic and plastic regime under multiple scales, we compute the general expression of the dissipated energy rate.

$$\dot{w} = (\underline{S} - \underline{b}) : \dot{\underline{\epsilon}}^p = \gamma \frac{\sigma_y - \lambda\Sigma_H}{s}. \quad (154)$$

From Eq.(149) and Eq.(152) in annex, we get:

$$E\gamma dt = \left\langle \|\underline{S} - \underline{b}\|_{trial} - \frac{\sigma_y - \lambda\Sigma_H}{s} \right\rangle / \left(\frac{1}{1 + \nu} + \frac{k}{E - k} \right) = \left\langle \|\underline{S} - \underline{b}\|_{trial} - \frac{\sigma_y - \lambda\Sigma_H}{s} \right\rangle \frac{(E - k)(1 + \nu)}{(E + k\nu)}, \quad (155)$$

where $\langle \rangle$ is Macaulay bracket symbol defined as $\langle m \rangle = 0$ if $m \leq 0$, otherwise $\langle m \rangle = m$.

We replace γ deduced from Eq.(155) in Eq.(154) to give the expression of local energy dissipation rate at scale s :

$$\dot{w} dt = \frac{(E - k)(1 + \nu)}{E(E + k\nu)} \left\langle \|\underline{S} - \underline{b}\|_{trial} - \frac{\sigma_y - \lambda\Sigma_H}{s} \right\rangle \frac{\sigma_y - \lambda\Sigma_H}{s}. \quad (156)$$

With Eq.(138), the final expression of energy dissipation W during time step dt writes:

$$\begin{aligned} W &= \dot{W} dt \\ &= \frac{1}{2} \sum_i \omega_i \dot{w} \left[\left(\frac{x_i + 1}{2} \right)^{\frac{1}{1-\beta}} \right] dt \\ &= \frac{(E - k)(1 + \nu)}{2E(E + k\nu)} \sum_i \omega_i \left\langle \|\underline{S} - \underline{b}\|_{trial} - \frac{\sigma_y - \lambda\Sigma_H}{\left(\frac{x_i + 1}{2} \right)^{\frac{1}{1-\beta}}} \right\rangle \frac{\sigma_y - \lambda\Sigma_H}{\left(\frac{x_i + 1}{2} \right)^{\frac{1}{1-\beta}}}. \end{aligned} \quad (157)$$

We have the damage accumulation deduced in Eq.(139):

$$g_{n+1} = g_n + \frac{\dot{W}dt}{W_F} = g_n + \frac{W}{W_F},$$

$$\text{with } D_n = \left[1 - \left(1 - g_n^{\frac{1}{1-\alpha}} \right)^{\frac{1}{\gamma+1}} \right].$$

Now we are able to put these formula into numerical tests.

6.3. Test on different load histories

6.3.1. One dimensional application to simple cyclic data

The test is first performed on a sinusoidal axial load $\Sigma = C \sin(t)$ with parameters in Table 5, giving a deviatoric amplitude $S_{max} = \sqrt{\frac{2}{3}}C$.

Parameters	Value
Load	$\Sigma = 5e8 \sin(t)$ Pa
Young's modulus	$E = 2e11$ Pa
Hardening parameter	$k = 6e8$ Pa
Weakening scales distribution exponent	$\beta = 3$
Hydrostatic pressure sensitivty	$\lambda = 0.5$
Macroscopic yield stress	$\sigma_y = 6.38e8$ Pa
Material parameter from Chaboche law(Wohler curve exponent)	$\gamma = 0.5$
Non-linearity of damage accumulation	$\alpha = 0.5$
Initial damage	$D = 0$
Initial time	$t = 0$ s
Dissipated energy to failure per unit volume	$W_F = 3e6$ J
Looping step	1e-4 s

Table 5: Material parameters in a simple cyclic load

We use matlab to realize our analytical method. We plot $(\underline{\Sigma} - \underline{b})_{trial}$ and $(\underline{\Sigma} - \underline{b})$ for two different scales ($s_1 = 21.21657929229650$ and $s_8 = 2.176132808422946$) in Fig. 40.

The nonlinearity is determined by

$$\alpha = 1 - a \left\langle \frac{\max_t \sqrt{J_{2,a}(t)} + a_c P_{max}(t) - b_c}{\sigma_u - 2 \max \sqrt{J_{2,a}}} \right\rangle,$$

which is predominated by Crossland criterion, for simplicity we take α as a constant. The damage evolves like in Fig. 41, where we compare the damage evolution as predicted by the cycle accumulation Eq.(130) and by the numerical strategy of section 4.

Now we compare the result to the one demonstrated in Fig. 39. The first cycle has 3 phases which have the energy loss identical to phase 1. The following cycles each have 4 times energy loss as phase 1. We can see from Fig. 42 and Fig. 43 the difference between cyclic load calculation and numerical method as function of time (time step = 1/5000s and 1/15000s separately). Because the step by step damage accumulation grows in a power law, so the amplitude of difference grows with time. However, the difference between the two methods swing around 0 and from Fig. 41 we can see the difference is not symmetrical, we could consider the numerical method converges in cyclic load calculation method.

The cyclic load calculation is only valid for very simple such as proportional loading in fatigue, nevertheless it can still be used as a comparison group to verify the numerical results. The outcome seems satisfactory. Hence, to be more general for any loading history, we adopt the numerical method.

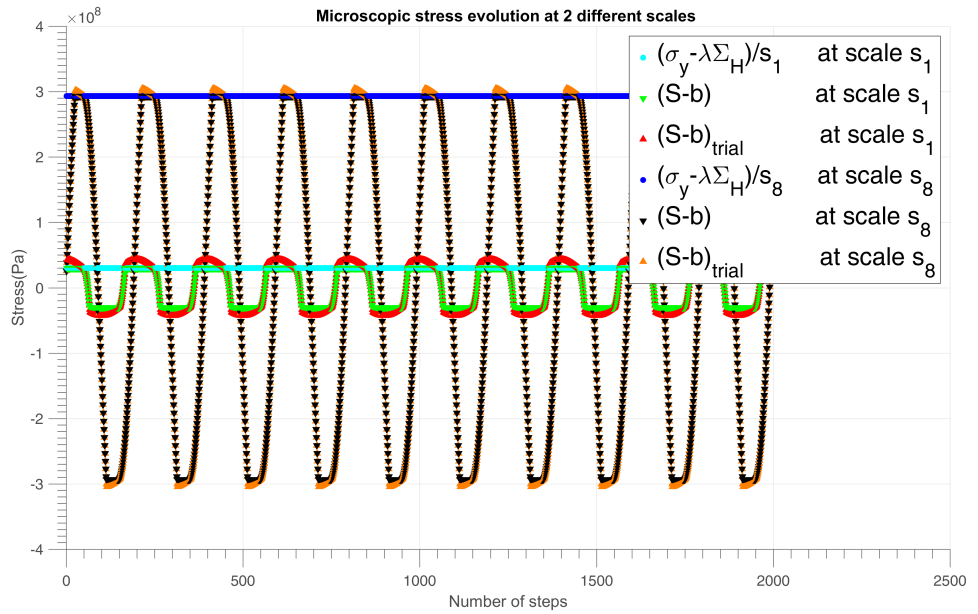


Fig. 40: Microscopic $(\underline{S} - \underline{b})_{trial}$ and $(\underline{S} - \underline{b})$ evolution with time under different weakening scales in sinusoidal load

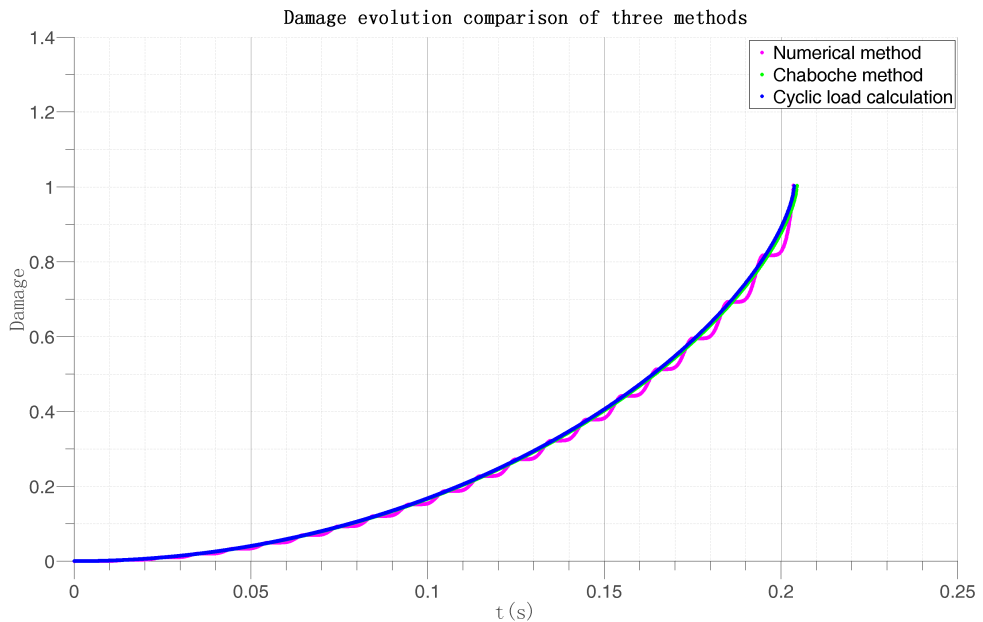


Fig. 41: Damage evolution with time under sinusoidal load with two different methods

6.3.2. One dimensional application to PSA data

In this test, we reconstruct a unidimensional macroscopic stress history from recorded force data proposed by PSA group.

The sample recording rate is 256 per second. In order to accumulate damage using very small steps, we have created 10 additional points between every 2 recorded points by linear interpolation. So the sample

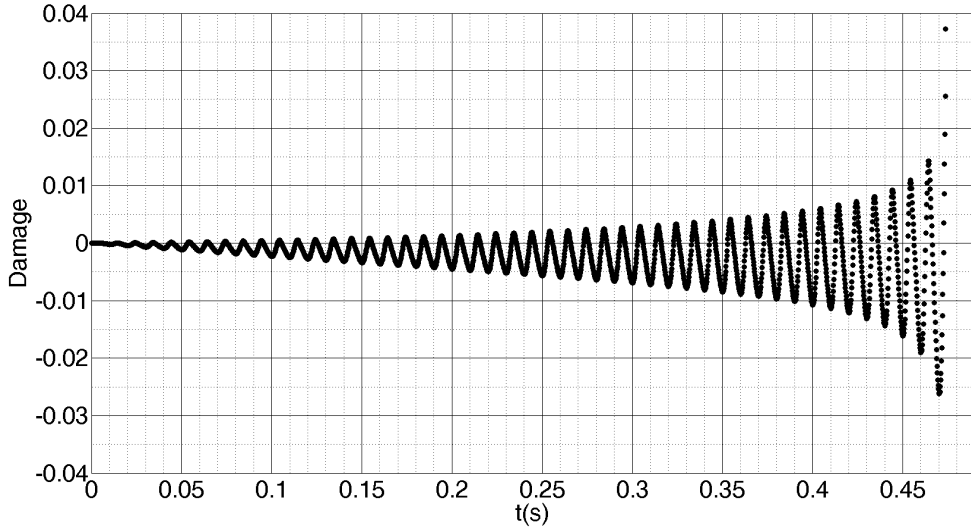


Fig. 42: Difference between cyclic load calculation and numerical method as function of time(time step=1/5000s)

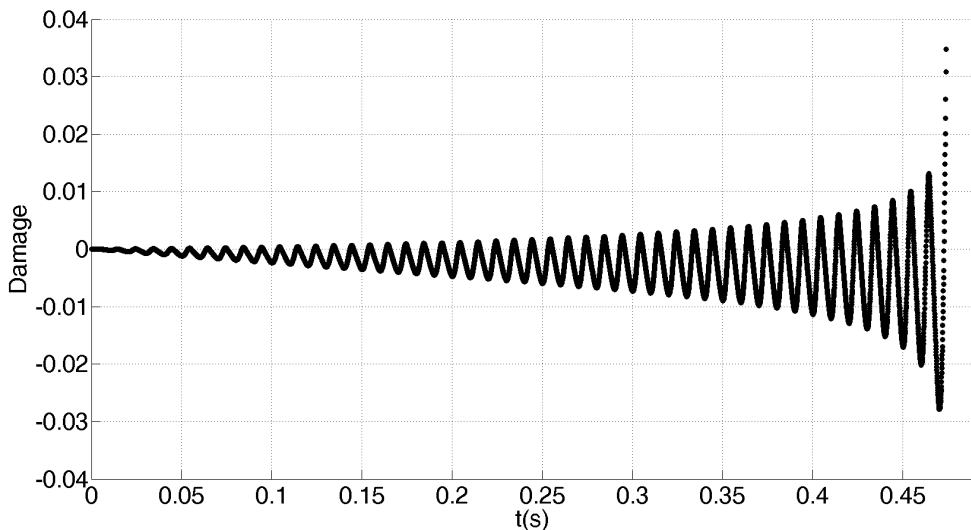


Fig. 43: Difference between cyclic load calculation and numerical method as function of time(time step=1/15000s)

rate is $256 * 10$ per second.

The force on wheel is firstly considered as under uniaxial loading F_x . Here we temporally set $\Sigma_x = F_x/A$ where $A = \frac{1}{1e6} m^2$ is the area of force, and $W_F = 3e6 J$. The other data are as Table 5. The plot of $(\underline{\underline{S}} - \underline{\underline{b}})_{trial}$ and $(\underline{\underline{S}} - \underline{\underline{b}})$ under 2 different scales ($s_1 = 21.21657929229650$ and $s_8 = 2.176132808422946$) are shown in Fig. 45. The damage evolves like Fig. 47.

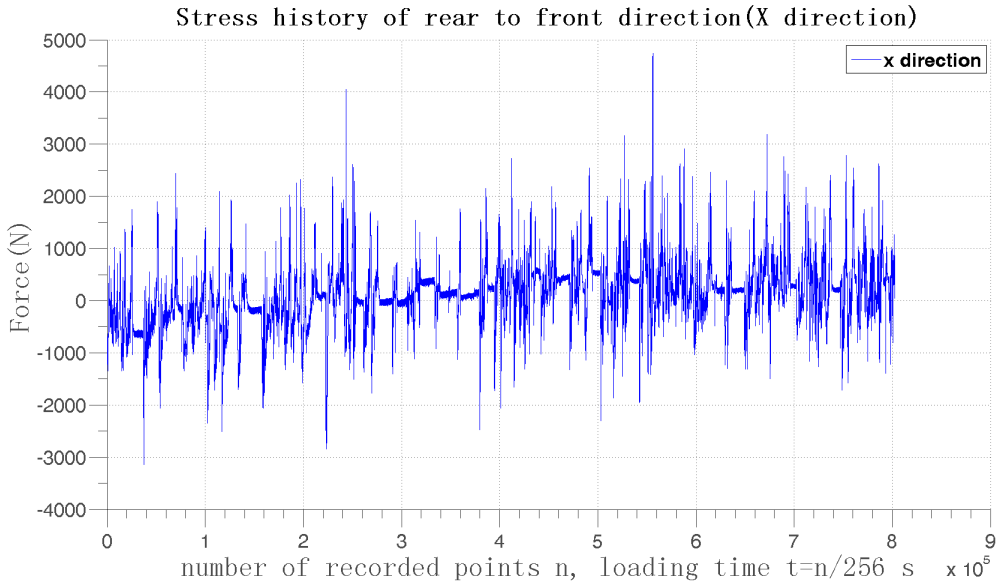


Fig. 44: Loading history of X direction, force vs the record index n, with 256 sample recorded per second

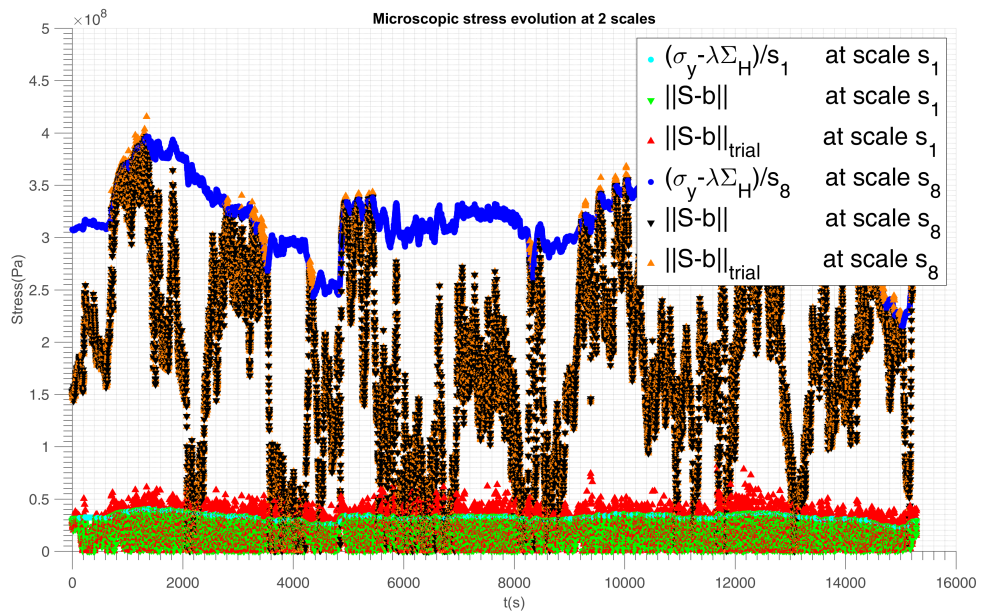


Fig. 45: $(\underline{S} - \underline{b})_{trial}$ and $(\underline{S} - \underline{b})$ evolution with time under different weakening scales in PSA load history

6.3.3. Multi-dimensional application to PSA data

We now consider a situation where we have force recorded measured in 3 different directions as shown in Fig. 48. In real case, the vertical force F_z is much larger than the axial and horizontal forces F_x and F_y , as shown in Fig. 48. However, in order to investigate large domains of interest, we first scale the axial and horizontal forces to reach comparable impact and transform them in principal stresses $c_x \frac{F_x}{A}$ applied along the stress principle vector \underline{e}_α (respectively \underline{e}_β) that we choose randomly (Fig. 49). We therefore consider the

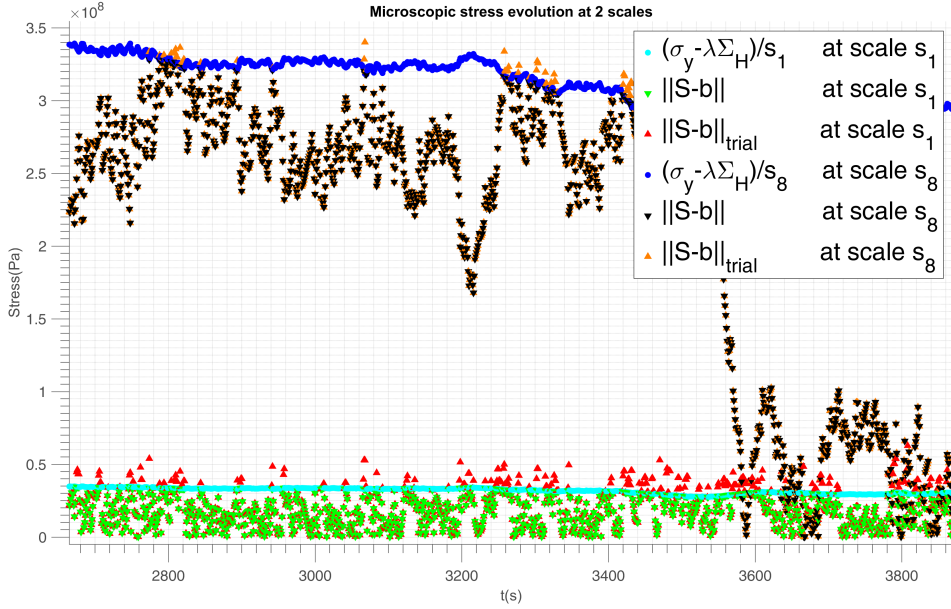


Fig. 46: Circled area magnification in Fig. 45 where there is more $(\underline{\underline{S}} - \underline{\underline{b}})_{trial} > \sigma_y$ (plasticity) at s_1 than at s_8

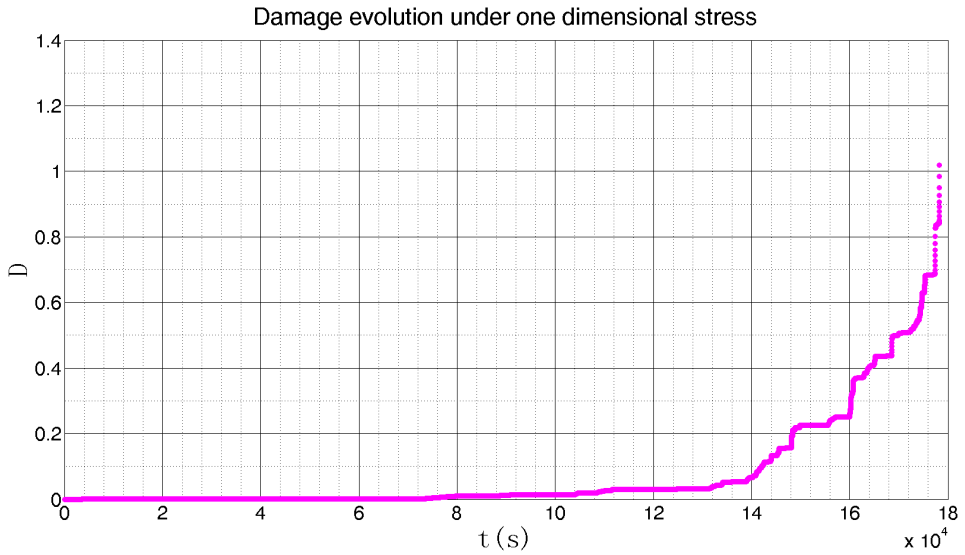


Fig. 47: Damage evolution with time at one dimension PSA load history

following macroscopic stress tensor:

$$\underline{\underline{\Sigma}} = \frac{F_z(t)}{A} \underline{\underline{e}}_1 \otimes \underline{\underline{e}}_1 + c_x \frac{F_x(t)}{A} \underline{\underline{e}}_\alpha \otimes \underline{\underline{e}}_\alpha + c_y \frac{F_y(t)}{A} \underline{\underline{e}}_\beta \otimes \underline{\underline{e}}_\beta \quad (158)$$

where $\underline{\underline{e}}_\alpha$ and $\underline{\underline{e}}_\beta$ are principal vectors whose spherical coordinate are $\theta_x, \varphi_x, \theta_y$ and φ_y respectively:

$$\underline{\underline{e}}_\alpha = \cos \theta_x \underline{\underline{e}}_1 + \sin \theta_x \cos \varphi_x \underline{\underline{e}}_2 + \sin \theta_x \sin \varphi_x \underline{\underline{e}}_3,$$

$$\underline{\underline{e}}_\beta = \cos \theta_y \underline{\underline{e}}_1 + \sin \theta_y \cos \varphi_y \underline{\underline{e}}_2 + \sin \theta_y \sin \varphi_y \underline{\underline{e}}_3.$$

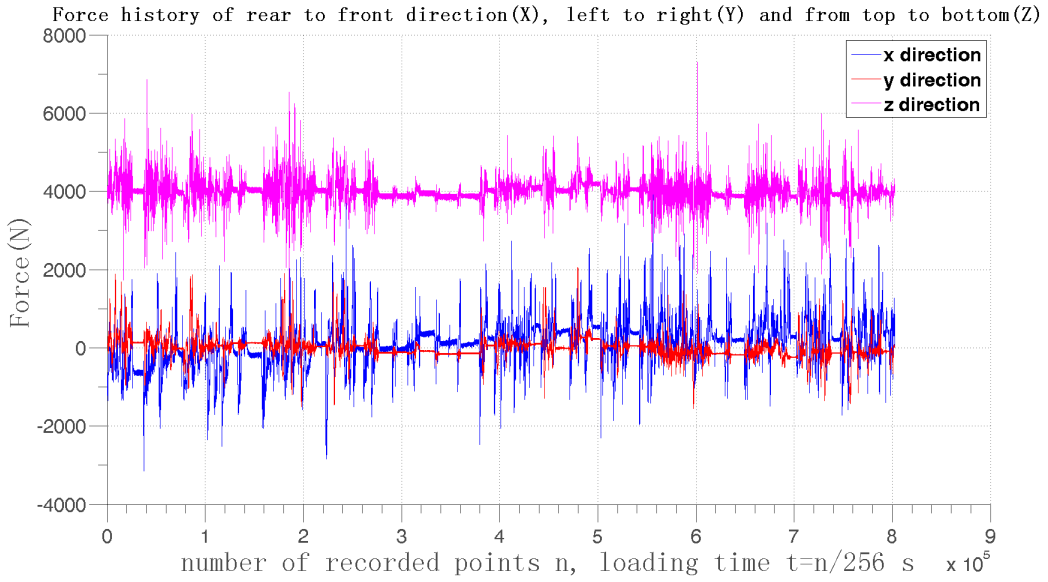


Fig. 48: Loading history of 3 different directions

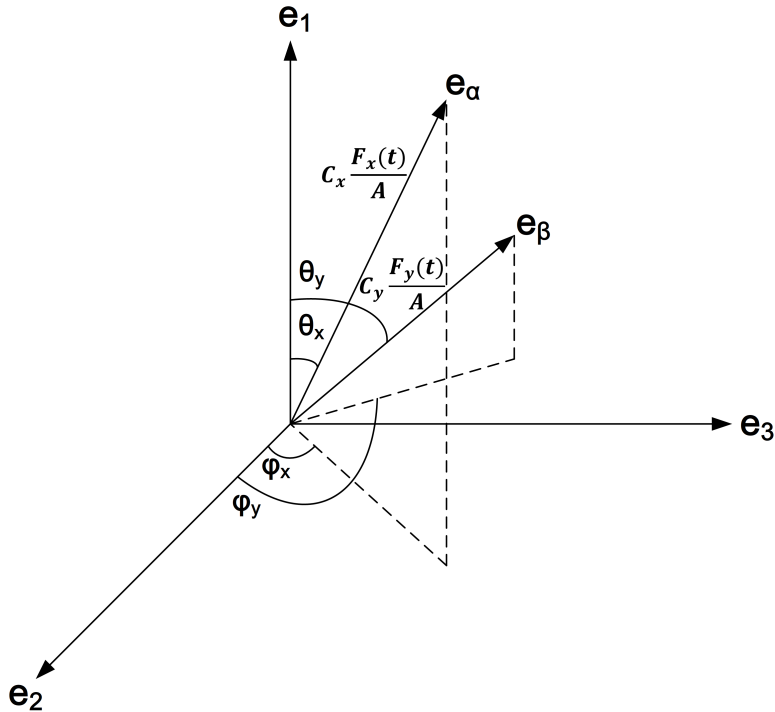


Fig. 49: Loading in 3 different directions

Here $F_x(t)$, $F_y(t)$, $F_z(t)$ are from test data, and θ_x , φ_x , θ_y , φ_y are structural parameters to be chosen randomly. The physical data are the same with parameters in Table 5. The structural data we choose is shown in Table 6.

The underlying assumption is that a unit load on wheel in direction e_x creates a stress tensor at point M

Parameter	$A(m^2)$	c_x	c_y	θ_x	φ_x	θ_y	φ_y
Value	1/6e4	10	60	0.5	0.3	0.6	0.4

Table 6: The structural data in 3D analysis

given by:

$$c_x \frac{F_x(t)}{A} \underline{e}_\alpha \otimes \underline{e}_\alpha,$$

where $\underline{e}_\alpha \otimes \underline{e}_\alpha$ defines the local structural response of the vehicle.

Replacing \underline{e}_α and \underline{e}_β in Eq.(158) we get the stress tensor in Eq.(159).

$$\begin{aligned}
\underline{\underline{\Sigma}} &= \frac{F_z}{A} \underline{e}_1 \otimes \underline{e}_1 + c_x \frac{F_x}{A} \underline{e}_\alpha \otimes \underline{e}_\alpha + c_y \frac{F_y}{A} \underline{e}_\beta \otimes \underline{e}_\beta \\
&= \frac{F_z}{A} \underline{e}_1 \otimes \underline{e}_1 + c_x \frac{F_x}{A} (\cos\theta_x \underline{e}_1 + \sin\theta_x \cos\varphi_x \underline{e}_2 + \sin\theta_x \sin\varphi_x \underline{e}_3) \otimes (\cos\theta_x \underline{e}_1 + \sin\theta_x \cos\varphi_x \underline{e}_2 + \sin\theta_x \sin\varphi_x \underline{e}_3) \\
&\quad + c_y \frac{F_y}{A} (\cos\theta_y \underline{e}_1 + \sin\theta_y \cos\varphi_y \underline{e}_2 + \sin\theta_y \sin\varphi_y \underline{e}_3) \otimes (\cos\theta_y \underline{e}_1 + \sin\theta_y \cos\varphi_y \underline{e}_2 + \sin\theta_y \sin\varphi_y \underline{e}_3) \\
&= \left(\frac{F_z}{A} + c_x \frac{F_x}{A} \cos^2 \theta_x + c_y \frac{F_y}{A} \cos^2 \theta_y \right) \underline{e}_1 \otimes \underline{e}_1 \\
&\quad + \left(c_x \frac{F_x}{A} \cos\theta_x \sin\theta_x \cos\varphi_x + c_y \frac{F_y}{A} \cos\theta_y \sin\theta_y \cos\varphi_y \right) (\underline{e}_1 \otimes \underline{e}_2 + \underline{e}_2 \otimes \underline{e}_1) \\
&\quad + \left(c_x \frac{F_x}{A} \cos\theta_x \sin\theta_x \sin\varphi_x + c_y \frac{F_y}{A} \cos\theta_y \sin\theta_y \sin\varphi_y \right) (\underline{e}_1 \otimes \underline{e}_3 + \underline{e}_3 \otimes \underline{e}_1) \\
&\quad + \left(c_x \frac{F_x}{A} \sin^2 \theta_x \cos^2 \varphi_x + c_y \frac{F_y}{A} \sin^2 \theta_y \cos^2 \varphi_y \right) \underline{e}_2 \otimes \underline{e}_2 \\
&\quad + \left(c_x \frac{F_x}{A} \sin^2 \theta_x \cos\varphi_x \sin\varphi_x + c_y \frac{F_y}{A} \sin^2 \theta_y \cos\varphi_y \sin\varphi_y \right) (\underline{e}_2 \otimes \underline{e}_3 + \underline{e}_3 \otimes \underline{e}_2) \\
&\quad + \left(c_x \frac{F_x}{A} \sin^2 \theta_x \sin^2 \varphi_x + c_y \frac{F_y}{A} \sin^2 \theta_y \sin^2 \varphi_y \right) \underline{e}_3 \otimes \underline{e}_3
\end{aligned} \tag{159}$$

The plot of $(\underline{\underline{\Sigma}} - \underline{\underline{b}})_{trial}$ and $(\underline{\underline{\Sigma}} - \underline{\underline{b}})$ under 2 different scales are shown in Fig. 50.

In the load history, when $(\underline{\underline{\Sigma}} - \underline{\underline{b}})_{trial} > \sigma_y$, the damage accumulates. However, under scale s_{10} , there are much less damage accumulation than under scale s_1 . In this way we do not neglect the small influences in load history and the big fluctuation in stress is magnified which reflects the real situation.

The damage evolves like in Fig. 51.

We can improve the result by inserting more arithmetic sequence points between every 2 recorded points. As is shown in Table.7 :

Table 7: Arithmetic sequence points density effect

Arithmetic sequence points between every two points	Total time to failure(s)
10	78.63711
20	72.24630
30	70.25793
50	68.69148
100	67.49223

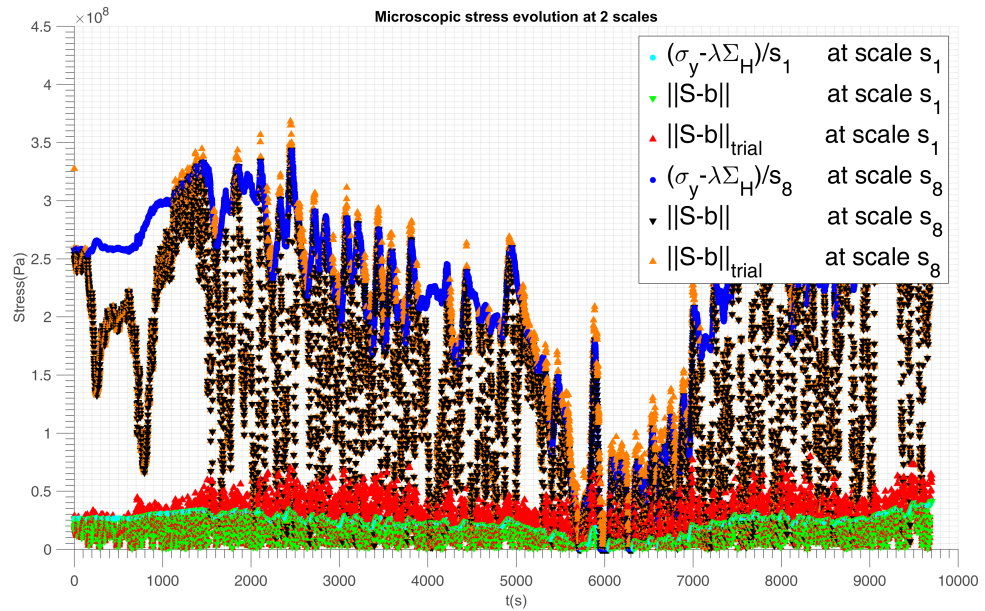


Fig. 50: $(\underline{S} - \underline{b})_{trial}$ and $(\underline{S} - \underline{b})$ evolution with time under different weakening scales in PSA load history

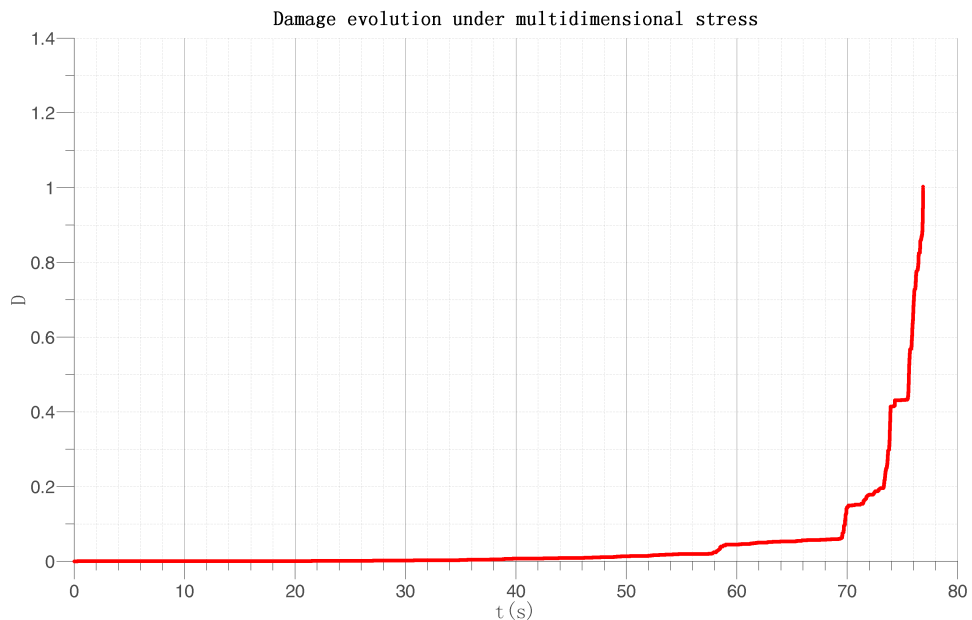


Fig. 51: Damage evolution under multidimensional stress

6.4. Discussion

The strategy can be made more complex by introducing a local space averaging process in the calculation of the local damage, and by taking more general plastic flows. The energy based fatigue approach takes into account impurities and hardness in the material which affect the fatigue life. The load sequence effects for complex multiaxial loading history are included in damage accumulation process. The small step-by-step

Loading direction	max(N)	mean(N)	min(N)
FX_RAVG	4739	113	-3145
FY_RAVG	2050	0	-1558
FZ_RAVG	7301	4012	1219
FZ_RARG	5858	3272	647

Table 8: Summary of the signals in the center of LFW

Table 9: My caption

Signal	nb of cycles	Max of Range	Min of Mean	Max of Mean
FX_RAVG	206636	7884	-3106	4704
FY_RAVG	205359	3608	-1489	2032
FZ_RAVG	237703	6082	2225	6224
FZ_RARG	340967	5211	1482	5122

Table 10: Rainflow counting results of the force data

strategy does not ignore small fluctuations in the load history. In addition, it can take into account any type of micro plasticity law and multiaxial load geometry.

Further research of energy based failure criteria should be focused on the following aspects:

1. The accommodation law might be more elaborate than kinematic hardening.
2. The differentiation of shear stress and normal stress effect on fatigue life should be clarified.
3. The non-linearity parameter α contains the stress σ , so it can evolve with time. But for complex loading history, should it change at every time step?

7 Multi-dimensional application

We have a 52 minutes recording of an average customer which have driven 18.3 kilometers. A complete set of forces were recorded at the center of the left front wheel (LFW in English but RAVG in French for Roue AVant Gauche). This wheel is driving and sustains the engine mass (half of it).

FX: Force in the axial direction (from rear to front), a positive (resp. negative) force corresponds to an acceleration (resp. deceleration) of the vehicle.

FY: Force in the horizontal direction (from driver to shotgun), a positive (resp. negative) force corresponds to an right (resp. left) turn.

FZ: Force in the vertical direction (from top to bottom), a more (resp. less) than average force corresponds to a bump (resp. pot hole) in the road, the average is the vehicle mass to the wheel.

The summary of the signals are :

From a comparison point of view, the rainflow counting in the Range/Mean diagram of these signals gives:

So all the signals present a significant amounts of fatigue cycles (above 2e5) but the rear wheel is richer (by 50%), hence it is presented here.

The starting point is the data of a loading history on different macroscopic directions $(F_i)_i = 1, N$. Typically, in the data sent recently by PSA, the elementary loads are the three components of the force applied at the rear center wheel $(q_i(t))_i = 1, N$. The objective is to construct from this data a multi-scale stochastic mesoscopic plastic damage accumulation at the different materials points M inside the structure, and identify the time to failure as the time when the cumulated energy dissipated by this mesoscopic plastic accumulation reaches a given material threshold.

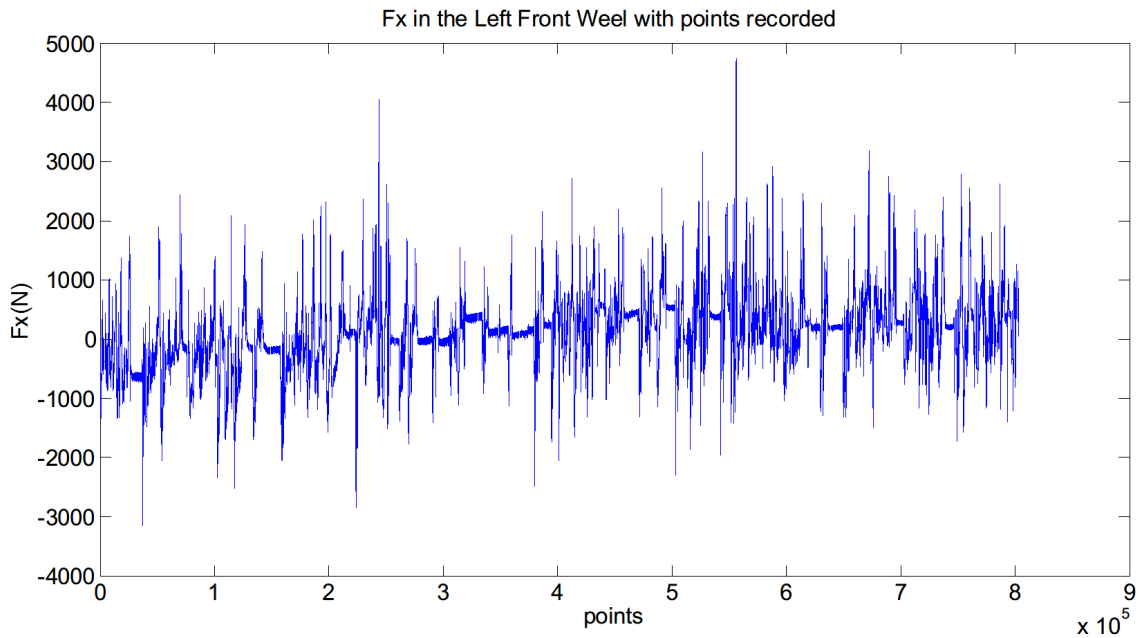


Fig. 52: Fx in the Left Front Weel with points recorded

The material under high cycle fatigue does not undergo local strain concentration. But physically the internal residual stress causes slip of grains in the weaker parts in the material. The grain slip system is determined by the orientation of the stress and the size of grain. To predict failure we have to consider both shear and hydrostatic stress of the loading.

The whole process of loading history has no macroscopic plastic deformation. But instead of thinking mesoscopic stress concentration, we assume there are local weak points where the stress yield limit is smaller than the macroscopic one. To put this thought into formula we assume the mesoscopic strain is the same as macroscopic strain:

$$\hat{\varepsilon} = E$$

And the mesoscopic shear stress is the difference between macroscopic stress and the local residual stress.

$$\hat{\sigma} = \Sigma - \sigma_R$$

To get the residual stress evolution with time we need to find a filter to get rid of the signals with small variation which have negligible influence on residual stress, see Fig. 53. The filtered rainflow signal 'shortened' the actual time that the material endured but this does not influent our damage prediction because we consider the trivial signals has no impact on fatigue life.

From the filtered loading history we use Dang Van or Habbibou's law to get the residual stress evolution history at given slip(orientation) or scale. By making the difference between the actual stress and residual stress we get $\hat{\sigma}$.

When the accumulated energy reached a certain limit then fatigue occurs. Locally we have the expression of dissipated energy:

$$\Delta W \doteq \int \hat{\sigma} : \hat{\varepsilon} dt$$

To start with simple case we assume our signal is sinusoidal. Now we want the distribution of orientation of the slips in the metal. Statistics method gives us the yield limit distribution.

Acknowledgments We are grateful for the financial and technical support of Chaire PSA.

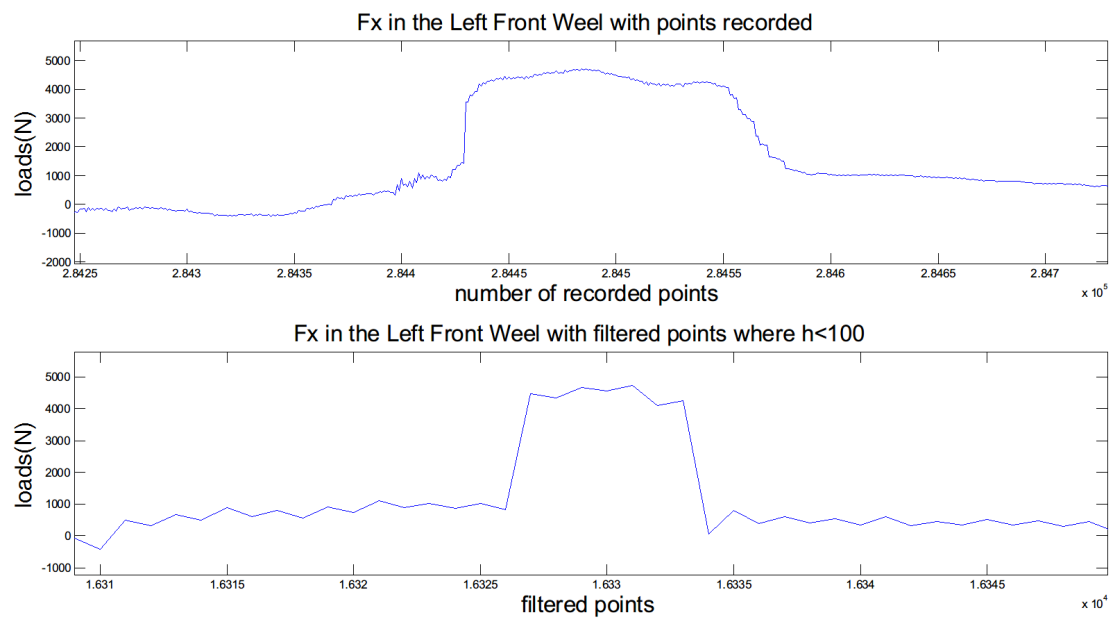


Fig. 53: Comparison between the recorded signal and filtered signal which removes the small variation points where the rainflow cycle amplitude $h \leq 100N$

References

- [1] DH Luu, MH Maitournam, and QS Nguyen. Formulation of gradient multiaxial fatigue criteria. *International Journal of Fatigue*, 2013.
- [2] Crossland B. Effect of large hydrostatic pressures on the torsional fatigue strength of an alloy steel. In: *Proceedings of the International Conference on Fatigue of Metals*, Institution of Mechanical Engineers, London., pages 138–149, 1956.
- [3] Ioannis V. Papadopoulos, Piermaria Davoli, Carlo Gorla, Mauro Filippini, and Andrea Bernasconi. A comparative study of multiaxial high-cycle fatigue criteria for metals. *International Journal of Fatigue*, 19(3):219 – 235, 1997.
- [4] P Ballard, K Dang Van, A Deperrois, and YV Papadopoulos. High cycle fatigue and a finite element analysis. *Fatigue & Fracture of Engineering Materials & Structures*, 18(3):397–411, 1995.
- [5] IV Papadopoulos. *Fatigue limit of metals under multiaxial stress conditions: the microscopic approach*. Joint Research Centre, ISEI, 1993.
- [6] Ioannis V Papadopoulos. Long life fatigue under multiaxial loading. *International Journal of Fatigue*, 23(10):839–849, 2001.
- [7] Li Yuan and Han Xu Liu Jie Jiang Chao. A prediction method on high-cycle fatigue parameters based on dissipated energy computation. *Chinese Journal of Theoretical and Applied Mechanics*, 3:008, 2013.
- [8] Thierry Palin-Luc and Serge Lasserre. An energy based criterion for high cycle multiaxial fatigue. *European Journal of Mechanics-A/Solids*, 17(2):237–251, 1998.
- [9] Tadeusz Łagoda, Ewald Macha, and Włodzimierz Bedkowski. A critical plane approach based on energy concepts: application to biaxial random tension-compression high-cycle fatigue regime. *International Journal of Fatigue*, 21(5):431–443, 1999.
- [10] F. Morel. A critical plane approach for life prediction of high cycle fatigue under multiaxial variable amplitude loading. *International Journal of Fatigue*, 22(2):101 – 119, 2000.
- [11] F Morel. A fatigue life prediction method based on a mesoscopic approach in constant amplitude multiaxial loading. *Fatigue and Fracture of Engineering Materials and Structures*, 21(3):241–256, 1998.
- [12] Subra Suresh. *Fatigue of materials*. Cambridge university press, 1998.
- [13] Ioannis V. Papadopoulos and Vassilis P. Panoskaltsis. Invariant formulation of a gradient dependent multiaxial high-cycle fatigue criterion. *Engineering Fracture Mechanics*, 55(4):513 – 528, 1996.
- [14] R. Amargier, S. Fourny, L. Champon, C. Schwob, and C. Poupon. Stress gradient effect on crack initiation in fretting using a multiaxial fatigue framework. *International Journal of Fatigue*, 32(12):1904 – 1912, 2010.
- [15] Mahaman Habibou Maitournam, Ky Dang Van, and Jean-François Flavenot. Fatigue design of notched components with stress gradients and cyclic plasticity. *Advanced Engineering Materials*, 11(9):750–754, 2009.
- [16] David Taylor. *The theory of critical distances: a new perspective in fracture mechanics*. Elsevier, 2010.
- [17] J.A. Arajo, L. Susmel, D. Taylor, J.C.T. Ferro, and E.N. Mamiya. On the use of the theory of critical distances and the modified whler curve method to estimate fretting fatigue strength of cylindrical contacts. *International Journal of Fatigue*, 29(1):95 – 107, 2007.
- [18] JF Flavenot and N Skalli. Lépaisseur de couche critique ou une nouvelle approche du calcul en fatigue des structures soumises des sollicitations multiaxiales. *Mec. Mater. Electr*, 397:15–25, 1983.
- [19] T Palin-Luc. Stress gradient and size effects in multiaxial fatigue. *Materials Week (Munich, Germany)*, 2000.
- [20] A. Banvillet, T. Palin-Luc, and S. Lasserre. A volumetric energy based high cycle multiaxial fatigue criterion. *International Journal of Fatigue*, 25(8):755 – 769, 2003.
- [21] Ioannis V Papadopoulos and Vassilis P Panoskaltsis. Invariant formulation of a gradient dependent multiaxial high-cycle fatigue criterion. *Engineering Fracture Mechanics*, 55(4):513–528, 1996.
- [22] William Nichols Findley, JJ Coleman, and BC Hanley. *Theory for Combined Bending and Torsion Fatigue with Data for SAE4340 Steel*. Division of Engineering, Brown University, 1956.
- [23] Jean Lemaitre and Jean-Louis Chaboche. *Mechanics of solid materials*. Cambridge university press, 1990.
- [24] J. L. Chaboche and P. M. Lesne. A non-linear continuous fatigue damage model. *Fatigue , Fracture of Engineering Materials , Structures*, 11(1):1–17, 1988.
- [25] Lu Xi and Zheng Songlin. Strengthening of transmission gear under low-amplitude loads. *Materials Science and Engineering: A*, 488(1):55–63, 2008.
- [26] Lu Xi and Zheng Songlin. Strengthening and damaging under low-amplitude loads below the fatigue limit. *International Journal of Fatigue*, 31(2):341–345, 2009.
- [27] Lu Xi and Zheng Songlin. Changes in mechanical properties of vehicle components after strengthening under low-amplitude loads below the fatigue limit. *Fatigue & Fracture of Engineering Materials & Structures*, 32(10):847–855, 2009.
- [28] GM Sinclair. An investigation of the coaxing effect in fatigue of metals. Technical report, DTIC Document, 1952.
- [29] Masaki Nakajima, Jae Woong Jung, Yoshihiko Uematsu, and Keiro Tokaji. Coaxing effect in stainless steels and high-strength steels. *Key Engineering Materials*, 345:235–238, 2007.
- [30] Richard M Christensen. Yield functions, damage states, and intrinsic strength. *Mathematics and Mechanics of Solids*, 5(3):285–300, 2000.
- [31] M.H. Maitournam, C. Krebs, and A. Galtier. A multiscale fatigue life model for complex cyclic multiaxial loading. *International Journal of Fatigue*, 33(2):232 – 240, 2011.
- [32] Stefano Bosia and Andrei Constantinescu. Fast time-scale average for a mesoscopic high cycle fatigue criterion. *International Journal of Fatigue*, 45:39 – 47, 2012.
- [33] Ma Zepeng. Structures under multiaxial fatigue taking consideration of gradients of the constraints with time and space variation.
- [34] Legendre Gauss Quadrature weights and nodes. <https://www.mathworks.com/matlabcentral/fileexchange/4540-legendre-gauss-quadrature-weights-and-nodes>. Accessed: 2004-05-11.

Appendices